POLITEHNICA UNIVERSITY OF TIMIŞOARA
Civil Engineering Faculty
Department of Steel Structures and Structural Mechanics

EXPERIMENTAL INVESTIGATIONS ON WELDED BUILT-UP COLD-FORMED STEEL BEAMS

Author: **Nguyen Thai HOANG, Civ. Eng.**

Supervisors: **Professor Viorel UNGUREANU, Ph.D.**
&
Asst. Professor Ioan BOTH, Ph.D.

Politehnica University of Timisoara, Romania

Study Program: **SUSCOS_M**

Academic year: **2017 / 2018**

EXPERIMENTAL INVESTIGATIONS ON WELDED BUILT-UP COLD-FORMED STEEL BEAMS

By

Nguyen Thai HOANG

Thesis submitted in partial fulfillment of the requirements for the degree of

MASTER OF SCIENCE

in

CIVIL ENGINEERING

European Erasmus Mundus Masters Course

Sustainable Construction Under Natural Hazards and Catastrophic Events

February 2018

Keywords: Spot welding, CMT welding, Corrugated web, built-up beam, cold-formed steel sections, experimental tests.

JURY MEMBERS

President:

Acad.Prof.Dr.Ing. Dan DUBINA
Member of the Romanian Academy
Politehnica University Timişoara
Srada Ioan Curea, 1
300224, Timişoara, Timiş, Romania

Members:

Prof.Dr.Ing. Viorel UNGUREANU
(Thesis Supervisor)
Politehnica University Timişoara
Srada Ioan Curea, 1
300224, Timişoara, Timiş, Romania

Prof.Dr.Ing. Adrian CIUTINA
Politehnica University Timişoara
Srada Ioan Curea, 1
300224, Timişoara, Timiş, Romania

Prof.Dr.Ing. Florea DINU
Politehnica University Timişoara
Srada Ioan Curea, 1
300224, Timişoara, Timiş, Romania

Conf.Dr.Ing. Adrian DOGARIU
Politehnica University Timişoara
Srada Ioan Curea, 1
300224, Timişoara, Timiş, Romania

Secretary:

Dr.Ing. Ioan MARGINEAN
Politehnica University Timişoara
Srada Ioan Curea, 1
300224, Timişoara, Timiş, Romania

ACKNOWLEDGMENTS

First and foremost, I would like to express my sincere appreciation and gratitude to the following people who help me to finish this master thesis.

I am thankful to Professor Viorel UNGUREANU for being my supervisor of this thesis. With his thorough guidance, constructive advice and generosity in time, I have found the motivation to work harder, made the best effort possible in my thesis and successfully completed it in the last 5 months. Besides helping me to complete a master dissertation, he encouraged and directed me in publishing conference papers. That is very precious as it has contributed to the promotion of my research career.

I greatly appreciate Asst. Professor Ioan BOTH for his constant support in laboratory for my thesis. His kind characteristic and pleasant presence have made my time in the office much better than it could be. Our meetings always involved funny stories that were related to what we dealt with. His sense of humor gave me comfort and distracted me from the stress. There is no doubt to say that he is a great supporter.

I would like to convey my gratitude to the all SUSCOS coordinators, especially Professor Dan DUBINA and Professor Adrian CIUTINA for making all the courses and thesis become a life-time experience, not only for me but also for all SUSCOS's students. I wish to take this opportunity to forward my utmost appreciation to all the lecturers in Steel structures and Structural Mechanics Department, Faculty of Civil Engnieering, Politehnica University of Timisoara. At the same time, I thank to all SUSCOS colleagues for their spirit, passion and companionship during the one and a half year. I was very fortunate to share part of the journey in my life particularly in Europe with these incredible people from different countries in the world.

Last but not least, I dedicate this master thesis to my family, my parents and elder sister. Their timely interest keeps the fire inside me in whatever I do and wherever I go. Huge thanks to them for understanding my passion and interest so that I can push myself beyond the limit. They are definitely the first and the last source of love and solace I would find in my academic and life journey.

ABSTRACT

The present thesis is dedicated to investigate the behaviour of cold-formed steel beams with composite section made of corrugated steel sheets for the web and thin-walled cold-formed steel profiles for the flanges, connected by spot-welding or CMT (Cold metal transfer) welding in the framework of the WELLFORMED research project, taking place at the Research Center CEMSIG of the Politehnica University of Timişoara.

It consists of two parts, "Experimental tests" and "Numerical simulation". At first, the tests on small flat specimens subjected to the shear, is executed to see the real properties of material. Then experimental programme continues with specimens, composed of two layers of steel sheets and connected by spot welding or CMT welding in order to comprehend and characterize the behavior of these types of joints. The resistance of the joints is calculated by applying the formulae in chapter 8.4 and 8.5 of Eurocode 1993-1-3. And the comparison between the theoritical results and the actual results from the test is implemented. After that, the experimental programme is applied on five full-scale beams in order to demonstrate the feasibility of the proposed solution and to evaluate their performances. Within the framework of the thesis, three out of five beams are performed the test in laboratory due to the limitation of time. In the second part, the finite element software ABAQUS version 6.14 is used to make the numerical simulation to optimize the details of the connections and the parameterisation of the solution, respectively.

As a general conclusion based on the current study, the results are encouraging and demonstrating the potential of this solution for standardization and industrial manufacturing.

TABLE OF CONTENTS

LIST OF FIGURES

LIST OF TABLES

CHAPTER 1: INTRODUCTION

1.1. Introduction

Built-up beams, with sinusoidal or trapezoidal corrugated web, represent a relatively new structural system that has developed in the last two decades, especially in Germany and Austria. The large number of applications was made by using this type of structural system. It is observed that it is being widely used more and more for the mainframe of single-storey steel buildings with large span and many steel bridges, respectively.

The increase in buckling resistance of the corrugated webs is the main advantage of this type of beam. The reduction of the number of the web stiffeners may result in a very economical design. In addition, the use of thinner webs leads to lower costs for materials, which results in an estimated cost saving of 10-30% compared to conventional fabricated sections and more than 30% compared with standard hot-rolled beams. The buckling resistance of sinusoidal corrugated sheet used for webs can be comparable with plane webs of 12 mm thickness or more. Furthermore, due to lower weight, the erection and transport cost can be reduced.

In the solutions developed previously, the flanges were made of flat sheets, welded to the sinusoidal sheet for the web, which required a specific welding technology. For these elements, the flanges are mainly responsible for providing the main bending resistance of the beam, with a small contribution of the sinusoidal corrugated web that offers shearing capacity. The failure modes of the web happens due to steel yielding or web buckling. Furthermore, lateral-torsional buckling of the girder and local flange buckling, separately or in interaction, represents other possible types of failure modes. The design of corrugated web beams is regulated by Annex D of EN 1993-1-5 [1] together with the specific aspects covered by EN 1993-1-1 [2] and EN 1993-1- 3 [3].

1.2. Report objective

Being developed within the WELLFORMED research project financed by the Executive Agency for Higher Education, Research, Development and Innovation Funding (UEFISCDI), Romania, carried out at the CEMSIG Research Center of the Politehnica University of Timisoara, this study presents a new jointing technological solution for such a system, composed of webs made of trapezoidal cold-formed steel sheet and flanges of built-up thin-walled cold-formed steel profiles, namely welding connection. The specific welding solution can bring the benefits that it helps to

redure the handwork and the cost of joining technology and prepare the automatic solution. Spot welding and CMT (Cold metal transfer) welding are proposed for the connections between flanges and web. Furthermore, due to the fact that all components are galvanized, high protection against corrosion is one of the major advantages indeed.

The research project involves a large experimental program conducted on small specimens, composed of two layers of steel sheets with different thickness subjected to shear through tensile test, connected by spot welding or CMT welding. The aim is to understand the real properties of materials and the behaviour of two types of joints. After that, the experimetal test is applied on 1:1 scale beams in order to demonstrate the feasibility of the proposed solution and to assess their performances, followed by numerical simulations to optimize the details of the joints and to extend the solution by parametric studies.

Figure 1.1: Field of broad use of corrugated web beam

This new solution can be applied in building construction as steel supporting framework: as roof girders, portal and low rise multi-story frames, short span pedestrian bridges. In addition, it can be a reliable alternative to purlins or secondary beams, where these have to cover large bays. Because of the high strength to weight ratio, the span lengths could be wider, so a less number of columns are needed.

1.3. Research methodology

The study consists of two parts, “Experimental tests” and “Numerical simulation”:

- Experimental test is applied on flat specimens, specimens connected by spot welding, specimens connected by CMT welding and the full scale beams. At first, the tests on small flat specimens subjected to the shear, is executed to see the real properties of material. Then, the experimental program continues with tensile tests on specimens composed of two layers of steel sheets with different thickness combination connected together by welding technique to characterize the behavior of these types of joints. In order to determine the behavior of all types of joints used to build-up the beams, the joints in four positions are taken into account, including: (1) Overlapping zone of corrugated sheets; (2) Connection between the corrugated sheet and shear panels; (3) Connection between the shear panels and the flanges; (4) Connection between the flanges and the corrugated web. There are six combinations of thicknesses to be studied, consisting of 0.8 mm, 1.0 mm, 1.2 mm, 1.5 mm, 2.0 mm and 2.5 mm. A total of 340 small specimens are performed by the test. The resistance of the joints is calculated by applying the formulae in chapter 8.4 and 8.5 of Eurocode 1993-1-3. And the comparison between the theoritical results and the actual results from the test is implemented. Finally, the experimental programme is completed by performing the test on five full-scale beams in order to demonstrate the feasibility of the proposed solution and to evaluate their performances.

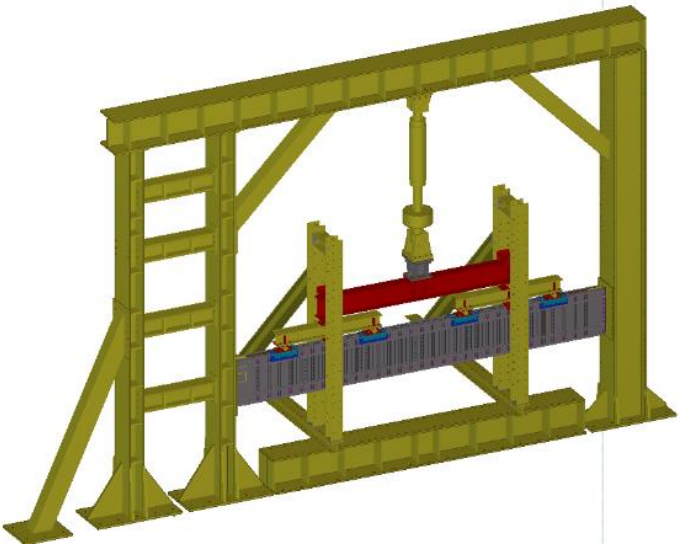

Figure 1.2: Experimental arrangement

Five types of beams with cold-formed steel profile flanges and a corrugated web, with a span of 5157 mm and a height of 600 mm are being tested (see Figure 1.2) considering different welding distributions, different thicknesses of the web and the shear panels.

- In the second part, the numerical simulation is made by using the finite element software ABAQUS version 6.14 to optimize the details of the connections and the parameterization of the solution, respectively.

CHAPTER 2: LITERATURE VIEW

2.1. Built-up cold-formed steel beams

One of the important aspects for the cold-formed steel elements or structures is the jointing technique. There are several types of built-up cold-formed steel beams on the market, prepared for industrialised fabrication, for which bolts, screws or spot welds are used for the connections between flanges and web.

A research programme was implemented by Zhao [4] at Queensland University of Technology to investigate the structural behaviour and design of hollow flange members in compression. The study focused on members with rectangular hollow flanges, where the sections are formed from a single steel strip, with various manufacturing methods such as spot welding, selfpierced riveting and screw fastening for the flange-to-web connections. It was concluded that the member compression capacity is not significantly affected by the type of fastening and spacing. Wanniarachchi [5] extended the work of Zhao [4] and developed a new cold-formed steel beam with two rectangular hollow flanges, rigid in torsion, and a slender web, cross-section assembled using intermittent screw fastening. He has found that intermittent screw fastening method is considerred to be structurally adequate and and it helps to reduce the fabrication cost.

In [6], the applicability of built-up cold-formed steel beams assembled by laser welding and their load bearing capacity was evaluated and assessed by Landolfo et al. The I-section with hollow flanges is fabricated from two special C-profiles back-to-back. The two profiles are joined with connections located on the web and on the flanges. Two reinforcing plates are placed inside the top and bottom hollow flanges of the I-section, providing an additional connection system between the two C-profiles.

A summary of the research and development in girders with corrugated web was reported by Elgaaly and Dagher [7] in order to study the shear capacity. In [8], Smith performed four tests on two beams with corrugated webs, which were welded to the flanges using intermittent welding. He found that the connection between the flange and the web is critical for the shear strength as the weld used in the test was subjected to high strength and web was easily ruptured at this point before it reached its buckling strength. A conclusion was drawn that intermittent welding of the corrugated webs to the flange is not advisable.

42 tests on 21 beams, which used four different corrugation configurations and two thicknesses, was performed by Hamilton [9]. Unlike Smith's [8] specimens using intermittent welding, the webs were continuously welded to the flanges from one side. It was found that the failure of all specimens was initiated by local buckling of one of the corrugation folds. Another conclusion was that dense corrugation profiles are prone to fail in global shear buckling. The test results done by Smith [8] and Hamilton [9] were verified by Elgaaly et al. [10] using nonlinear FEM and it was found that the results of the finite element analysis were very close to the test results.

In [11], a geometrical parametric study and comparison between the numerical results with existing empirical and analytical formulae were done by Luo and Edlund using non-linear finite element analysis. They have found that the ultimate shear capacity increases proportionally with the girder depth and does not seem to be dependent on the ratio of girder length over girder depth, while the post-buckling shear capacity not only increases with the girder depth, but also appears to be dependent on the ratio of girder length over girder depth. They have also found that the corrugation depth did not seem to have much effect on the ultimate shear capacity but affected the degree of the localization of the buckling mode.

For the type of corugated-web beams, the flanges mainly provide the flexural strength of the beam, with a small contribution of the sinusoidal or trapezoidal corrugated web that offers shearing capacity. To understand the bending behaviour of steel girders with corrugated webs, a lot of work has been done so far.

It has been observed that the web's contribution to the ultimate moment capacity of a beam with corrugated web is negligible, and the flange yield stress is the deciding factor for the ultimate moment capacity of the beam itself. A series of experimental and analytical studies were performed by Elgaaly et al. [12]. They took into account six specimens that had corrugated webs in the centre panel and flat panels adjacent to the supports for experimental test. As a result, all the specimens failed due to flange yielding followed by vertical buckling of the compression flange into the web. It was found that the contribution of the web to the bending capacity of the beam is small it could be neglected.

Chan et al. [13] studied the influence of web corrugation on the bending capacity of the beam using FEM. Beams with different types of webs were studied, included plan web, horizontally corrugated web and vertically corrugated web. They found that the vertically corrugated web provides a stronger support against the flange buckling than those with horizontally corrugated and flat webs.

In addition, the corrugation radius was investigated and found that higher bending moment could be provided by larger corrugation radius. It was also found that, the vertically corrugated beam had a 10.6% reduction in weight when compared with the beam with flat web.

Numerically and in experimental tests were performed by Johnson and Cafolla [14] to investigate the effect of the vertically corrugated webs on the local buckling of the compressive flange and the flexural behaviour of beams with corrugated webs. They found that the contribution of the web to flexural capacity was small. Also, they found that depending on the shape of the corrugations, the slenderness should be based on the distances from the horizontal fold to the edges of the flange.

The experimental tests to study the lateral-torsional behaviour of steel girders with corrugated webs was carried out by Lindner [15] and it was found that the torsional section constant I_T for a beam with corrugated was not different from that of a beam with flat web, but the warping section constant I_w is not similar.

The effect of the corrugation profiles of the web on the lateral torsional buckling strength of I-girders was also studied [16,17]. Pasternak et al. [18,19] presented a new proposal for Annex D of EN 1993-1-5: 2006 [1].

By using finite element analysis, Moon et al. [20] studied the lateral-torsional buckling strength of an I-girder with corrugated steel webs under linear moment gradient. It was found that the buckling behaviour of the I-girder with corrugated steel webs differed depending on the number of periods of the corrugation. A simple equation for the moment gradient correction factor for these types of beams was suggested.

Concerning beams with trapezoidal corrugated webs under patch loading, Leiva-Aravena and Edlund [21] performed six tests that considered three parameters, included the load patch width, the load path location and the web thickness. As a comparison between the test and finite element analysis results, it can be concluded that the FE model is able to depict the behaviour of girders with corrugated webs subjected to in plane compressive patch loading and caculate the failure load with a good level of accuracy.

In [22], Elgaaly and Seshadri performed five tests on four different types of corrugation profiles. It was observed that there are two distinct modes of failure: web crippling and web yielding. Furthermore, the interaction between partial compressive edge loading and bending or shear was also studied, using FEM.

Luo and Edlund [23] studied the effect of four factors that influence the buckling strength of the beams, consisting of (1) strain hardening model; (2) corner effect; (3) initial imperfections; (4) loading position, by performing nonlinear finite element analysis. They used elastic-perfectly plastic and Ramberg–Osgood's models and found that with a Ramberg–Osgood strain-hardening model for webs, the ultimate strength of the girder is about 8–12% higher than using an elastic-perfectly plastic model. In addition, the effect of the corners due to cold-forming does not have any significant effect on the ultimate strength.

Nguyen et al. [24] investigated the moment modification factors of I-girder with trapezoidal web corrugations under moment gradient and various end restraint conditions and proposed closed-form expressions for the moment modification factors.

The performance of the strength, the rotational stiffness, and the ductility of the composite and non-composite connection using trapezoidal web profiled steel sections was studied by Tahir et al. [25]. Eight full scales testing of beam-to-column connections have been carried out, comprised of four specimens for composite and four for non-composite connection with different geometrical configurations. A good agreement between the experimental and the predicted values was shown. It is also observed by the test that composite connections have higher moment resistance, higher stiffness, and less ductile compared with the non-composite connections.

The stress distribution in the flange of the girders with corrugated webs was investigated in [26] by Kövesdi et al. During the experimental tests, the different locations on flanges and web were considerred to measure the stress distributions as a basis for parametric analyses.

An attempt of Dubina et al. [27] related to the type of beams completely composed by cold-formed steel elements was a numerical study in order to prove the efficiency of such solution against cold-formed steel trusses.

In the framework of PRECASTEEL project [28], a similar solution has been proposed and analysed, but using blind rivets as seam fasteners for the corrugated web and bolts for web-to-flange connections. For flanges, back-to-back lipped channel or two types of hat-sections have been used. Deep corrugation web sheeting of longitudinal intermediate stiffeners have been applied in this solution. However, it was observed from the test results that the sensitivity to distortion of corrugation still remains high.

Within the Research Center CEMSIG (http://www.ct.upt.ro/en/centre/cemsig) of the Politehnica University of Timisoara, a technological solution of such a built-up beam, consisting of trapezoidal corrugated web and parallel flanges made of thin-walled cold-formed steel lipped channel sections, was proposed and carried out, in which the flanges and the web were connected by self-drilling screws (see Figure 2.1).

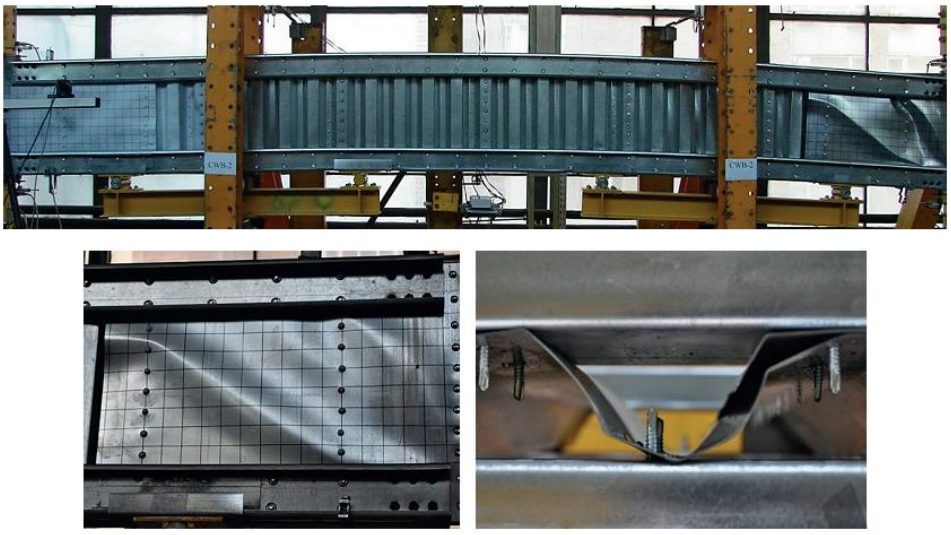

Figure 2.1: Built-up corrugated web beam with self-drilling screw fastener

Five beams with corrugated webs, with a span of 5157 mm and a depth of 600 mm, were tested, with different arrangements of self-drilling screws and shear panels. It should be noticed that this type of system is constituted of 100% of cold-formed steel elements in order to distinguish with the combination of two types of products that the web made of cold-formed elements and the flanges composed of hot-rolled steel. The detailed presentation of this solution was presented by Dubina et al. [29,30]. In the case developed later, it was applied further to evaluate the behaviour and capacity of a beam with 12 m span and trapezoidal shape with the FEM model validated.

With the aim of promoting the physical and mechanical limits of welding technology, new welding processes have been improved and progressed in order to meet the high standards of the automative industry. Fronius is well known as the market leader in the field of robotic welding systems, with over 50 years of experience in the automotive and components supply industry. it brings the world the very latest technologies for arc welding and resistance spot-welding. These technologies, due to their advantages, have also started to be used in the steel structure domain.

2.2. Spot welding technology

One of the noticeable technique for jointing technology is resistance spot welding (RSW). it is considered as one of the quickest and cleanest welding processes available and as the dominant process for joining sheet metals in automotive manufacturing factory.

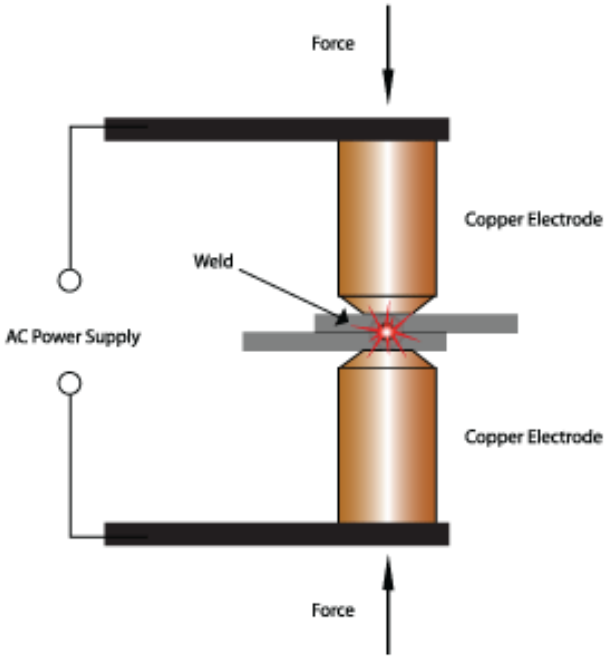

Figure 2.2: Spot welding technology

Spot welding is a technique for joining of overlapping pieces of metal, usually steel, without additional material. It is the most commonly joining method in the automative industry because of its advantages. Spot welding can bring great benefits due to high speed of fabrication, low cost of operation and ability to weld a wide range of joint configurations with the same gun. It will be formed when a large amount of current is passed through the panels for the correct amount of time and with the correct amount of pressure. The details of the weld forming process are shown in Figure 2.2. With the use of two copper alloy electrodes in the welding area, a compressive force is applied and electric current is transmitted, which locally heats the parts. Thus, the material between the electrodes is melting and after the welding current has stopped, the materials solidify and the joint results, creating a welded spot.

A comparative study on self-pierce riveting (SPR), resistance spot welding (RSW) and spot friction joining (SFJ) was performed by Paul Briskham et al. [31]. As a conclusion, resistance pot welding is the most economical process for highvolume production and its process offers the flexibility to

make different joint configurations on a single gun and the ability to switch between steel and aluminium. However, RSW is more sensitive to the condition of the sheet surface and thickness of the oxide layer than either SPR or SFJ so that a significant increase in oxide thickness due to poor storage conditions can lead to over heating of the weld resulting in reduced electrode life.

Gregory L. Snow [32] conducted a research in order to see how arc spot weding is aftected by arc time used while forming the weld. Thicknesses were studied consisting of 0.85 mm, 1 mm, 1.3 mm and 1.6 mm. The test was performed for each gauge material in single-, double- and four-layer configurations. This research has proven that arc time has a tremendous influence on arc spot weld shear strength. Therefore, using proper arc time to ensure weld forming is necessary.

It is indicated in [33] that four variables needed to take into account with resistance spot welding, including: Pressure, weld time, electric current and tip diameter. The weld current and weld time are inversly proportional to each other through a function of weld temperature to bring the metal to reach a temperature of 2550 degree F.

In [34], the prediction of resistance spot weld failure modes in shear tension tests of advanced high-strength automotive steels was made by performing the experimental test and verified by finite element simulation. As a result, it is generally observed that there are two different failure modes, namely full button pull-out and interfacial fracture. The research pointed out that the load-bearing capacity of these welds is not significantly affected by the fracture mode. Thus, the mode of failure should not be the only criteria used to judge the results of the shear-tension test. The load-carrying capacity of the weld should be considered the most important parameter when evaluating the shear-tension test results in advanced high-strength automotive steels.

An analytical model predicting failure mode of resistance spot welds was perfomred by M. Pouranvari et al. [35]. It was found that spot welds that fail in nugget pullout mode provide higher peak loads and energy absorption levels than spot welds that fail in interfacial fracture mode. Therefore, the analytical model was proposed to estimate minimum fusion zone size to ensure pull-out failure mode of resistance spot welds during tensile-shear test. According to this model, ratio of fusion zone hardness to failure location hardness is the key metallurgical factor governing failure mode of spot welds during tensile-shear test, in addition to sheet thickness. It was also noticed in [36] that sheet thickness, fusion zone size, and hardness characteristics of the welds are key factors controlling the failure mode of spot welds during cross-tension test. Results showed that increasing

the fusion zone size improved the peak load of spot welds in both cross-tension and tensile-shear tests.

In [37], Y.J.Chao showed that the plastic collapse is the cause of nugget pullout failure and the interfacial failure is governed by crack or fracture mechanics. These two failure mechanisms compete with each other and the failure of a spot weld occurs when the fracture criterion for one of the mechanisms is satisfied first.

Strength tests were performed by Chao [38] to reveal the failure mechanisms of spot weld in lapshear and cross tension test samples. Based on the observed failure mechanism, stress distribution was assumed. A theoretical model was developed to the mixed normal/shear loading condition.

Axial compression tests of thin-walled beams joined by spot welding was presented by E. Rusinski [39]. the effect of the size of the weld's diameter and the pitch of the weld on the amount of absorbed energy are parameters to be studied. A numerical simulation was made and FEM strength computations of the thin-walled beams, taking into account physical and geometrical nonlinearities, were performed.

2.3. CMT (Cold metal transfer) welding technology

The cold welding process CMT means outstanding results with all materials. it guarantees the most stable electric arc in the world and precise control of the process, offering welded bead and soldering without welding drops and able to weld ultra-light gauge sheets from only 0.3 mm.

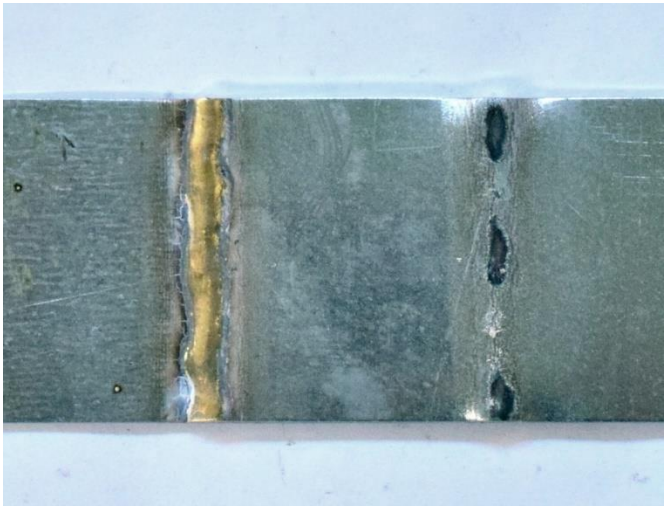

Figure 2.3: CMT welding technology

In [40], it indicates that CMT exhibits a high wire melting coefficient requiring in the region of 20 - 30% less thermal energy for welding compared to conventional MIG welding processes. It brings a lot of advantages such as: reducing part distortion, minimizing the problem of weld spatter due to low thermal input, greatly reducing the requirement for rework, and providing good gap bridging capabilities.

A cold metal transfer (CMT) fusion joining technique was performed within research of Paul R. Cao et al [41]. The fusion welding of 1-mm-thick Mg AZ31 to 1-mm-thick galvanized mild steel lap joints was studied. Based on the experimental results, it was found that CMT welding of Mg can be applied to steel if the steel has a zinc coating because of the lower melting temperature of the zinc compared to the steel, in which interacts with the molten Mg alloy to provide a braze joint.

The use of low-energy and standard welding methods (CMT and MIG-Pulse) for joining elements made of hard-to-weld 6xxx series aluminium alloys was presented by Janusz Rykała et al in [42]. The determination of the usability of the CMT and MIG-Pulse methods for welding butt joints made of 2.0 mm thick sheets was also caried out. The authors indicate that CMT welding provides high quality and aesthetics of welded joints made of aluminium alloys regarded as difficulty to weld.

In [43], mechanical properties and acoustic emission (AE) characteristics occurring in cold metal transfer (CMT)-welded specimens subjected to corrosion process and tensile testing were investigated by Piyapong et al. Specimens with Al alloy AlMg3 sheets and zinc-coated steel DX51D sheets joined by using CMT welding with AlSi5 as filler material are prepared for the experimental test. There are two parts for the experiment, including: first is studying AE signals detected from test specimens being under salt-spray testing, and second part is conducting tensile testing of both corrosive CMT-welded specimens and non-corrosive CMT-specimens with AE technique. As a result, it clearly showed that the strength of test specimens is decreased due to corrosion process appearing on them. Furthermore, the AE technique performed the ability to display AE signals generated by test specimens during tensile testing. Therefore, the manufacturing process in industry could be improved effectively and safely if the AE method can be applied to examine the CMT welding quality.

Lin Jian et al. [44] performed both experimental observation and numerical simulation whithin a research, applied to specimens composed of dissimiliar materials using CMT brazed lap joints. The aim was to evaluate the shear strength and investigate the faliure modes of this type of

specimens. The interface layer of CMT brazed lap joint was modeled by the interface element. The authors proposed the failure stress and the failure energy at the interface element as the failure criteria for the prediction of shear strength of CMT welding connections. It was found that with the thicker steel sheets, the stress distribution at the interface layer elements has some change, leading to improvement of shear stength at the interface layer. As a result, the failure occuring at the interface element may transfer to the fusion line at the side of the alluminum alloy sheet.

Research progresses on arc welding techniques are described by Kodama et al. [45], focusing on the automotive members. It is indicated that arc welding is a versatile joining method applicable to a wide variety of joint confiuration such as butt, lapping, and T joints. Static strength and fatigue strength performance of welded joints are improved for high-strength steels by CMT applied arc spot welding.

CHAPTER 3: EXPERIMENTAL TESTS

The following chapter describes the testing procedure that was followed and the results that were taken from each test. Details related to the procedure such as specimen dimensions, material properties and instrumentation are included. The detailed results are presented by the tables and figures which are shown in the Appendix.

Procedure of the tensile test is followed by the international standard ISO 6892-1, Metallic materials - Tensile testing - Part 1: Method of test at room temperature. Experimental tests were conducted using the UTS universal testing machine. The test pieces are gripped by the clamps at both ends. It is needed to be sure that test pieces are held in such a way that the force is applied as axially as possible, in order to minimize bending. In order to obtain a straight test piece and ensure the alignment of the test piece and grip arrangement, a preliminary force may be applied provided it does not exceed a value corresponding to 5 % of the specified or expected yield strength [46].

3.1. Tensile tests

3.1.1. Specimen preparation

The purpose of the test is to obtain the real properties of material. Tensile tests were performed on six series of specimens in different thicknesses. The specimens with the nominal width of 20 mm and the thicknesses of the steel sheet including 0.8 mm, 1.0 mm, 1.2 mm, 1.5 mm, 2.0 mm and 2.5 mm, were tested. The dimensions were chosen so as to adequately fit into the grips of the testing machine.

The status of all specimens before and after the tensile test is displayed in Appendix A: Pre- and post- status of specimens for tensile test of this thesis

The dimensions for each specimens are shown in the Table 3.1. The thickness and the width were measured in three different positions along the length of specimen in order to get the average values.

Table 3.1: Specimen dimensions for tensile test

Specimens	Width (mm)				Thickness (mm)			
	1st	2nd	3rd	Average	1st	2nd	3rd	Average
T - 0.8 - 1	21.60	21.40	21.35	**21.45**	0.80	0.82	0.83	**0.82**
T - 0.8 - 2	21.51	21.54	21.77	**21.61**	0.80	0.79	0.80	**0.80**
T - 0.8 - 3	21.68	21.49	21.51	**21.56**	0.79	0.80	0.80	**0.80**
T - 0.8 - 4	21.60	21.55	21.68	**21.61**	0.79	0.80	0.79	**0.79**
T - 0.8 - 5	21.09	20.64	20.18	**20.64**	0.80	0.80	0.80	**0.80**
T - 0.8 - 6	22.04	21.80	21.65	**21.83**	0.80	0.80	0.79	**0.80**
T - 1.0 - 1	20.76	20.75	20.74	**20.75**	1.01	1.01	1.01	**1.01**
T - 1.0 - 2	20.70	20.52	20.54	**20.59**	1.02	1.02	1.00	**1.01**
T - 1.0 - 3	20.54	20.53	20.54	**20.54**	1.00	1.01	1.00	**1.00**
T - 1.0 - 4	20.85	20.82	20.81	**20.83**	1.02	1.01	1.00	**1.01**
T - 1.0 - 5	20.75	20.72	20.70	**20.72**	1.00	1.00	1.01	**1.00**
T - 1.0 - 6	20.90	20.92	20.91	**20.91**	1.02	1.01	1.00	**1.01**
T - 1.0 - 7	21.26	21.25	21.24	**21.25**	0.99	1.00	1.01	**1.00**
T - 1.2 - 1	20.78	20.79	20.83	**20.80**	1.21	1.21	1.20	**1.21**
T - 1.2 - 2	21.04	20.96	20.97	**20.99**	1.20	1.20	1.21	**1.20**
T - 1.2 - 3	21.17	21.18	21.17	**21.17**	1.20	1.21	1.20	**1.20**
T - 1.2 - 4	20.76	20.77	20.78	**20.77**	1.21	1.21	1.21	**1.21**
T - 1.2 - 5	21.02	21.06	21.04	**21.04**	1.21	1.20	1.21	**1.21**
T - 1.5 - 1	20.69	20.70	20.72	**20.70**	1.52	1.50	1.51	**1.51**
T - 1.5 - 2	20.55	20.56	20.55	**20.55**	1.52	1.52	1.52	**1.52**
T - 1.5 - 3	20.75	20.75	20.75	**20.75**	1.50	1.51	1.53	**1.51**
T - 1.5 - 4	20.70	20.72	20.70	**20.71**	1.55	1.53	1.54	**1.54**
T - 1.5 - 5	20.77	20.77	20.77	**20.77**	1.54	1.54	1.55	**1.54**
T - 1.5 - 6	19.51	19.55	19.57	**19.54**	1.47	1.50	1.47	**1.48**
T - 2.0 - 1	20.31	20.33	20.35	**20.33**	1.97	1.97	1.97	**1.97**
T - 2.0 - 2	20.31	20.32	20.35	**20.33**	1.95	1.96	1.96	**1.96**
T - 2.0 - 3	20.30	20.36	20.37	**20.34**	1.97	1.97	1.96	**1.97**
T - 2.0 - 4	20.35	20.34	20.34	**20.34**	1.96	1.96	1.97	**1.96**
T - 2.0 - 5	20.32	20.32	20.35	**20.33**	1.95	1.96	1.96	**1.96**
T - 2.5 - 1	20.35	20.37	20.39	**20.37**	2.49	2.51	2.51	**2.50**
T - 2.5 - 2	20.43	20.44	20.46	**20.44**	2.49	2.50	2.50	**2.50**
T - 2.5 - 3	20.43	20.44	20.46	**20.44**	2.49	2.50	2.50	**2.50**
T - 2.5 - 4	20.40	20.44	20.44	**20.43**	2.51	2.50	2.51	**2.51**
T - 2.5 - 5	20.50	20.53	20.57	**20.53**	2.52	2.52	2.53	**2.52**

3.1.2. Stress-strain curve

The relationship between stress and strain for each combination of thickness are dispalyed below.

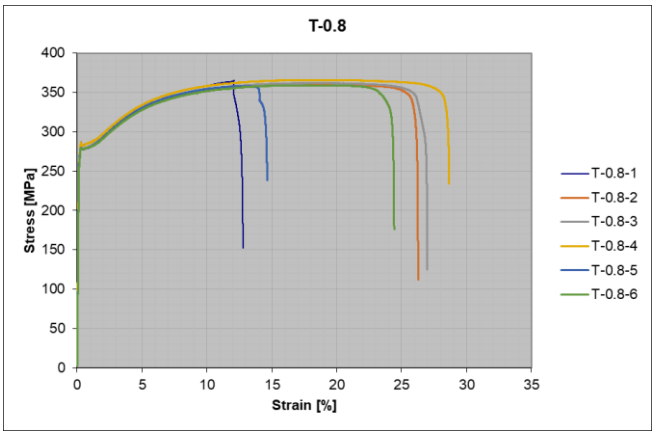

Figure 3.1: Stress-strain curve for series of T-0.8

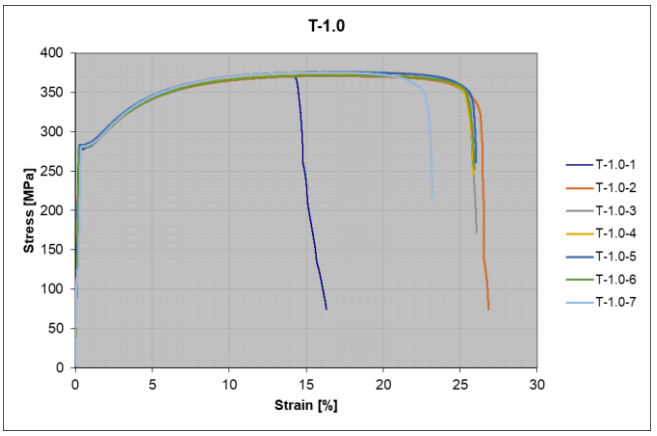

Figure 3.2: Stress-strain curve for series of T-1.0

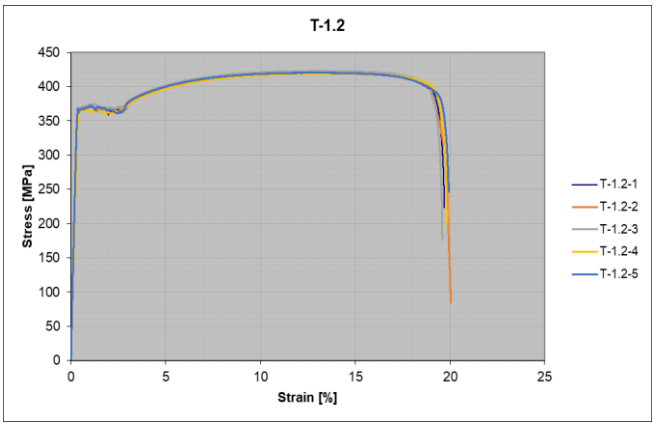

Figure 3.3: Stress-strain curve for series of T-1.2

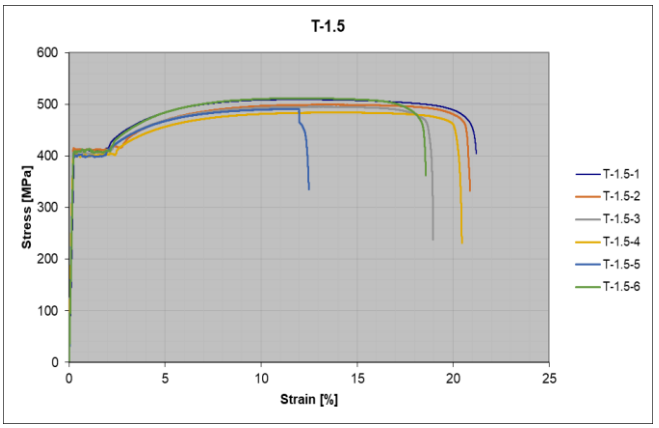

Figure 3.4: Stress-strain curve for series of T-1.5

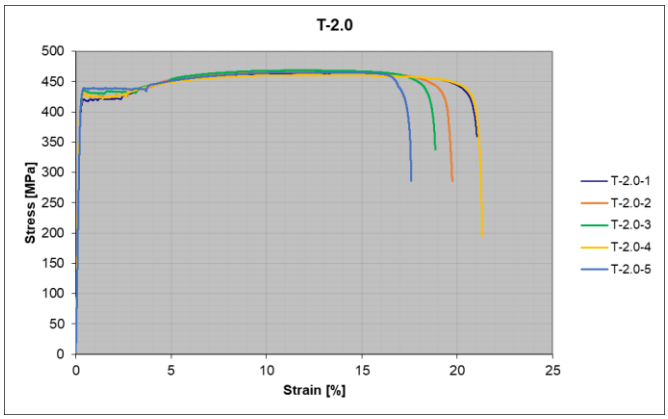

Figure 3.5: Stress-strain curve for series of T-2.0

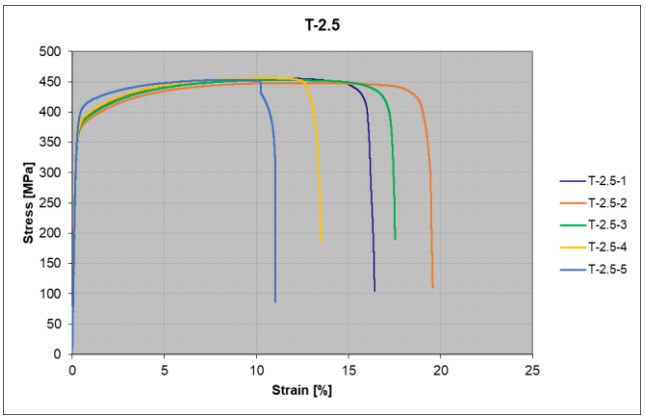

Figure 3.6: Stress-strain curve for series of T-2.5

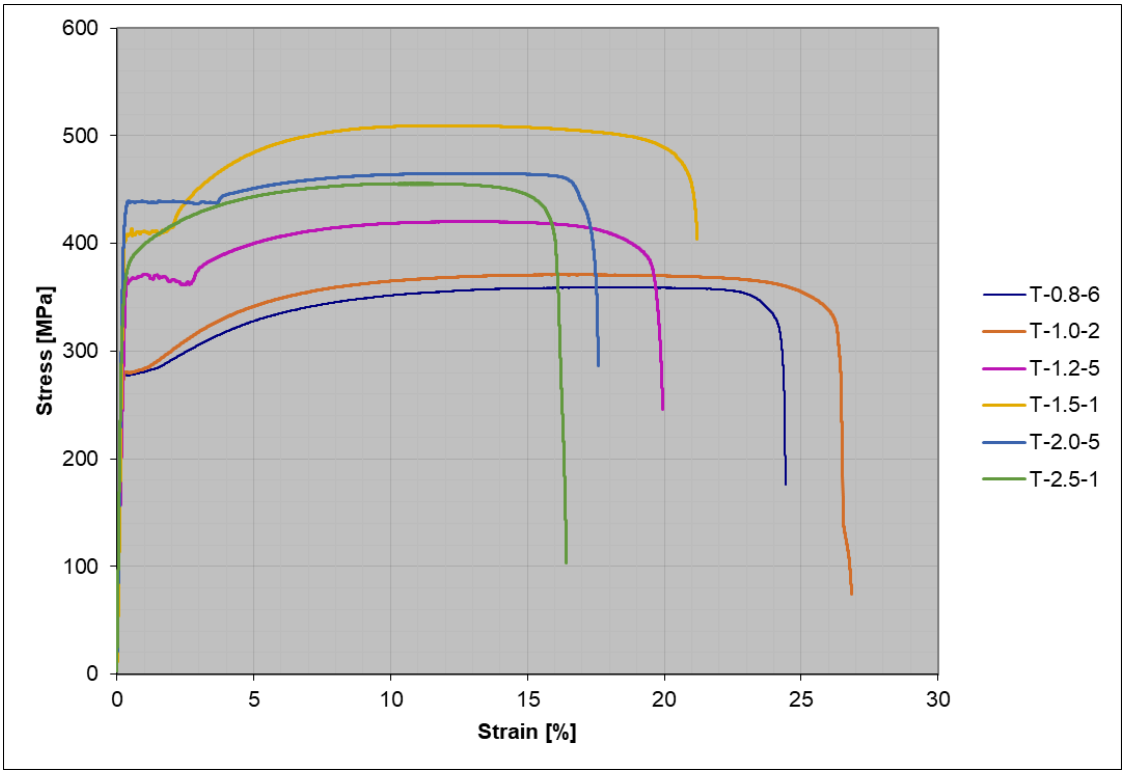

Figure 3.7: Comparison of stress-strain curves for six combinations of specimens

Figure 3.7 presents for stress-strain relationship of six typical ones among all specimens used for the test and the comparison between them. It can be seen from the graph that all combinations show very good ductility under tensile test. A series of T-1.5 witnessed the highest value of ultimate strength while the highest value of yield strength is recorded by the performance of T-2.0 series.

3.1.3. The material properties

Table 3.2 presents the average characteristics of material obtained after performing the test.

Table 3.2: The average material properties

Series	L_o	$R_{p0.2}$	R_{eH}	e_{ReH}	A_e	R_{eL}	R_m	A_g	A_{gt}	A	A_t
	mm	MPa	MPa	%	%	MPa	MPa	%	%	%	%
T-0.8	140	279.78	282.87	0.29	0.34	279.16	361.76	16.26	16.46	30.85	22.13
T-1.0	140	280.93	-	-	-	-	373.40	18.76	19.19	33.80	28.85
T-1.2	140	366.45	367.81	0.48	2.86	360.49	420.68	15.15	15.60	27.54	23.52
T-1.5	140	406.41	407.45	0.31	1.94	403.31	498.49	12.34	12.60	26.07	18.79
T-2.0	140	431.86	430.43	0.43	2.28	423.55	464.46	11.55	11.79	27.46	19.77
T-2.5	140	379.29	-	-	-	-	453.04	10.66	10.90	21.49	15.42

Where:

R_{eH}: Upper yield strength.

R_{eL}: Lower yield strength.

R_m: Tensile strength.

$R_{p0.2}$: Basic yield strength.

L_o: Length between gauge length marks on the piece measured at room temperature before the test. Gauge length: length of the parallel portion of the test piece on which elongation is measured at any moment during the test.

A_e: Percentage yield point extension.

A_g: Percentage plastic extension at maximum force.

A_{gt}: Percentage total extension at maximum force.

A: Percentage elongation after fracture.

A_t: Percentage total extension at fracture.

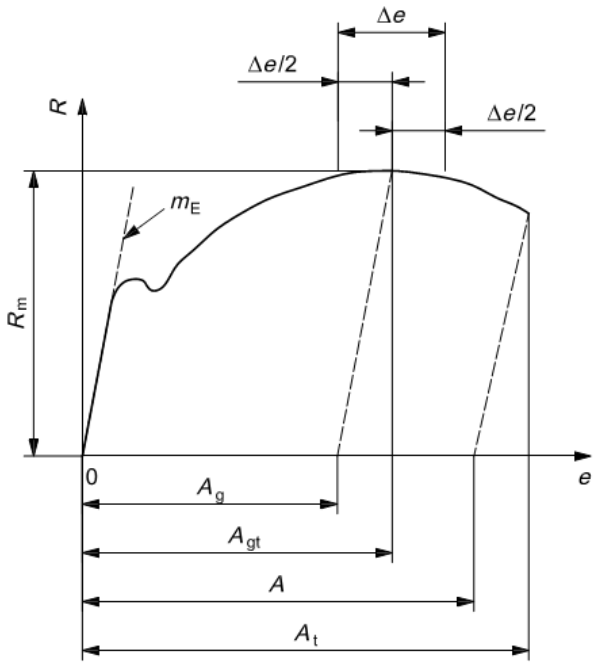

Figure 3.8: Definitions of extension

The experimental results are taken to compare with the nominal ones that are provided in the Table 3.1b, Chapter 3, EN 1993-1-3 for the type of steel: Continuous hot dip zinc coated carbon steel sheet of structural quality. The difference between nominal values and experimental values of basic yield strength f_{yb} and ultimate tensile strength f_u are calculated and shown as in the Table 3.3.

Table 3.3: Comparison between nominal values and experimental values of tensile test

Series	Steel grade	f_y (Mpa)			f_u (Mpa)		
		$f_{y,nom}$	$f_{y,exp}$	δ	$f_{u,nom}$	$f_{u,exp}$	δ
T-0.8	S280GD+Z	280	279.78	-0.08%	360	361.76	0.49%
T-1.0	S280GD+Z	280	280.93	0.33%	360	373.40	3.72%
T-1.2	S350GD+Z	350	366.45	4.70%	420	420.68	0.16%
T-1.5	S350GD+Z	350	406.41	16.12%	420	498.49	18.69%
T-2.0	S350GD+Z	350	431.86	23.39%	420	464.46	10.58%
T-2.5	S350GD+Z	350	379.29	8.37%	420	453.04	7.87%

3.1.4. Evaluation of test results

Test results should be appropriately adjusted to allow for variations between the actual measured properties of the test specimens and their nominal values.

- **For basic yield strength f_{yb}:**

The adjustment of basic yield strength was made according to Chapter A.6.2 and A.6.3 of EN1993-1-3 as following:

The adjusted value $R_{adj,i}$ of the test result for test i should be determined from the actual measured test result $R_{obs,i}$ using:

$$R_{adj,i} = R_{obs,i} / \mu_R \quad \text{(Eq 3.1)}$$

in which μ_R is the resistance adjustment coefficient given by:

$$\mu_R = \left(\frac{f_{yb,obs}}{f_{yb}}\right)^{\alpha} \left(\frac{t_{obs,cor}}{t_{cor}}\right)^{\beta} \quad \text{(Eq 3.2)}$$

The exponent α for use in expression (Eq 3.2) should be obtained as follows:

- if $f_{yb,obs} \leq f_{yb}$: $\alpha = 0$

- if $f_{yb,obs} > f_{yb}$: $\alpha = 1$

The exponent β for use in expression (Eq 3.2) should be obtained as follows:

- if $t_{obs,cor} \leq t_{cor}$: $\beta = 1$

- if $t_{obs,cor} > t_{cor}$: $\beta = 2$ (for tests on profiled sheets or liner trays)

The core thickness can be taken as t_{nom} - 0.04 in the unit of mm.

The characteristic value R_k determined on the basis of at least 4 tests may be obtained from:

$$R_k = R_m - k.s \quad \text{(Eq 3.3)}$$

where:

k is the appropriate coefficient from Table 3.4;

R_m is the mean value of the adjusted test results R_{adj};

s is the standard deviation;

$$s = \sqrt{\frac{\sum_{i=1}^{n}(x_i - \bar{x})^2}{n-1}} \qquad \text{(Eq 3.4)}$$

Table 3.4: Values of coefficient k

n	4	5	6	7	8	10	20	30	∞
k	2.63	2.33	2.18	2.09	2	1.92	1.76	1.73	1.64

n is the number of tests.

- **For ultimate strength f_u:**

The adjustment of ultimate strength was followed by European Recommendations (ECCS_124, 2008):

The European Recommendations (ECCS_124, 2008) use the same expression (Eq 3.3) as in EN1993-1-3 to evaluate the characteristic value of resistance, R_k:

$$R_k = R_m - k.s$$

in which:

k is the appropriate coefficient from Table 3.4 depending on the number of tests;

s is the standard deviation calculated by formula: $s = \sqrt{\frac{\sum_{i=1}^{n}(x_i - \bar{x})^2}{n-1}}$;

R_m is the mean value of the adjusted test results R_{adj} from a minimum of five tests;

$$R_{adj,i} = R_{obs,i} / \mu_R$$

The adjustment coefficient, μ_R, is given by:

$$\mu_R = \left(\frac{f_{u,obs}}{f_u}\right)^{\alpha} \left(\frac{t_{obs,cor}}{t_{cor}}\right) \qquad \text{(Eq 3.5)}$$

where:

$f_{u,obs}$ is the actual measured ultimate resistance;

f_u is nominal ultimate resistance;

$\alpha = 1$, if $f_{u,obs} > f_u$ and $\alpha = 0$, if $f_{u,obs} \leq f_u$;

The core thickness can be taken as t_{nom} - 0.04 in the unit of mm.

The tables showing the detailed calculations for each series of specimens are presented in Appendix B: Evaluation of tensile test results of this thesis.

Table 3.5 presents the final results of basic yield strength f_{yb} and ultimate strength f_u after adjustment. And it should be noticed that the adjusted value of ultimate strength here will be used to calculate the resistance for spot welds and CMT welds in the following chapters.

Table 3.5: Comparison between nominal values and adjusted values of tensile test

Series	Steel grade	f_y (Mpa)			f_u (Mpa)		
		$f_{y,nom}$	$f_{y,adj}$	δ	$f_{u,nom}$	$f_{u,adj}$	δ
T-0.8	S280GD+Z	280	266.65	-4.77%	360	350.98	-2.51%
T-1.0	S280GD+Z	280	269.18	-3.86%	360	353.58	-1.78%
T-1.2	S350GD+Z	350	342.56	-2.13%	420	414.03	-1.42%
T-1.5	S350GD+Z	350	324.45	-7.30%	420	404.44	-3.71%
T-2.0	S350GD+Z	350	354.22	1.21%	420	425.06	1.21%
T-2.5	S350GD+Z	350	341.57	-2.41%	420	414.78	-1.24%

3.2. Test for spot-welding specimens

3.2.1. Specimen preparation

The dimensions of the specimens (see Figure 3.9) were chosen in accordance with the specifications given in Chapter 8.4 of EN1993-1-3 [3]. According to Table 3.6 and EN1993-1-3 [3], all types of connections have been tested using a single welding spot. A total number of 140 specimens were produced to perform the test.

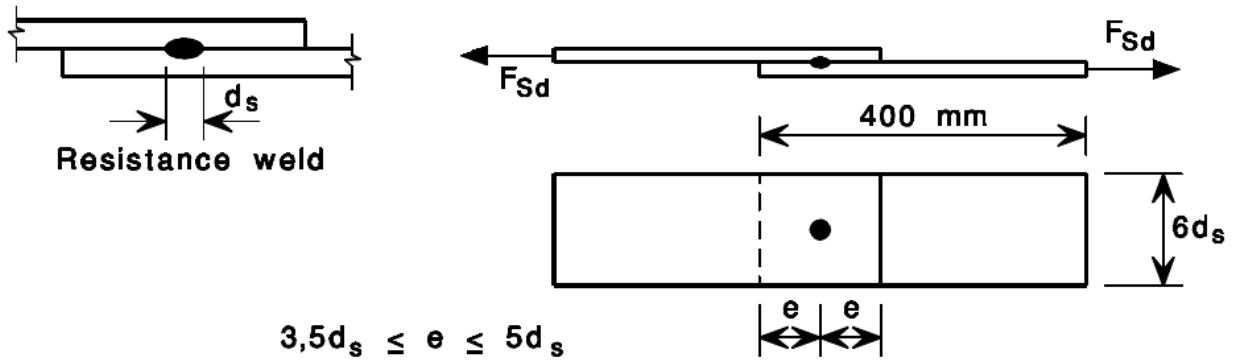

Figure 3.9: The dimensions of the specimens according to EN1993-1-3

The spot welding combinations between different sheet thicknesses, experimentally tested, are displayed in Table 3.6. The notations t_1 and t_2 represent the thicknesses of the steel sheets in the connection and d_s is the diameter of the spot-welding. A weld nugget diameter d_s are taken to be $5\sqrt{t_1}$ as recommended in EN1993-1-3 [3] for the type of resistance welding, where t_1 is the smallest thickness of the connected steel sheets.

Table 3.6: Types of spot welding connections

Name	t_1 [mm]	t_2 [mm]	No. of tests	d_s [mm]
SW-0.8-0.8	0.8	0.8	7	4.5
SW-0.8-1.0	0.8	1.0	7	4.5
SW-0.8-1.2	0.8	1.2	7	4.5
SW-0.8-1.5	0.8	1.5	7	4.5
SW-0.8-2.0	0.8	2.0	7	4.5
SW-0.8-2.5	0.8	2.5	7	4.5
SW-1.0-1.0	1.0	1.0	7	5.0
SW-1.0-1.2	1.0	1.2	7	5.0
SW-1.0-1.5	1.0	1.5	7	5.0
SW-1.0-2.0	1.0	2.0	7	5.0
SW-1.0-2.5	1.0	2.5	7	5.0
SW-1.2-1.2	1.2	1.2	7	5.5
SW-1.2-1.5	1.2	1.5	7	5.5
SW-1.2-2.0	1.2	2.0	7	5.5
SW-1.2-2.5	1.2	2.5	7	5.5
SW-1.5-1.5	1.5	1.5	7	6.1
SW-1.5-2.0	1.5	2.0	7	6.1
SW-1.5-2.5	1.5	2.5	7	6.1
SW-2.0-2.0	2.0	2.0	7	7.1
SW-2.0-2.5	2.0	2.5	7	7.1

3.2.2. Resistance spot welding parameters

Figure 3.10 presents the welding equipment used for obtaining the required spot welded specimens, so-called Inverspotter 14000 Smart Aqua from Telwin.

Figure 3.10: Welding equipment Inverspotter 14000 Smart Aqua

The UTS universal testing machine was used to performed the experimental tests. The distance between the extensometer's sensors was 80 mm.

Another important aspect of the investigation was the welding regime. The welding equipment has default factory settings for different thickness combinations, the so-called "SMART" settings, but there is also the possibility to use user-defined programs. Table 3.7 shows, for example, the parameters analyzed for a series of SW-1.2-1.5 specimens, where the following parameters were considered: welding intensity I_s (A), clamping force F (daN) between the electrodes, pressure (bar) and welding time, t_s (ms) for the electrode of 13 mm diameter and 32 mm radius of the tip.

Table 3.7: Welding regimes for the set of SW-1.2-1.5

	Name	I_s	Power	F	Pressure	t_s
		(A)	(%)	(daN)	(bar)	(ms)
REG 1	**SW-1.2-1.5-1**	10366	70	365	6	380
REG 2	**SW-1.2-1.5-2**	10336	70	365	-	380
REG 3	**SW-1.2-1.5-3**	11088	75	483	6.8	600
REG 4	**SW-1.2-1.5-4**	11088	75	472	6.6	600
REG 5	**SW-1.2-1.5-5**	11055	-	457	6.4	600
REG 6	**SW-1.2-1.5-6**	11775	80	449	6.2	600

The most effective and common parameter that influences welding result of a given material configuration is the welding current. A too low current will not provide adequate heat to create a nugget while the expulsion will be consequence if a too high current is applied and even temperatures above the boiling point. The welding time is of importance when calculating heat generation and resulting weld formation. As being indicated in [33], the weld current and weld time are inversly proportional to each other. Thus, a shorter weld time is desirable and is more likely to be compensated by higher weld current to give sustainable spot welds.

Another variable which will affect the outcome of the weld is the magnitude of compressive force produced by two electrodes. If the force is too big, it will cause damage to the work piece or excessive deformations. Wheares, a too low force will increase the risk of geometrical instability of the welding process.

The amount of pressure that is applied to the weld is also important. If too little pressure is applied, the joining area will be small and weak. If too much pressure is applied, then cracking can occur in the weld because of the quenching effect of the welding tips. Also, high pressure can cause thinning of the metal and cause a weakness [33].

Figure 3.11 shows the set of six SW-1.2-1.5 specimens with the parameters shown in Table 3.7, before, after and during testing.

Figure 3.11: Specimens SW-1.2-1.5 before and after testing, using different welding regimes

3.2.3. Force-displacement curve

Figure 3.12 describes the force-displacement curves for the set of the specimens SW-1.2-1.5 and takes the comparison between them. It can be seen that the specimens shown in Figure 3.12 have very good capacity and ductility, the maximum recorded force exceeding 12 kN.

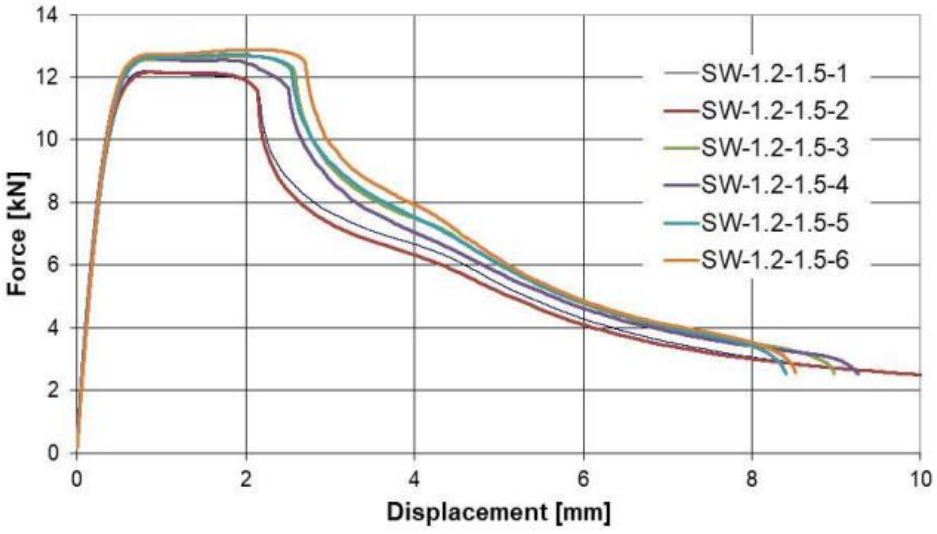

Figure 3.12: Force-displacement curves for SW-1.2-1.5 specimens (one spot weld)

Based on the results of the experimental test performed on all the specimens presented in Table 3.6, the following general conclusion can be drawn that both the capacity and the ductility obtained for the tested specimens are very good.

3.2.4. Failure modes

It is observed through the tensile test that spot welds can fail in two completely distinct modes, namely full button pullout (nugget pullout) and interfacial fracture.

Two types of failure modes are shown as below in Figure 3.13 and Figure 3.14, respectively.

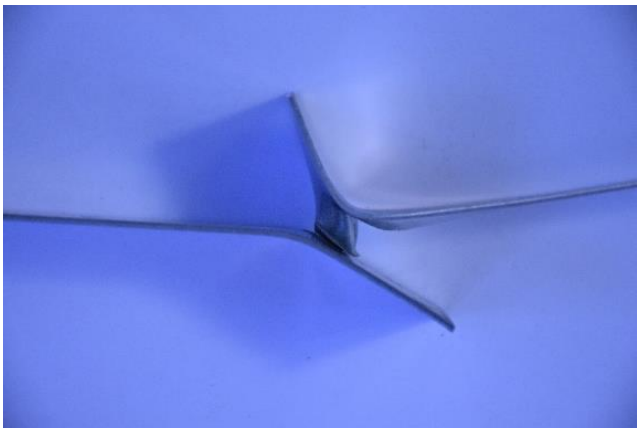

Figure 3.13: Full button pullout (Nugget pullout)

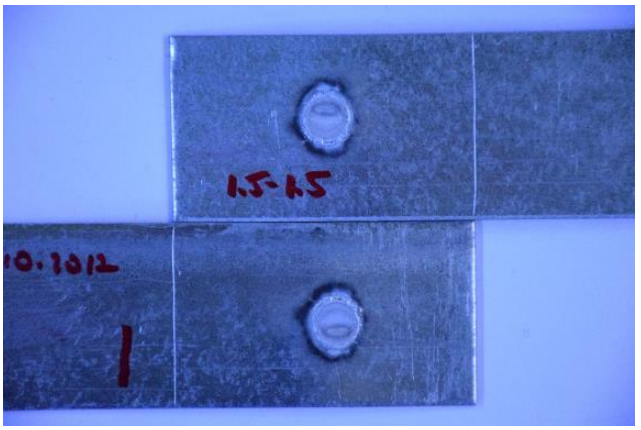

Figure 3.14: Interfacial fracture

In the full button pullout (see figure 3.13), fracture occurs in the base metal or in the weld heat affected zone at the perimeter of the weld. In this failure mode, the weld nugget is completely torn from one of the sheets with the weld remaining intact. This is the most common failure mode for specimens within this study.

Another type of failure mode is the interfacial fracture (see figure 3.14), in which the weld fails at the interface of the two sheets, leaving half of the weld nugget in one sheet and half in the other.

A conclusion can be drawn that in the case of full button pullout, the strain in the base material outside the weld nugget is greater than that developed at the weld interface and the opposite is true for the case of the weld interfacial failure. In addition from the experimental results, it is noticed that the load-bearing capacity of the weld is not affected by the fracture mode. In the case of the set SW-1.5-2.0 (see Figure 3.15), almost specimens encountered in the situation of nugget pullout for the failure mode except for SW-1.5-2.0-2 in the case of interfacial fracture. However, it can be obviously seen from the graph that the maxumim force recorded for that specimen is over 20 kN that is approximately the same with the rest of specimens. This was previously agreed by J. Radakovic et al. [34].

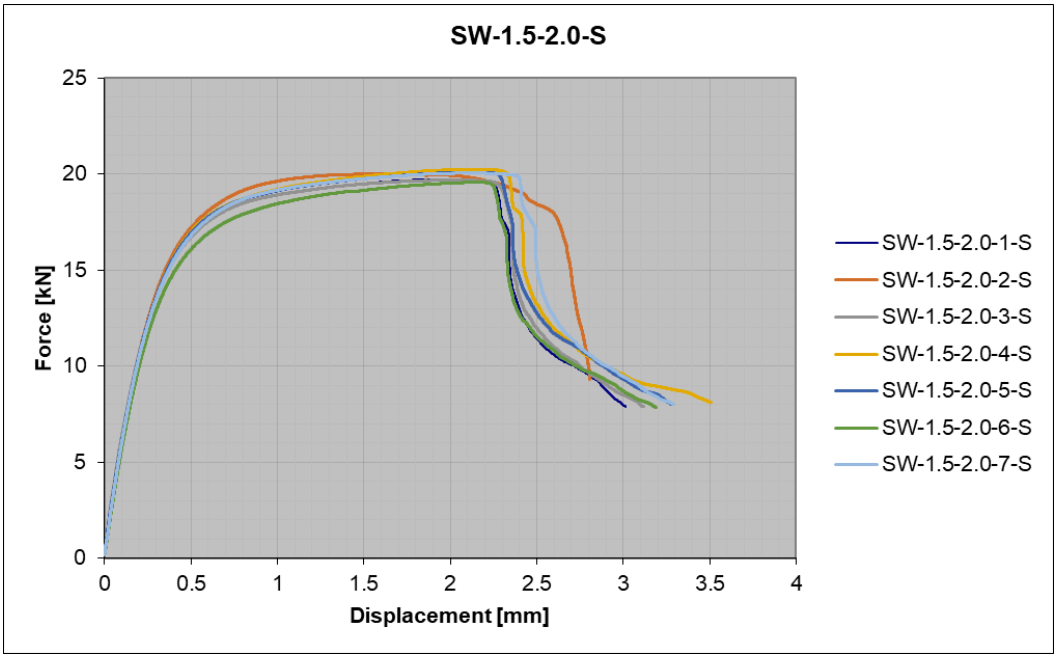

Figure 3.15: Force-displacement curve for SW-1.5-2.0 specimens

All detailed information regarding the measured dimensions, the load-displacement curves, the types of failure modes, the pictures that shows status of specimens before and after the test for all sets of spot-welding specimens are summarized and provided in Appendix C of this thesis.

3.2.5. Determination of elastic range

The methodology used to determine the elastic range within load-displacement curve is so-called linear correlation. The Pearson correlation coefficient is used to measure the strength of a linear association between variables, where the value r = 1 means a perfect correlation.

$$r_{xy} = \frac{n\sum x_i y_i - \sum x_i \sum y_i}{\sqrt{n\sum x_i^2 - (\sum x_i)^2}\sqrt{n\sum y_i^2 - (\sum y_i)^2}}$$

Where:

n is the number of observations;

x is variable represented for displacement;

y is variable represented for force.

The results obtained for all combinations of specimens are shown in the following page (see from Figure 3.16 to Figure 3.20). The values of Pearson correlation coefficient are obtained approximately 0.99 for all sets. In fact, the elastic range is theoretically perfectly linear. However, in the graphs, the scale of horizontal axis is modified in order to easily see the curves separately.

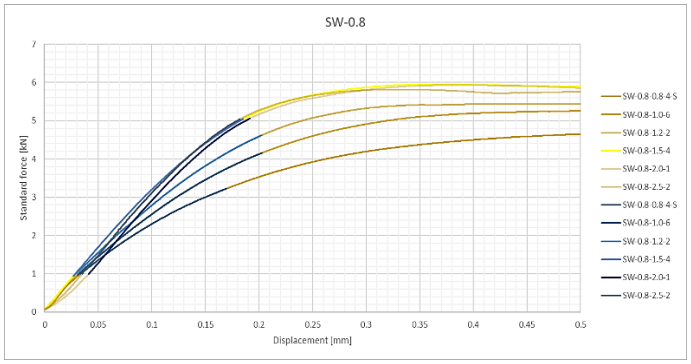

Figure 3.16: Elastic range for the set of SW-0.8

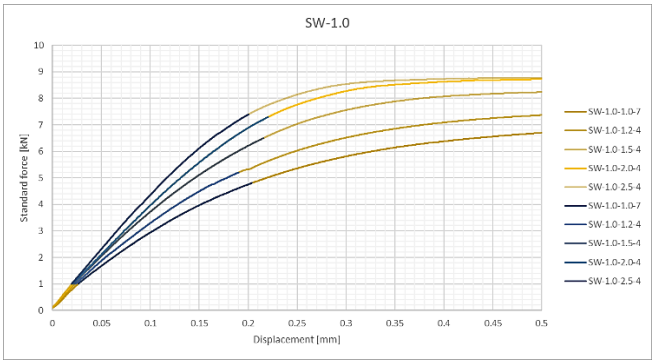

Figure 3.17: Elastic range for the set of SW-1.0

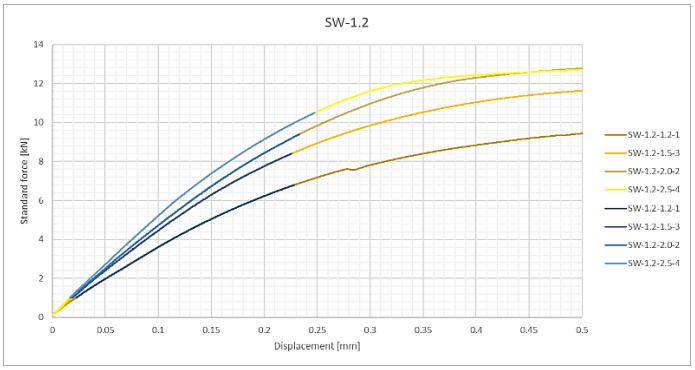

Figure 3.18: Elastic range for the set of SW-1.2

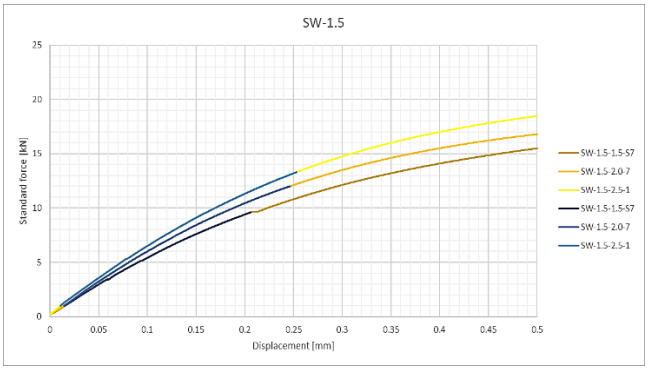

Figure 3.19: Elastic range for the set of SW-1.5

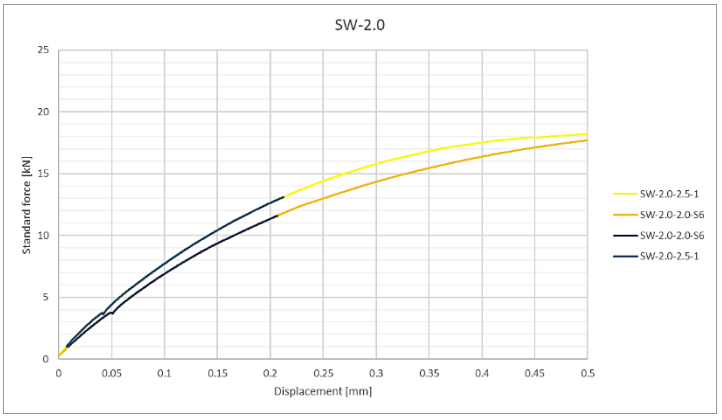

Figure 3.20: Elastic range for the set of SW-2.0

The blue curves represent the elastic range within load-displacement curves which are displayed by the yellow ones. It is noticed that the maximum forces recorded in the elastic ranges are taken to be considered as the experimental resistances for spot welds corresponding to each set of specimens in the next chapter.

3.2.6. Calculation of resistance for spot welds

The resistance of a spot weld loaded in shear should be determined using Table 8.5, Chapter 8.4, EN1993-1-3 [3].

Spot welds loaded in shear:
Tearing and bearing resistance: - if $t \le t_1 \le 2.5t$ $F_{tb,Rd} = 2.7 \cdot \sqrt{t} \cdot d_s \cdot f_u / \gamma_{M2}$ [with t in mm] - if $t_1 \ge 2.5t$ $F_{tb,Rd} = 2.7 \cdot \sqrt{t} \cdot d_s \cdot f_u / \gamma_{M2}$, but $F_{tb,Rd} \le 0.7 \cdot d_s^2 \cdot f_u / \gamma_{M2}$ and $F_{tb,Rd} \le 3.1 \cdot t \cdot d_s \cdot f_u / \gamma_{M2}$ End resistance: $F_{e,Rd} = 1.4 \cdot t \cdot e_1 \cdot f_u / \gamma_{M2}$ Net section resistance: $F_{n,Rd} = A_{net} \cdot f_u / \gamma_{M2}$ Shear resistance: $F_{v,Rd} = \frac{\pi}{4} \cdot d_s^2 \cdot f_u / \gamma_{M2}$
Conditions: $F_{v,Rd} \ge 1.25 \cdot F_{tb,Rd}$ or $F_{v,Rd} \ge 1.25 \cdot F_{e,Rd}$ or $\sum F_{v,Rd} \ge 1.25 \cdot F_{n,Rd}$

Where:

A_{net} is the net cross-sectional area of the connected part;

t is the thickness of the thinner connected part or sheet;

t_1 is the thickness of the thicker connected part or sheet;

e_1 is the distance from the edge of overlapping area to the center of spot weld;

f_u is ultimate strength of material obtained in Table 3.5 of this thesis;

The partial factor γ_{M2} is recommended to be 1.25 for calculating the design resistances of spot welds.

In the framework of this study, the comparison between the theoretical and experimental results is carried out (see Table 3.9), therefore, the value of γ_{M2} should be taken as 1.0. From Table 3.8, it can be seen that the design of a spot weld for all combinations is governed by the tearing and bearing resistance.

Table 3.8: Summary of results for spot welding specimens

Name	Nominal values									Measured values									Experimental test	
	min(t) (mm)	**d_s (mm)**	**b = 6d_s (mm)**	**e (mm)**	**f_u (MPa)**	**$F_{tb,Rk}$ (kN)**	**$F_{e,Rk}$ (kN)**	**$F_{n,Rk}$ (kN)**	**$F_{V,Rk}$ (kN)**	**min(t) (mm)**	**d_s (mm)**	**b (mm)**	**e (mm)**	**f_u (MPa)**	**$F_{tb,Rk}$ (kN)**	**$F_{e,Rk}$ (kN)**	**$F_{n,Rk}$ (kN)**	**$F_{V,Rk}$ (kN)**	**F_{exp} (kN)**	**Failure mode**
SW-0.8-0.8-4S	0.80	4.47	27	20.00	360.00	**3.89**	8.06	7.73	5.65	0.80	5.10	27.02	19.92	350.98	**4.35**	7.93	7.59	7.17	**3.23**	Nugget pullout
SW-0.8-1.0-6S	0.80	4.47	27	20.00	360.00	**3.89**	8.06	7.73	5.65	0.81	5.10	27.30	20.60	350.98	**4.35**	8.20	7.76	7.17	**4.16**	Nugget pullout
SW-0.8-1.2-2S	0.80	4.47	27	20.00	360.00	**3.89**	8.06	7.73	5.65	0.80	5.30	27.76	20.64	350.98	**4.49**	8.11	7.79	7.74	**4.62**	Nugget pullout
SW-0.8-1.5-4S	0.80	4.47	27	20.00	360.00	**3.89**	8.06	7.73	5.65	0.80	5.50	27.47	20.45	350.98	**4.66**	8.04	7.71	8.34	**5.04**	Nugget pullout
SW-0.8-2.0-1S	0.80	4.47	27	20.00	360.00	**3.89**	8.06	7.73	5.65	0.80	5.50	27.74	21.41	350.98	**4.66**	8.42	7.79	8.34	**5.05**	Nugget pullout
SW-0.8-2.5-2S	0.80	4.47	27	20.00	360.00	**3.89**	8.06	7.73	5.65	0.79	6.00	27.57	21.38	350.98	**5.05**	8.30	7.64	9.92	**5.04**	Nugget pullout
SW-1.0-1.0-7S	1.00	5.00	30	25.00	360.00	**4.86**	12.60	10.80	7.07	0.99	5.40	30.48	25.15	353.58	**5.16**	12.45	10.67	8.10	**4.80**	Nugget pullout
SW-1.0-1.2-4S	1.00	5.00	30	25.00	360.00	**4.86**	12.60	10.80	7.07	1.00	5.40	30.48	27.54	353.58	**5.16**	13.63	10.78	8.10	**5.20**	Nugget pullout
SW-1.0-1.5-4S	1.00	5.00	30	25.00	360.00	**4.86**	12.60	10.80	7.07	1.01	5.50	30.69	25.42	353.58	**5.28**	12.71	10.96	8.40	**6.50**	Nugget pullout
SW-1.0-2.0-4S	1.00	5.00	30	25.00	360.00	**4.86**	12.60	10.80	7.07	1.01	6.00	30.85	26.31	353.58	**5.76**	13.15	11.02	10.00	**7.30**	Nugget pullout
SW-1.0-2.5-4S	1.00	5.00	30	25.00	360.00	**4.86**	12.60	10.80	7.07	1.01	6.20	30.60	27.73	353.58	**5.95**	13.86	10.93	10.67	**7.40**	Nugget pullout
SW-1.2-1.2-1S	1.20	5.48	33	25.00	420.00	**6.80**	17.64	16.56	9.90	1.19	5.60	33.13	24.70	414.03	**6.83**	17.04	16.32	10.20	**6.80**	Nugget pullout
SW-1.2-1.5-3S	1.20	5.48	33	25.00	420.00	**6.80**	17.64	16.56	9.90	1.21	5.80	33.07	26.00	414.03	**7.13**	18.24	16.57	10.94	**8.40**	Nugget pullout
SW-1.2-2.0-2S	1.20	5.48	33	25.00	420.00	**6.80**	17.64	16.56	9.90	1.21	6.00	33.46	27.55	414.03	**7.38**	19.32	16.76	11.71	**9.40**	Nugget pullout
SW-1.2-2.5-4S	1.20	5.48	33	25.00	420.00	**6.80**	17.64	16.56	9.90	1.20	6.40	33.33	27.23	414.03	**7.84**	18.94	16.56	13.32	**10.50**	Nugget pullout
SW-1.5-1.5-4S	1.50	6.12	37	30.00	420.00	**8.51**	26.46	23.15	12.37	1.53	6.50	37.24	29.75	404.44	**8.78**	25.77	23.04	13.42	**9.60**	Interfacial fracture
SW-1.5-2.0-7S	1.50	6.12	37	30.00	420.00	**8.51**	26.46	23.15	12.37	1.54	7.00	37.32	31.00	404.44	**9.49**	27.03	23.24	15.56	**12.00**	Nugget pullout
SW-1.5-2.5-1S	1.50	6.12	37	30.00	420.00	**8.51**	26.46	23.15	12.37	1.52	7.50	37.48	31.57	404.44	**10.10**	27.17	23.04	17.87	**13.30**	Nugget pullout
SW-2.0-2.0-3S	2.00	7.07	42	35.00	420.00	**11.34**	41.16	35.64	16.49	1.99	7.50	42.15	36.28	425.06	**12.17**	43.18	35.65	18.78	**11.60**	Interfacial fracture
SW-2.0-2.5-1S	2.00	7.07	42	35.00	420.00	**11.34**	41.16	35.64	16.49	1.97	7.80	42.61	35.99	425.06	**12.56**	42.19	35.68	20.31	**13.10**	Interfacial fracture

NOTE: F_{exp} is maximum force in the elastic range determined by method of linear correlation.

Table 3.9: Comparison between theoretical and experimental results for SW

Specimens	$F_{tb,Rk,nom}$ (kN)	δ_{nom}	$F_{tb,Rk,measured}$ (kN)	$\delta_{measured}$	F_{exp} (kN)
SW-0.8-0.8-4S	3.89	16.99%	4.35	25.81%	3.23
SW-0.8-1.0-6S	3.89	-6.96%	4.35	4.39%	4.16
SW-0.8-1.2-2S	3.89	-18.78%	4.49	-2.80%	4.62
SW-0.8-1.5-4S	3.89	-29.72%	4.66	-8.18%	5.04
SW-0.8-2.0-1S	3.89	-29.98%	4.66	-8.40%	5.05
SW-0.8-2.5-2S	3.89	-29.58%	5.05	0.31%	5.04
SW-1.0-1.0-7S	4.86	1.19%	5.16	6.84%	4.80
SW-1.0-1.2-4S	4.86	-7.03%	5.16	-0.90%	5.20
SW-1.0-1.5-4S	4.86	-33.76%	5.28	-23.20%	6.50
SW-1.0-2.0-4S	4.86	-50.22%	5.76	-26.83%	7.30
SW-1.0-2.5-4S	4.86	-52.28%	5.95	-24.42%	7.40
SW-1.2-1.2-1S	6.80	0.04%	6.83	0.40%	6.80
SW-1.2-1.5-3S	6.80	-23.47%	7.13	-17.79%	8.40
SW-1.2-2.0-2S	6.80	-38.16%	7.38	-27.41%	9.40
SW-1.2-2.5-4S	6.80	-54.36%	7.84	-34.01%	10.50
SW-1.5-1.5-4S	8.51	-12.88%	8.78	-9.35%	9.60
SW-1.5-2.0-7S	8.51	-41.10%	9.49	-26.51%	12.00
SW-1.5-2.5-1S	8.51	-56.38%	10.10	-31.72%	13.30
SW-2.0-2.0-3S	11.34	-2.32%	12.17	4.68%	11.60
SW-2.0-2.5-1S	11.34	-15.54%	12.56	-4.28%	13.10

3.3. Test for CMT welding specimens

3.3.1. Specimen preparation

The configuration of the specimens connected by CMT (Cold metal transfer) welding is shown in Figure 3.21. All types of connections have been tested using CMT welds. A total number of 140 specimens were manufactured to perform the test.

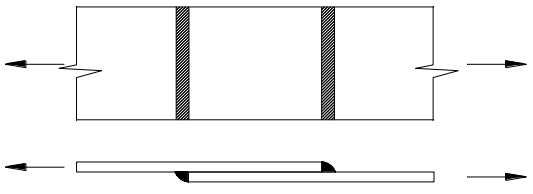

Figure 3.21: Configurarion of CMT welding specimens

The CMT welding combinations between different sheet thicknesses, experimentally tested, are displayed in Table 3.10. The notations t_1 and t_2 represent the thicknesses of the steel sheets in the connection.

Table 3.10: Types of CMT welding connections

Name	t_1 [mm]	t_2 [mm]	No. of tests	Name	t_1 [mm]	t_2 [mm]	No. of tests
CMT-0.8-0.8	0.8	0.8	7	**CMT-1.2-1.2**	1.2	1.2	7
CMT-0.8-1.0	0.8	1.0	7	**CMT-1.2-1.5**	1.2	1.5	7
CMT-0.8-1.2	0.8	1.2	7	**CMT-1.2-2.0**	1.2	2.0	7
CMT-0.8-1.5	0.8	1.5	7	**CMT-1.2-2.5**	1.2	2.5	7
CMT-0.8-2.0	0.8	2.0	7	**CMT-1.5-1.5**	1.5	1.5	7
CMT-0.8-2.5	0.8	2.5	7	**CMT-1.5-2.0**	1.5	2.0	7
CMT-1.0-1.0	1.0	1.0	7	**CMT-1.5-2.5**	1.5	2.5	7
CMT-1.0-1.2	1.0	1.2	7	**CMT-2.0-2.0**	2.0	2.0	7
CMT-1.0-1.5	1.0	1.5	7	**CMT-2.0-2.5**	2.0	2.5	7
CMT-1.0-2.0	1.0	2.0	7				
CMT-1.0-2.5	1.0	2.5	7				

3.3.2. Force-displacement curve

Figure 3.22 and Figure 3.23 depict the force-displacement curves for the set of CMT-1.0-1.2 specimens and the set of SW-1.0-1.2 specimens and takes the comparison between them.

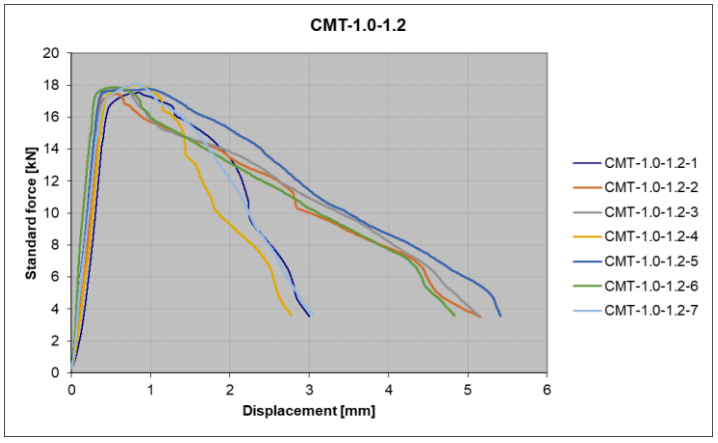

Figure 3.22: Force-displacement curves for CMT-1.0-1.2 set

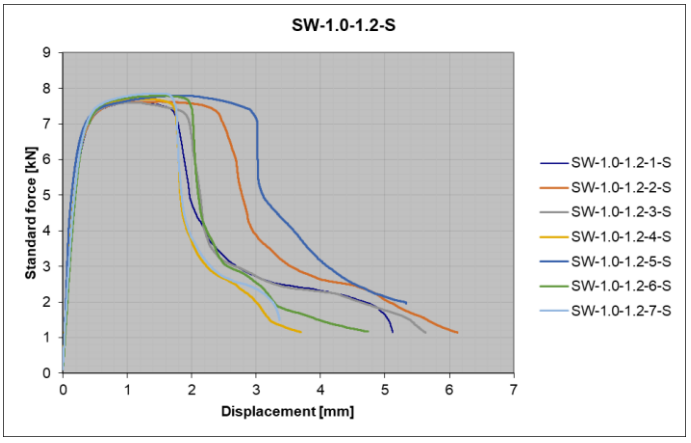

Figure 3.23: Force-displacement curves for SW-1.0-1.2 set

It can be seen that the specimens connected by CMT welding shown in Figure 3.22 have very good capacity, the maximum recorded force approximately 18 kN compared to nearly 8 kN for spot welding specimens with the same thicknesses. However, the ductility of the set of specimens connected by spot welds is higher than that in the CMT welding specimens.

3.3.3. Failure modes

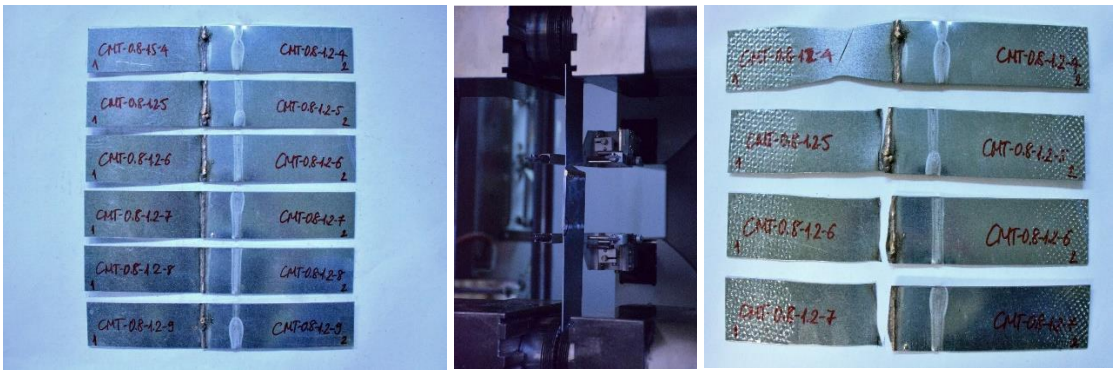

Figure 3.24: Specimens CMT-0.8-1.5 before, during and after testing

Figure 3.24 displays the status of specimens before the test, during the test and after the test. One thing should be noticed that the distance between the extensometer's sensors was 80 mm.

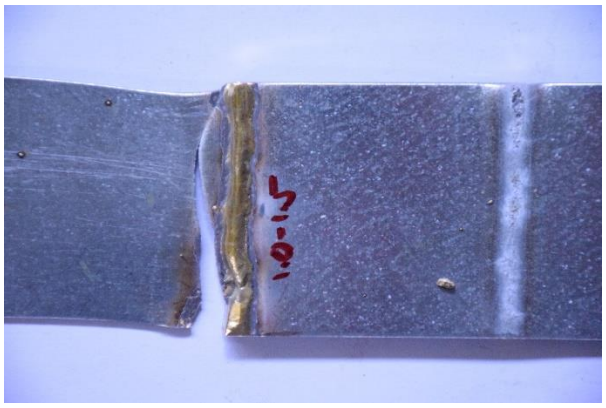

Figure 3.25: Nearly weld fracture

Figure 3.26: Breaking out of heat affected zone

There are two types of failure modes for specimens connected by CMT welding. The first type is that the fracture occurs near the welded position (see Figure 3.25) and the most specimens encountered this situation. Another type of failure mode is breaking out of heat affected zone displayed in Figure 3.26 and there are only a few specimens facing this situation.

All detailed information regarding the measured dimensions, the load-displacement curves, the types of failure modes, the pictures that shows status of specimens before and after the test for all sets of CMT welding specimens are summarized and provided in Appendix D of this thesis.

3.3.4. Determination of elastic range

The methodology used to determine the elastic range within load-displacement curve is so-called linear correlation presented in chapter 3.2.5 of this study. The results obtained for all combinations

of CMT welding specimens are shown as following (see from Figure 3.27 to Figure 3.31). The values of Pearson correlation coefficient are obtained approximately 0.99 for all sets.

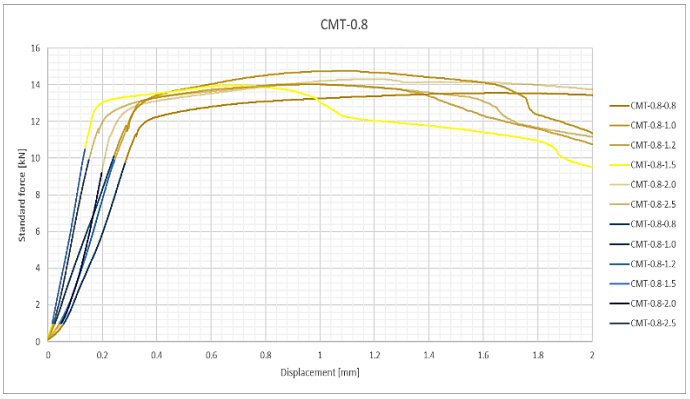

Figure 3.27: Elastic range for the set of CMT-0.8

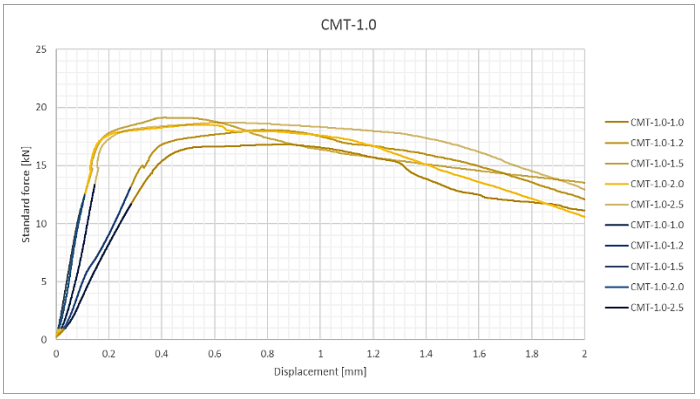

Figure 3.28: Elastic range for the set of CMT-1.0

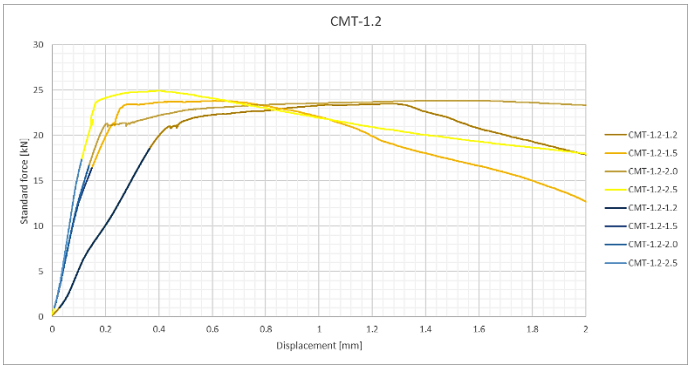

Figure 3.29: Elastic range for the set of CMT-1.2

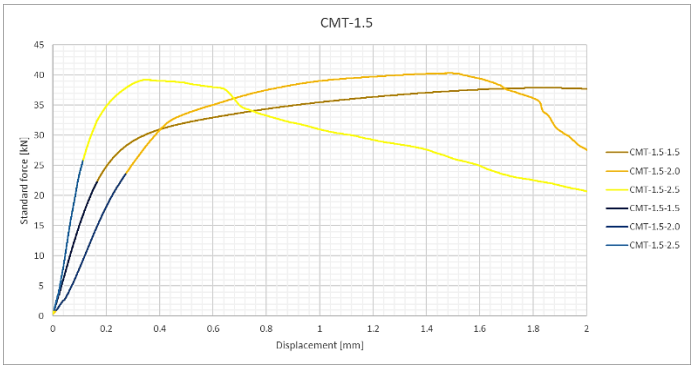

Figure 3.30: Elastic range for the set of CMT-1.5

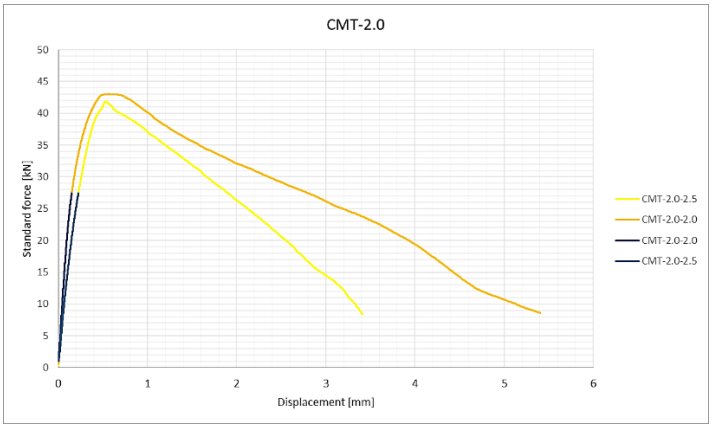

Figure 3.31: Elastic range for the set of CMT-2.0

The blue curves represent the elastic range within load-displacement curves which are displayed by the yellow ones. It is noticed that the maximum forces recorded in the elastic ranges are taken to be considered as the experimental resistances for CMT welds corresponding to each set of specimens in the next chapter.

3.3.5. Calculation of resistance for CMT welds

The design resistance $F_{w,Rd}$ of a CMT welded connection shall be determined from the following in accordance with formula 8.4c in Chapter 8.5.2, EN1993-1-3 [3].

For end fillet:

$$F_{w,Rd} = t \cdot L_{w,e} \cdot (1 - 0.3 \cdot L_{w,e} / b) \cdot f_u / \gamma_{M_2} \text{ [for one weld and if } L_{w,s} \le b \text{]}$$

Where: b is the width of the connected part or sheet;

$L_{w,e}$ is the effective length of the end fillet weld;

$L_{w,s}$ is the effective length of a side fillet weld;

f_u is ultimate strength of material obtained in Table 3.5 of this thesis;

The partial factor γ_{M2} is recommended to be 1.25 for calculating the design resistances of CMT welds.

In the framework of this study, the comparison between the theoretical and experimental results is implemented (see Table 3.11), therefore, the value of γ_{M2} should be taken as 1.0. The summary of the results for CMT welding specimens are presented in Table 3.12.

Table 3.11: Comparison between theoretical and experimental results for CMT

Specimens	$F_{w,Rk,nom}$ (kN)	δ_{nom}	$F_{w,Rk,measured}$ (kN)	$\delta_{measured}$	F_{exp} (kN)
CMT-0.8-0.8-4	10.08	3.70%	9.66	-0.50%	9.71
CMT-0.8-1.0-4	10.08	-0.21%	9.66	-4.59%	10.10
CMT-0.8-1.2-6	10.08	1.88%	9.72	-1.72%	9.89
CMT-0.8-1.5-6	10.08	-4.21%	9.84	-6.73%	10.50
CMT-0.8-2.0-5	10.08	8.69%	9.88	6.89%	9.20
CMT-0.8-2.5-5	10.08	1.79%	9.98	0.77%	9.90
CMT-1.0-1.0-3	12.60	7.11%	12.35	5.23%	11.70
CMT-1.0-1.2-7	12.60	-4.00%	12.27	-6.76%	13.10
CMT-1.0-1.5-7	12.60	2.35%	12.24	-0.55%	12.30
CMT-1.0-2.0-6	12.60	1.01%	12.28	-1.53%	12.47
CMT-1.0-2.5-6	12.60	-5.88%	12.39	-7.67%	13.34
CMT-1.2-1.2-4	17.64	-5.13%	17.02	-8.96%	18.55
CMT-1.2-1.5-6	17.64	6.77%	17.25	4.64%	16.45
CMT-1.2-2.0-7	17.64	5.69%	17.33	4.01%	16.64
CMT-1.2-2.5-6	17.64	1.74%	17.40	0.38%	17.33
CMT-1.5-1.5-7	22.05	-0.88%	21.06	-5.61%	22.25
CMT-1.5-2.0-4	22.05	-7.04%	20.99	-12.44%	23.60
CMT-1.5-2.5-6	22.05	-16.90%	21.04	-22.50%	25.78
CMT-2.0-2.0-6	29.40	6.77%	29.67	7.62%	27.41
CMT-2.0-2.5-4	29.40	6.80%	28.72	4.61%	27.40

Table 3.12: Summary of results for CMT welding specimens

Name	Nominal values							Measured values							Experimental test	
	t_1 (mm)	t_2 (mm)	min(t) (mm)	b (mm)	$L_{w,e}$ (mm)	f_u (MPa)	$F_{w,Rk}$ (kN)	t_1 (mm)	t_2 (mm)	min(t) (mm)	b (mm)	$L_{w,e}$ (mm)	f_u (MPa)	$F_{w,Rk}$ (kN)	F_{exp} (kN)	Failure mode
CMT-0.8-0.8-4	0.80	0.80	0.8	50	50	360	10.08	0.79	0.79	0.79	49.76	49.76	350.98	9.66	9.71	Nearly weld fracture
CMT-0.8-1.0-4	0.80	1.00	0.8	50	50	360	10.08	0.79	1.00	0.79	49.76	49.76	350.98	9.66	10.10	Nearly weld fracture
CMT-0.8-1.2-6	0.80	1.20	0.8	50	50	360	10.08	0.80	1.21	0.80	49.78	49.78	350.98	9.72	9.89	Nearly weld fracture
CMT-0.8-1.5-6	0.80	1.50	0.8	50	50	360	10.08	0.81	1.51	0.81	49.77	49.77	350.98	9.84	10.50	Nearly weld fracture
CMT-0.8-2.0-5	0.80	2.00	0.8	50	50	360	10.08	0.81	2.00	0.81	49.67	49.67	350.98	9.88	9.20	Nearly weld fracture
CMT-0.8-2.5-5	0.80	2.50	0.8	50	50	360	10.08	0.82	2.50	0.82	49.82	49.82	350.98	9.98	9.90	Nearly weld fracture
CMT-1.0-1.0-3	1.00	1.00	1.0	50	50	360	12.60	1.02	1.05	1.02	49.16	49.16	353.58	12.35	11.70	Nearly weld fracture
CMT-1.0-1.2-7	1.00	1.20	1.0	50	50	360	12.60	1.00	1.21	1.00	49.84	49.84	353.58	12.27	13.10	Nearly weld fracture
CMT-1.0-1.5-7	1.00	1.50	1.0	50	50	360	12.60	0.99	1.51	0.99	49.94	49.94	353.58	12.24	12.30	Nearly weld fracture
CMT-1.0-2.0-6	1.00	2.00	1.0	50	50	360	12.60	1.00	2.00	1.00	49.64	49.64	353.58	12.28	12.47	Nearly weld fracture
CMT-1.0-2.5-6	1.00	2.50	1.0	50	50	360	12.60	1.00	2.48	1.00	50.06	50.06	353.58	12.39	13.34	Nearly weld fracture
CMT-1.2-1.2-4	1.20	1.20	1.2	50	50	420	17.64	1.20	1.19	1.19	49.56	49.56	414.03	17.02	18.55	Nearly weld fracture
CMT-1.2-1.5-6	1.20	1.50	1.2	50	50	420	17.64	1.20	1.50	1.20	49.59	49.59	414.03	17.25	16.45	Nearly weld fracture
CMT-1.2-2.0-7	1.20	2.00	1.2	50	50	420	17.64	1.20	1.98	1.20	49.84	49.84	414.03	17.33	16.64	Nearly weld fracture
CMT-1.2-2.5-6	1.20	2.50	1.2	50	50	420	17.64	1.21	2.48	1.21	49.82	49.82	414.03	17.40	17.33	Nearly weld fracture
CMT-1.5-1.5-7	1.50	1.50	1.5	50	50	420	22.05	1.50	1.51	1.50	49.77	49.77	404.44	21.06	22.25	Nearly weld fracture
CMT-1.5-2.0-4	1.50	2.00	1.5	50	50	420	22.05	1.49	2.00	1.49	49.76	49.76	404.44	20.99	23.60	Nearly weld fracture
CMT-1.5-2.5-6	1.50	2.50	1.5	50	50	420	22.05	1.50	2.48	1.50	49.72	49.72	404.44	21.04	25.78	Nearly weld fracture
CMT-2.0-2.0-6	2.00	2.00	2.0	50	50	420	29.40	2.00	2.00	2.00	49.99	49.99	425.06	29.67	27.41	Nearly weld fracture
CMT-2.0-2.5-4	2.00	2.50	2.0	50	50	420	29.40	1.93	2.49	1.93	50.02	50.02	425.06	28.72	27.40	Nearly weld fracture

NOTE: F_{exp} is maximum force in the elastic range determined by method of linear correlation.

$F_{w,Rk}$ is characteristic resistance for CMT welds calculated by applying formula 8.4c, Chapter 8.5.2, EN1993-1-3.

3.4. Test for corrugated web beams

3.4.1. Description of experimental test setup

The experimental program is developed in the CEMSIG Research Center of Politehnica University of Timisoara, in which five corrugated web beams (see Table 3.13) with flanges of cold-formed C-shape profiles, back to back, is tested, having a span of 5157 mm and a height of 600 mm with different arrangements and configurations for welding position and for the additional shear panels.

There are three phases in the process of fabrication of beams: (1) Building up the web by connecting corrugated steel sheets together by applying welding technique; (2) Connecting the shear panels to the corrugation in both sides of the web, and (3) Connecting the flanges to the top and the bottom of the entire web.

The components of the built-up beams are shown in Figure 3.32 and are detailed below:

- C-section sections, back-to-back, for flanges - 2 × C120 / 2.0;
- Corrugated steel sheets with diffrent thicknesses between the intermediate and outer sheets;
- Additional shear panels - flat plates are positioned at the ends of the beam, where the shear force is maximum;
- Reinforcing profiles U 150 / 2.0 used under load application points;
- Bolts M12 grade 8.8 for flange to endplate connection.

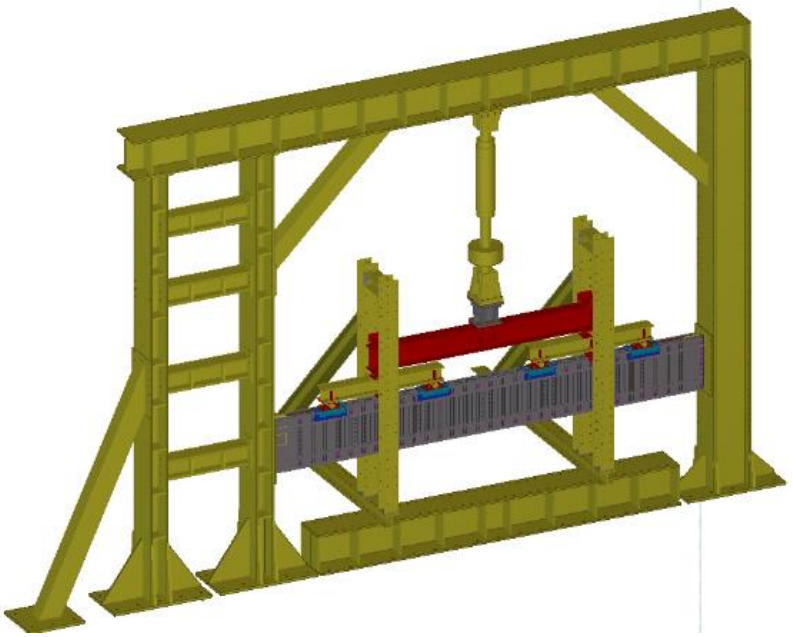

Figure 3.32: Test setup for welded built-up corrugated web beams

Figure 3.32 shows the test setup. A six-point bending test, monotonically conducted, was applied to each specimen with a loading rate of 2 mm/min. The full-scale testing programme was completed with tensile tests to determine both the material properties for beam components and the behaviour of welding connections which were presented in Chapters 3.1, 3.2 and 3.3 of this thesis.

The distinction between the five beams is shown in Table 3.13 below.

Table 3.13: Types of corrugated web beams

Name	Welding type	Thickness			Length of shear panels
		Outer corrugated sheets	Inner corrugated sheets	Shear panels	
CWB SW-1	Spot welding	1.2 mm	0.8 mm	1.0 mm	470 mm; 570 mm
CWB SW-2	Spot welding	1.2 mm	0.8 mm	1.2 mm	510 mm; 630 mm
CWB CMT-1	CMT welding	1.2 mm	0.8 mm	1.2 mm	470 mm; 570 mm
CWB CMT-2	CMT welding	0.8 mm	0.8 mm	1.0 mm	470 mm; 570 mm
CWB CMT-3	CMT welding	1.0 mm	0.8 mm	1.0 mm	470 mm; 570 mm

3.4.2. Experimental test result

In the framework of this master thesis, there were three beams being tested, namely CWB SW-1, CWB CMT-1 and CWB SW-2 respectively.

The first tested specimen was CWB SW-1 beam and its configuration before testing has been presented in Figure 3.33. In this case, the failure mode of the beam started with the buckling of shear panel, followed by the breaking of some spot-welding connections and then the small distortions of the corrugated web. The details of the development of the buckling of shear panels at both ends of the beam and web distorsion at failure are shown in Figure 3.34 and Figure 3.35 respectively. The behaviour of CWB SW-1 beam was ductile, with an initial stiffness of $K_{0\text{-}Exp}$ = 16483.5 N/mm and the maximum load is reached at F_{max} = 283.8 kN. The collapse appears for a displacement of around 123 mm. Figure 3.36 presents the deformed shape of the beam at collapse, while the load - displacement curve for CWB SW-1 beam is drawn in Figure 3.37.

Figure 3.33: CWB SW-1 beam before testing

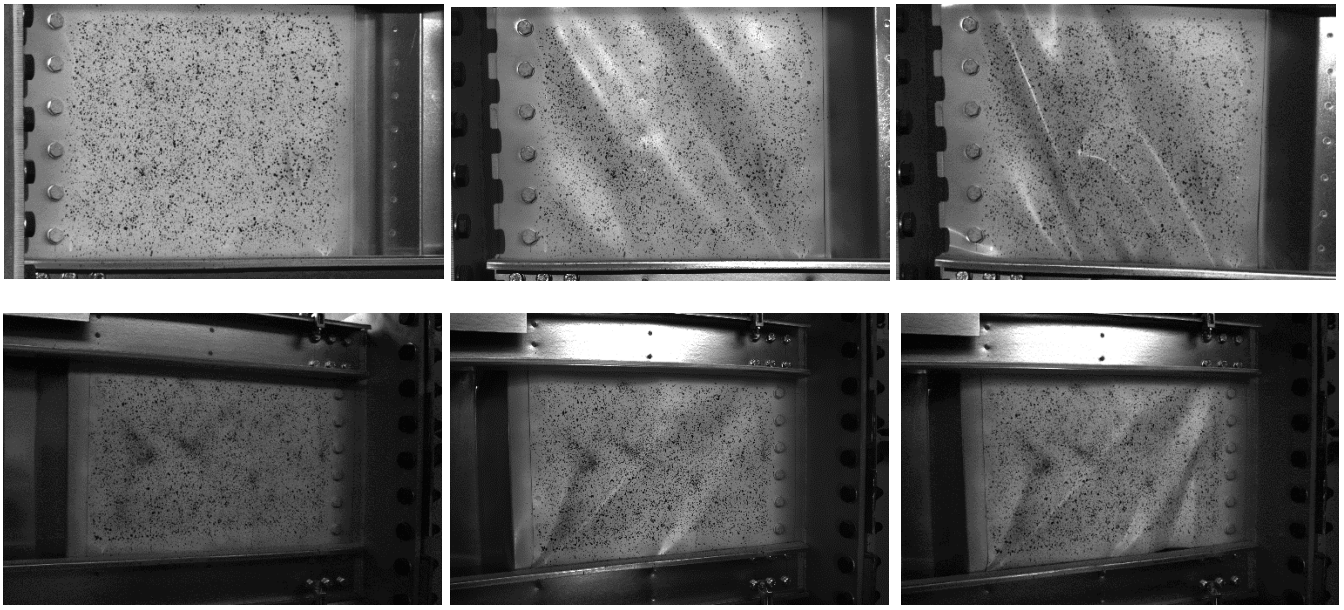

Figure 3.34: Development of the buckling of the end shear panels of CWB SW-1 beam

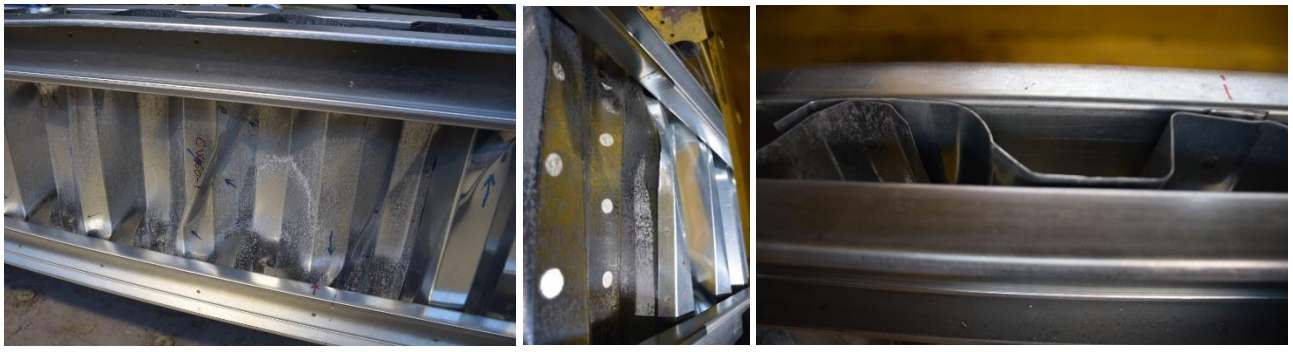

Figure 3.35: Distortion of the web corrugation of CWB SW-1 beam

Figure 3.36: Deformed shape of CWB SW-1 beam at failure

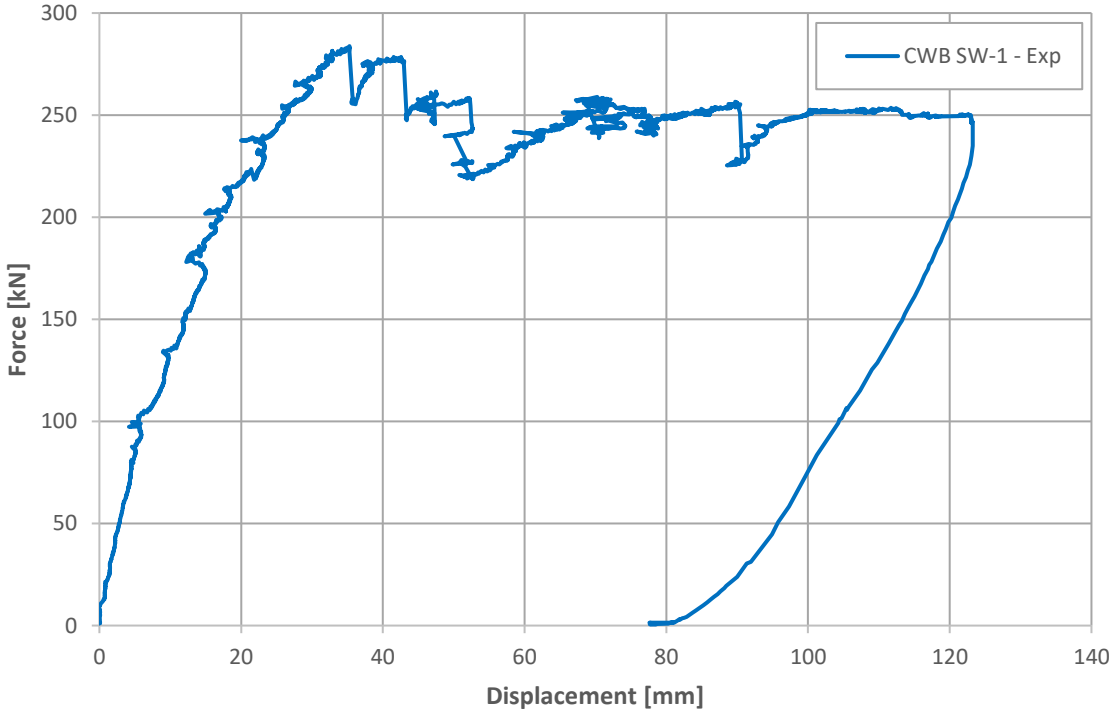

Figure 3.37: Load-displacement curve for CWB SW-1 beam

In case of CWB CMT-1 beam, detailed status of the welds and the beam before the experimental test are displayed in Figure 3.38. The mechanism of failure began with the buckling of shear panel (see Figure 3.39), followed by the distortion of the corrugated web. In this case, the corrugated web of the beam endured a big distortion at the end of the test as shown in Figure 3.40. The behaviour was ductile, with an initial stiffness of $K_{0\text{-}Exp}$ = 20973.4 N/mm and the maximum load is reached at F_{max} = 368.2 kN. The collapse appears for a displacement of 96 mm. The deformed shape of the beam at collapse is displayed in Figure 3.41, while in Figure 3.42 the load - displacement curve of CWB CMT-1 beam is plotted.

Figure 3.38: CWB CMT-1 beam before testing

Figure 3.39: Deformed shape of the end shear panel of CWB CMT-1 beam

Figure 3.40: Deformed shape of the flange and distortion of the web corrugation of CWB CMT-1 beam

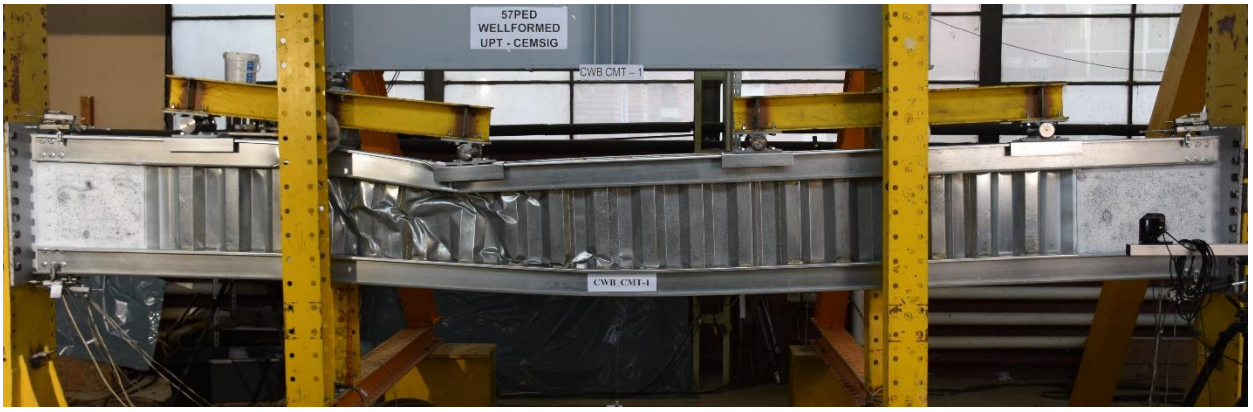

Figure 3.41: Deformed shape of CWB CMT-1 beam at failure

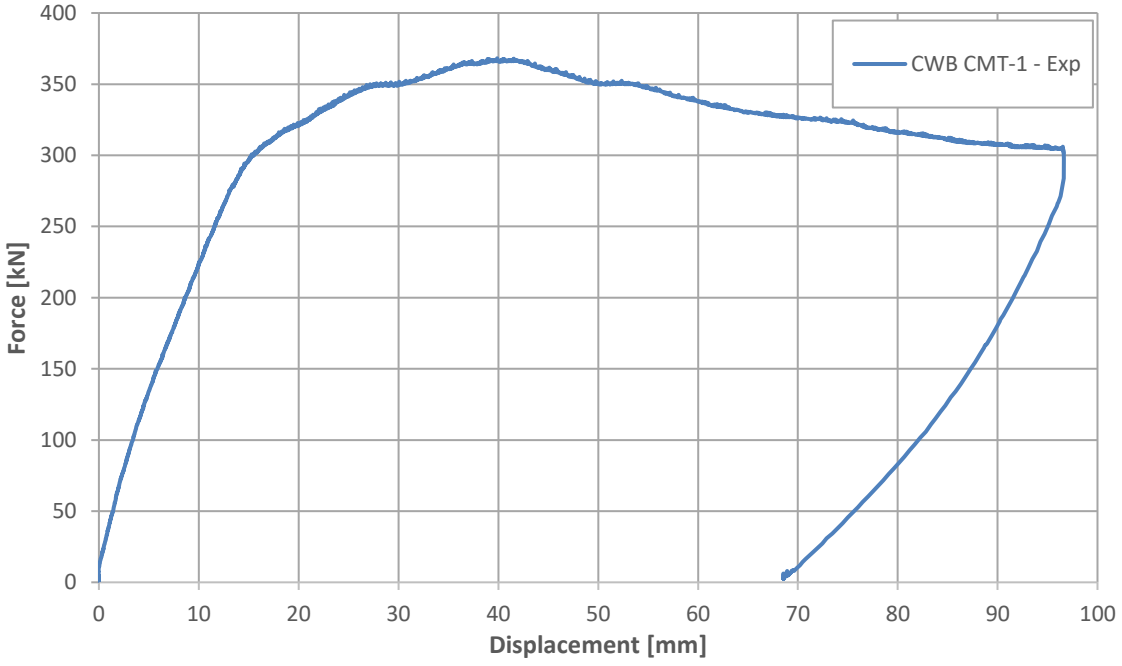

Figure 3.42: Load-displacement curve for CWB CMT-1 beam

The last tested beam within this thesis is CWB SW-2. The difference between CWB SW-2 and CWB SW-1 beams is not only in the thickness of the shear panels, but also in the arrangement of spot welds to connect the corrugated sheets of the web together. The configuration of the beam before experimental test has been shown in Figure 3.43. The mechanism of the failure mode developed from the stage of the buckling of the shear panel at one end of the beam, then breaking of spot welds at some positions before starting to get buckled of the shear panels at another end, and followed by the distorsion of the web. The buckling process of the shear panels is displayed in Figure 3.44, and Figure 3.45 presents the status of welding connections at some positions of the beam and the distortion of the web at the end of the test. The behaviour was ductile, with an initial stiffness of $K_{0\text{-}Exp}$ = 15007.3 N/mm and the maximum capacity is achieved at F_{max} = 276.0 kN. The collapse appears for a displacement of 71 mm. Figure 3.46 shows the deformed shape of the beam CWB SW-2 at collapse, while Figure 3.47 expresses the recorded load - displacement curve.

Figure 3.43: CWB SW-2 beam before testing

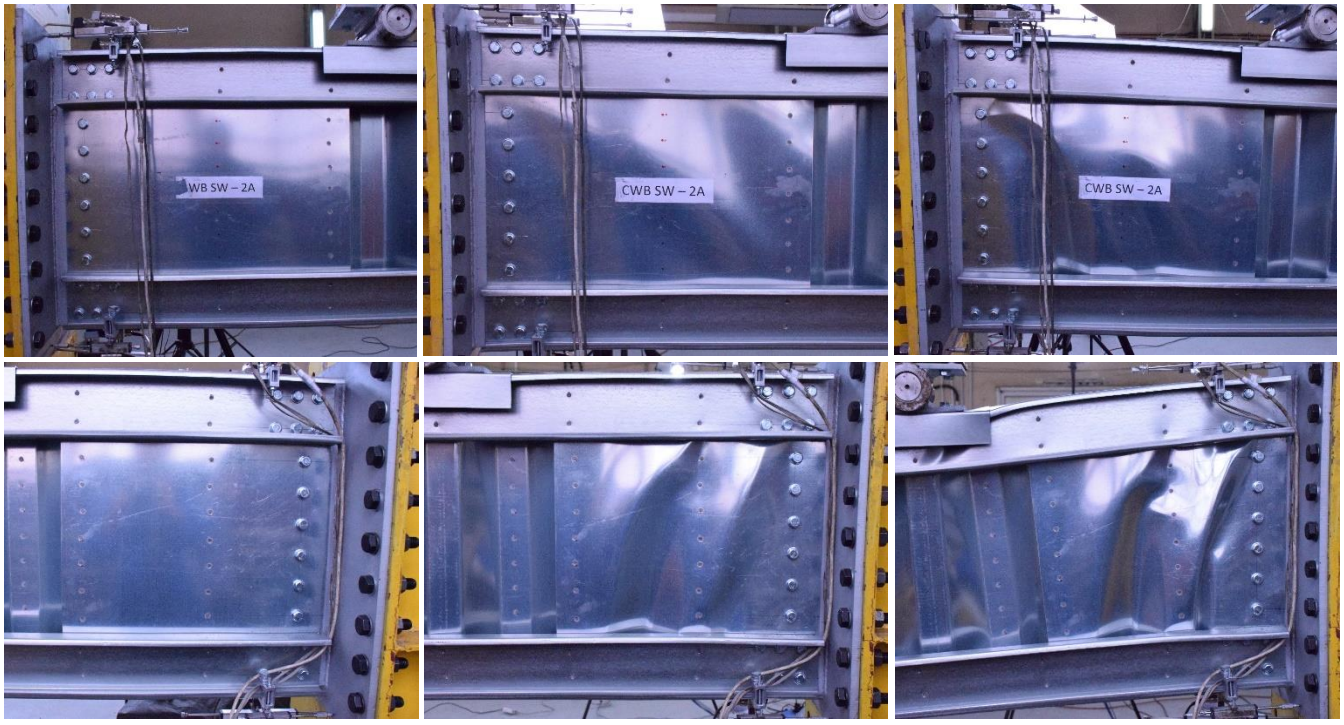

Figure 3.44: Development of the buckling of the end shear panels of CWB SW-2 beam

Figure 3.45: Breaking of some spot-welds and distortion of the web corrugation of CWB SW-2 beam

Figure 3.46: Deformed shape of CWB SW-2 beam at failure

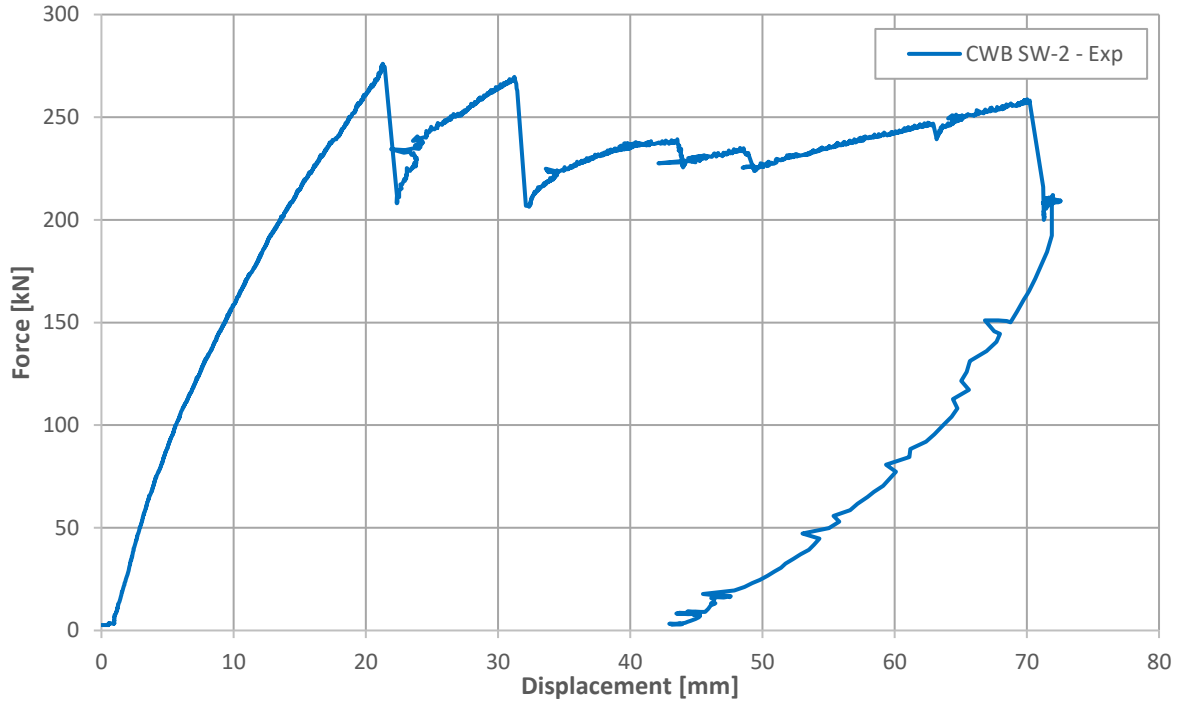

Figure 3.47: Load-displacement curve for CWB SW-2 beam

3.4.3. Comparison with the previous study

In the solutions developed previously within the Research Center CEMSIG (http://www.ct.upt.ro/en/centre/cemsig) of the Politehnica University of Timisoara, a technological solution of such a built-up beam, consisting of trapezoidal corrugated web and parallel flanges made of thin-walled cold-formed steel lipped channel sections, was proposed and carried out, in which the flanges and the web were connected by self-drilling screws. Five beams with corrugated webs, with a span of 5157 mm and a depth of 600 mm, were tested, with different arrangements of self-drilling screws and shear panels. The detailed presentation of this solution was presented by Dubina et al. [29,30].

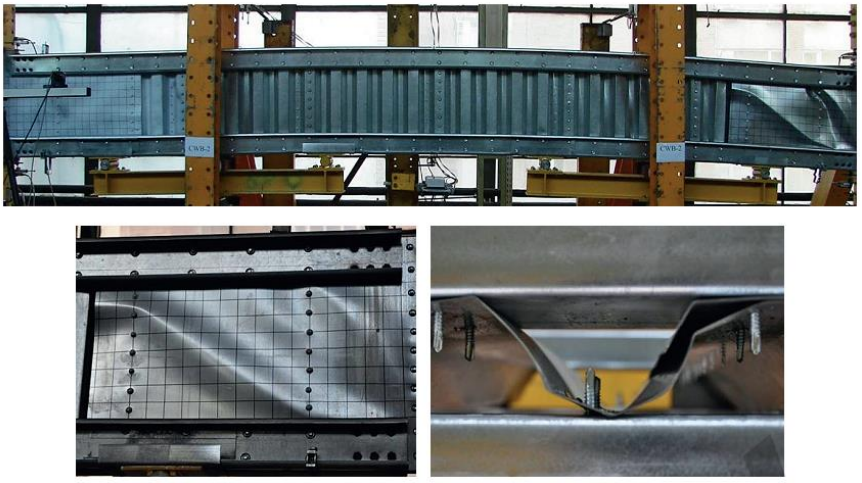

Figure 3.48: Built-up corrugated web beam with self-drilling screw fastener

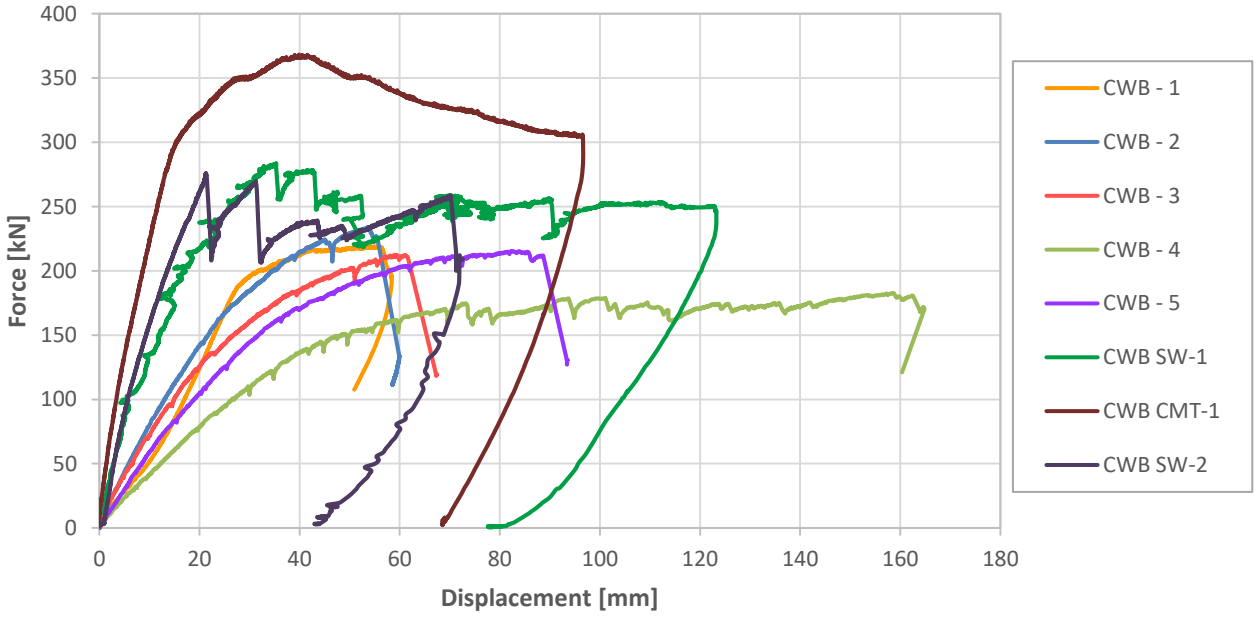

Figure 3.49: Load - displacement curves for several types of corrugated web beams

Table 3.14: Initial stiffness and ultimate load of corrugated web beams

Beam type	Type of fasteners	$K_{0\text{-}Exp}$ (N/mm)	$F_{max\text{-}Exp}$ (kN)
CWB-1	Self-drilling screws	6862.2	218.9
CWB-2	Self-drilling screws	7831.5	231.3
CWB-3	Self-drilling screws	7184.9	209.5
CWB-4	Self-drilling screws	3985.0	181.9
CWB-5	Self-drilling screws	5516.2	214.6
CWB SW-1	Spot welding	16483.5	283.8
CWB SW-2	Spot welding	15007.3	276.0
CWB CMT-1	CMT welding	20973.4	368.2

Some remarkable conclusions can be drawn by taking the comparison of the load - displacement curves (see Figure 3.49) between welded built-up cold-formed steel beams and other beams applied self-drilling screw fasteners which are displayed in Figure 3.48. It can be visibly seen from the graph that the beams with the welding connections provide higher values in terms of both initial stiffness and ultimate load compared to the beams with self-drilling screws. It is twice as high as, even three times regarding initial stiffness for the case of welding beams in comparison with the self-drilling screws corrugated-web beams. Especially, it is observed that the very high load-bearing capacity is offered by the beam used CMT welding technique. The specific results have been shown in Table 3.14. To conclude, the experiments in this study have proven that the beams used welding technique offer superior advantages over other beams.

CHAPTER 4: NUMERICAL ANALYSES

Experimental studies is the most reliable and essential way in order to investigate the performance of a structure. However, it is difficult to take into account for the influence of small changes and the large variability of the parameters since a lot of resources are required such as budget and time to performe experiments. That is why numerical simulation appears to be a practical solution, which enables to carry out larger number of analyses with lesser resources.

This chapter consists of three parts. Firstly, the information on numerical modeling is described. Secondly, the parametric study is implemented by changing some parameters of the beam components. And thirdly, the comparison of results between experimental study and numerical simulation is investigated.

4.1. Description of numerical models

After performing the full-scale experimental test in laboratory, the beams are simulated by using the finite element analysis software ABAQUS/CAE version 6.14. The details of the differences of five beams are provided in Table 3.13 of previous chapter.

The approach involves two analyses that run with the same model definition:

- In the first analysis, an eigenvalue buckling analysis will be performed with Abaqus/Standard in the type of "Frequency" on the perfect structure to establish probable collapse modes. Several Eigenmodes with different values of frequency will be provided from the result. However, the lowest modes are frequently assumed to provide the most critical imperfections. In other words, the result from the mode 1 is chosen to input into the original model to perform the second analysis.
- In the second analysis, Abaqus/Explicit will be used to introduce an imperfection in the geometry by adding these buckling modes to the “perfect” geometry. Then a load-displacement analysis on the perturbed structure will be performed. In order to define an imperfection based on Eigenmode data, the following code is used to import into the Keywords of the original model:

*IMPERFECTION, FILE=*results_file*, STEP=*step*

where:

step is defined in the type of "Dynamic, Explicit";

results_file is the name of the job for imperfection analysis.

4.1.1. Part module

Four parts of the beam components (see Figure 4.1) were drawn in the part module using following characteristics (see Table 4.1). All components of the beam are modeled with shell elements.

Table 4.1: Part module for beam components

Modeling space	3D
Type	Deformable
Shape	Shell
Type	Extrusion

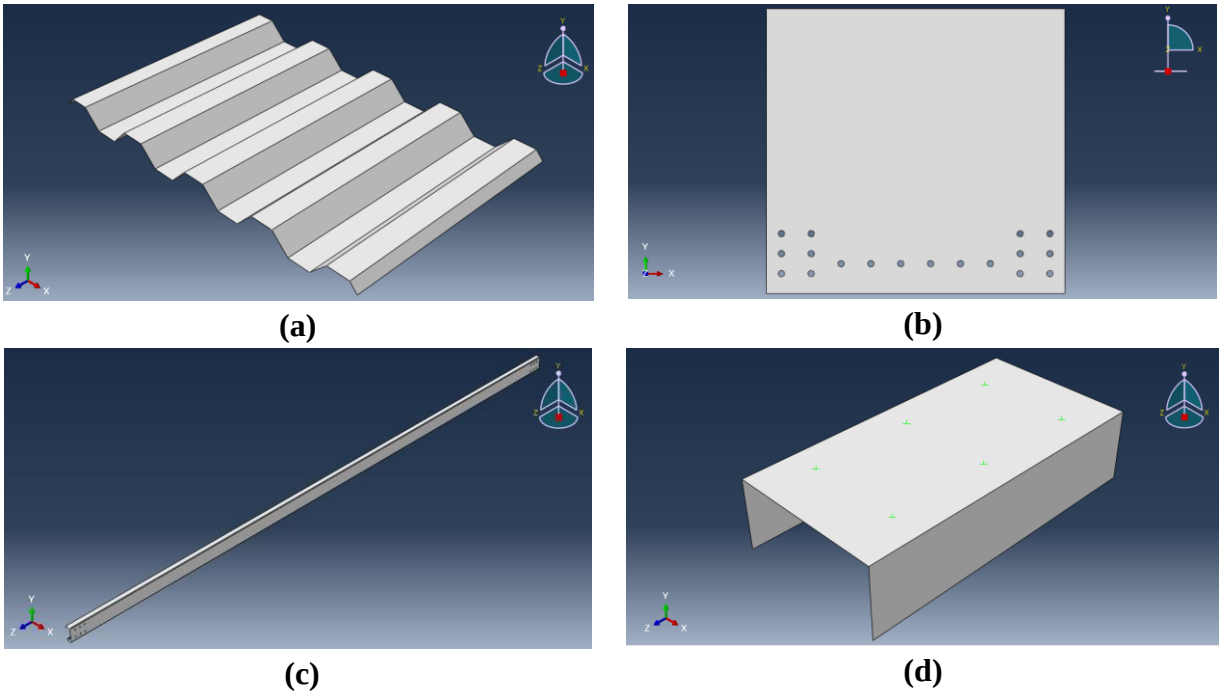

(a) **(b)** **(c)** **(d)**

Figure 4.1: Beam components

(a) Corrugated sheet; (b) Shear panel; (c) Flange;

(d) Reinforcing profiles used under the load application

4.1.2. Property module

In property module, material properties defined to each part of the beam are presented in the following tables. Both elastic and plastic material properties need to be defined in this module.

Table 4.2: Property module for beam components

Material property		Value	Unit
Density	Mass Density	7.85×10^{-9}	Tons/mm^3
Elastic	Young's Modulus	210000	N/mm^2
	Poisson's Ratio	0.3	-

These properties represent the material behavior in the elastic region. However, after the yield strain, the material behavior is not linear any more. Thus, entering other material data is necessary.

Before performing numerical investigation of the full-scale beam, the material model of steel is calibrated based on the result of the tensile test on material. From the tensile test presented in Chapter 3.1 of this thesis, the force-displacement curves for different combinations of thickness of steel samples were obtained, but the change of the area of the specimen along with force was not considered in the curve. It is so-called engineering stress and strain. It is not real stress and strain on specimens. That is why it is required to find true stress and strain which are used as an input data for the plastic behavior of steel beam components including flange, shear panel and corrugated web in numerical simulation. For the material calibration in Abaqus, the Engineering Stress-Strain curves were transformed to True Stress-Strain curves using the following equations from EN1993-1-5-Annex C [1].

$$\sigma_T = \sigma_E(1 + \varepsilon_E) \quad \text{(Eq 4.1)}$$

$$\varepsilon_T = \ln(1 + \varepsilon_E) \quad \text{(Eq 4.2)}$$

$$\varepsilon_{plastic} = \varepsilon_T - \varepsilon_{yield} \quad \text{(Eq 4.3)}$$

Where:

σ_T is the true stress;

ε_T is the true strain;

σ_E is the engineering stress;

ε_E is the engineering strain;

$\varepsilon_{plastic}$ is the true plastic strain;

ε_{yield} is true strain at true yielding stress.

These equations are only valid up to the ultimate strength. The following tables represents for the true stress and strain which were used in numerical modeling, calculated by applying the equations 4.1, 4.2 and 4.3. And the graphs illustrate the difference between engineering stress and strain

curve and true stress and stress curve. In fact, the difference between these two curves at small deformation is extremely low. However, the true stress is much larger than the engineering stress when the strain increases. The results from the first and the third columns of each table should be entered in ABAQUS material properties for plasticity.

Table 4.3: Material properties of T-0.8 used in ABAQUS

T-0.8		
True Stress (Mpa)	**True Strain**	**True plastic strain**
267.25	0.00207	0
285.17	0.01158	0.00951
308.89	0.02609	0.02402
334.77	0.04185	0.03978
354.52	0.05739	0.05532
362.29	0.06513	0.06306
378.35	0.08367	0.08160
388.99	0.09853	0.09646
397.04	0.11180	0.10973
405.63	0.12667	0.12460
412.81	0.14126	0.13919
419.59	0.15635	0.15428
426.06	0.17149	0.16942
429.46	0.17974	0.17767
435.57	0.19726	0.19519

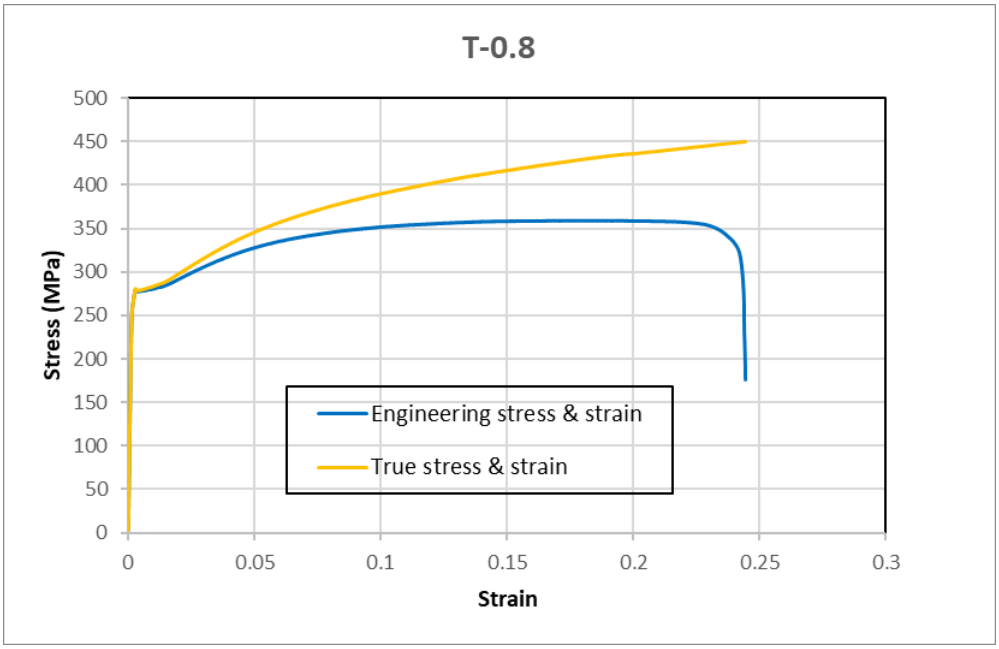

Figure 4.2: Material calibration for T-0.8

Table 4.4: Material properties of T-1.0 used in ABAQUS

T-1.0		
True Stress (Mpa)	**True Strain**	**True plastic strain**
269.78	0.00228	0
288.18	0.01116	0.00888
325.51	0.02857	0.02629
355.22	0.04629	0.04401
375.77	0.06371	0.06143
385.65	0.07423	0.07195
399.35	0.09225	0.08997
408.74	0.10708	0.10480
418.08	0.12347	0.12119
425.63	0.13852	0.13624
432.76	0.15441	0.15213
439.13	0.17006	0.16778
444.86	0.18546	0.18318
448.61	0.19771	0.19543

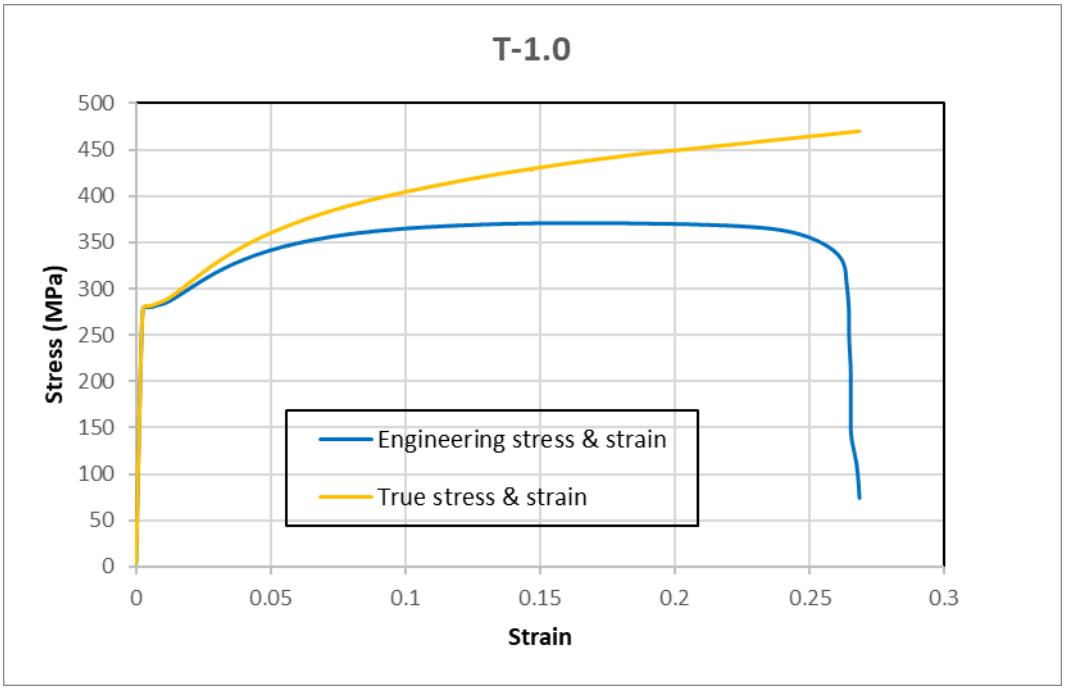

Figure 4.3: Material calibration for T-1.0

Table 4.5: Material properties of T-1.2 used in ABAQUS

T-1.2		
True Stress (Mpa)	**True Strain**	**True plastic strain**
343.65	0.00303	0
371.14	0.00722	0.00419
373.93	0.01534	0.01231
395.92	0.03312	0.03009
410.20	0.04164	0.03861
430.56	0.05809	0.05506
443.08	0.07119	0.06816
452.69	0.08354	0.08051
461.21	0.09665	0.09362
468.79	0.11023	0.10720
475.26	0.12364	0.12061
481.07	0.13687	0.13384
483.78	0.14442	0.14139

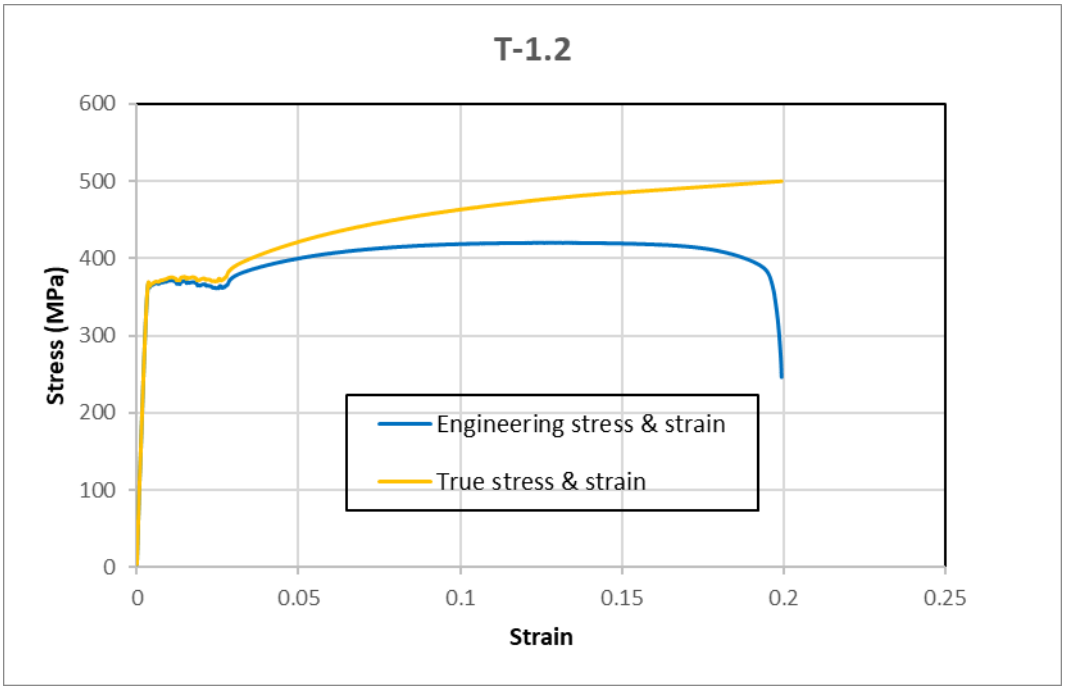

Figure 4.4: Material calibration for T-1.2

Table 4.6: Material properties of T-2.0 used in ABAQUS

T-2.0		
True Stress (Mpa)	**True Strain**	**True plastic strain**
354.93	0.00200	0
444.03	0.01260	0.01060
448.47	0.02303	0.02103
461.09	0.03786	0.03586
474.10	0.04916	0.04716
486.94	0.06293	0.06093
495.50	0.07352	0.07152
503.66	0.08483	0.08283
510.86	0.09613	0.09413
517.13	0.10700	0.10500
523.46	0.11850	0.11650
529.32	0.12990	0.12790
532.50	0.13673	0.13473

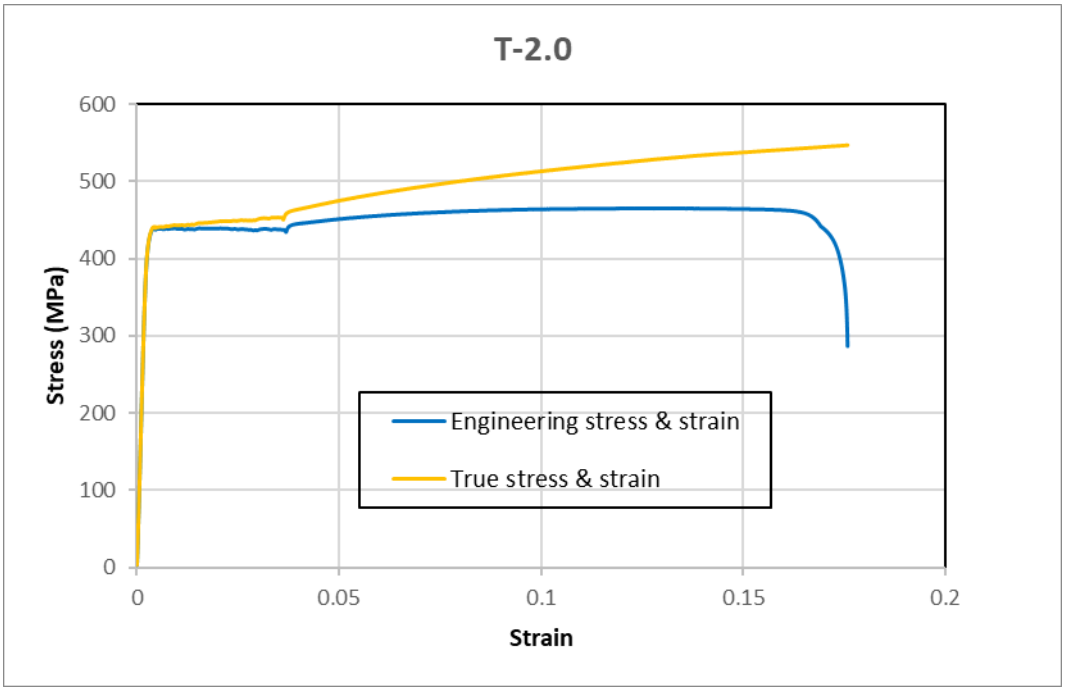

Figure 4.5: Material calibration for T-2.0

4.1.3. Assembly module

This module is used to assemble all separated components in Part module in order to form an entire beam similar to the one that was tested in laboratory. The reference point RP-7 (see Figure 4.6) is defined to apply the load for the beam CWB SW-1.

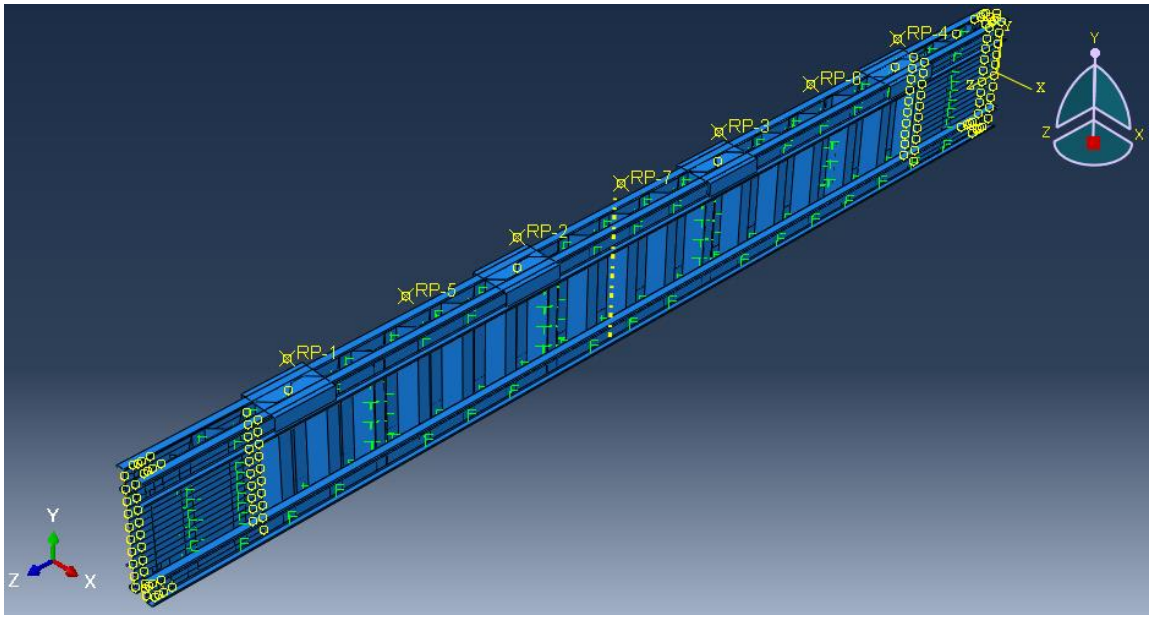

Figure 4.6: Model of the beam CWB SW-1 in ABAQUS

4.1.4. Step module

The imperfection analysis is firstly run in the copy of the perfect model with the type of "*Frequency*". After that, the type of "*Dynamic, Explicit"* is used to run the load-displacement analysis of the beam in the original model.

4.1.5. Interaction module

The friction coefficient of 0.1 is assigned in "Tangential behavior" with friction formulation of penalty, and hard contact was used for specifying "Normal behavior" in contact property options. In addition, separation was allowed after the general contact takes place.

4.1.6. Load module

The control of displacement and rotation is used in the boundary condition as following:

- At the positions to connect the flanges and shear panels to the endplates, both displacement and rotation are restricted: U1 = U2 = U3 = 0, and UR1 = UR2 = UR3 = 0.
- At the positions to connect shear panels to the endplates, only displacement is restricted and rotation is free: U1 = U2 = U3 = 0.

- The control of displacement of 60 mm is assigned to the reference point RP-7 in the y-axis (see Figure 4.6): U2 = - 60, U1 = U3 = 0, UR2 = 0. The amplitude for RP-7 is defined as following.

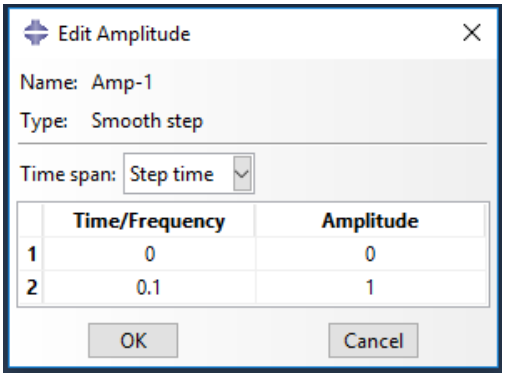

Figure 4.7: Amplitude assigned in boundary condition

4.1.7. Mesh module

The global mesh size of 15 mm was used for the web, flanges and shear panels, and 25 mm was used for the reinforcing profiles under the load application. Mesh size was further reduced around the bolt holes to connect the shear panels to the endplate.

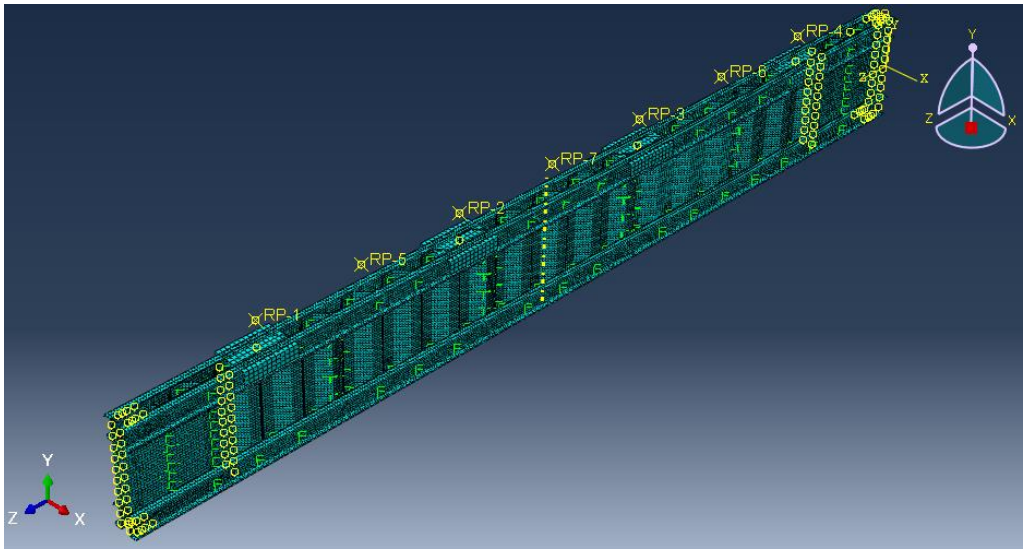

Figure 4.8: The mesh assigned for the beam CWB SW-1 in ABAQUS

4.1.8. Results in visualization module

Visualization module was used for getting results.

Figure 4.9 presents the Eigenmode 1 of the beam CWB SW-1 for imperfection analysis.

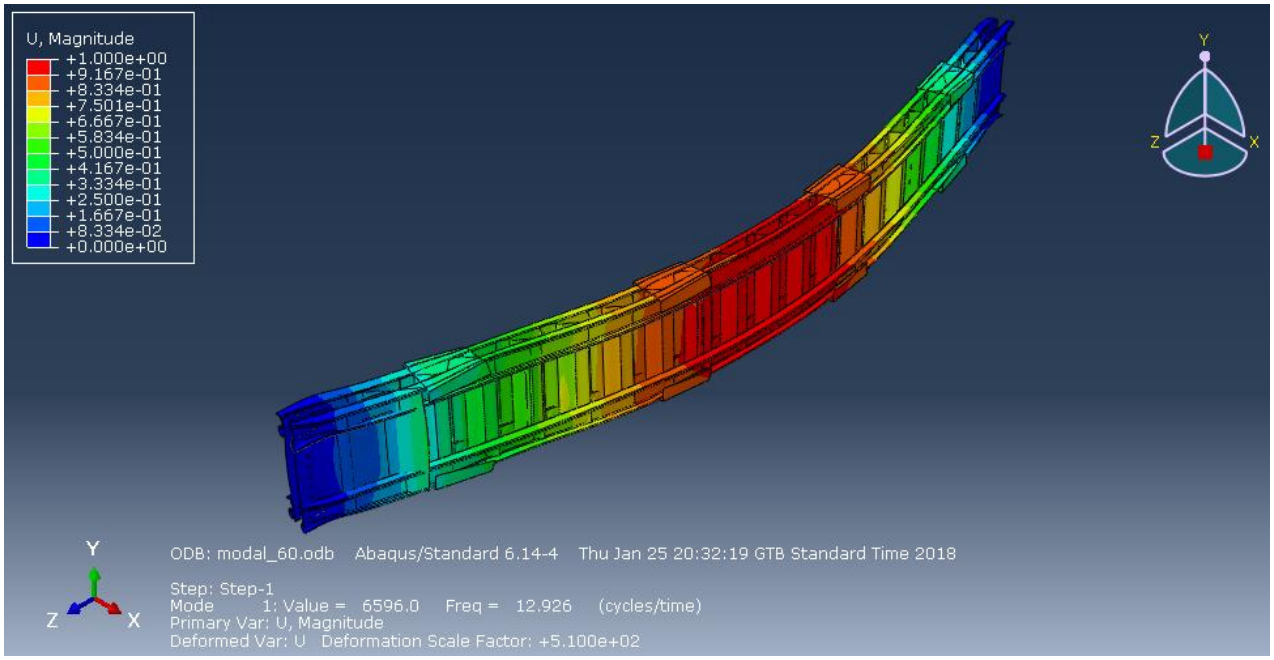

Figure 4.9: Eigenmode 1 of the beam CWB SW-1

Following figures show the development of the mises stresses on the beams at two stages:

1. At displacement of 20 mm;
2. At displacement of 60 mm as being assigned in boundary condition.

Followed by the force-displacement curves for two spot-welding beams (see Figure 4.15) and three CMT-welding beams (see Figure 4.16).

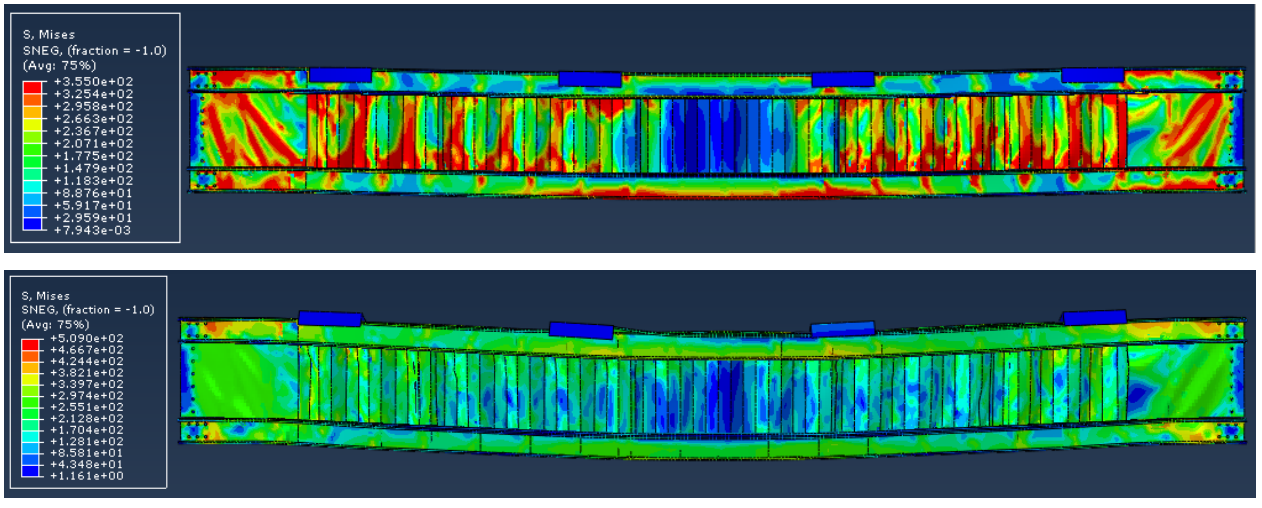

Figure 4.10: Development of the mises stresses on CWB SW-1 beam

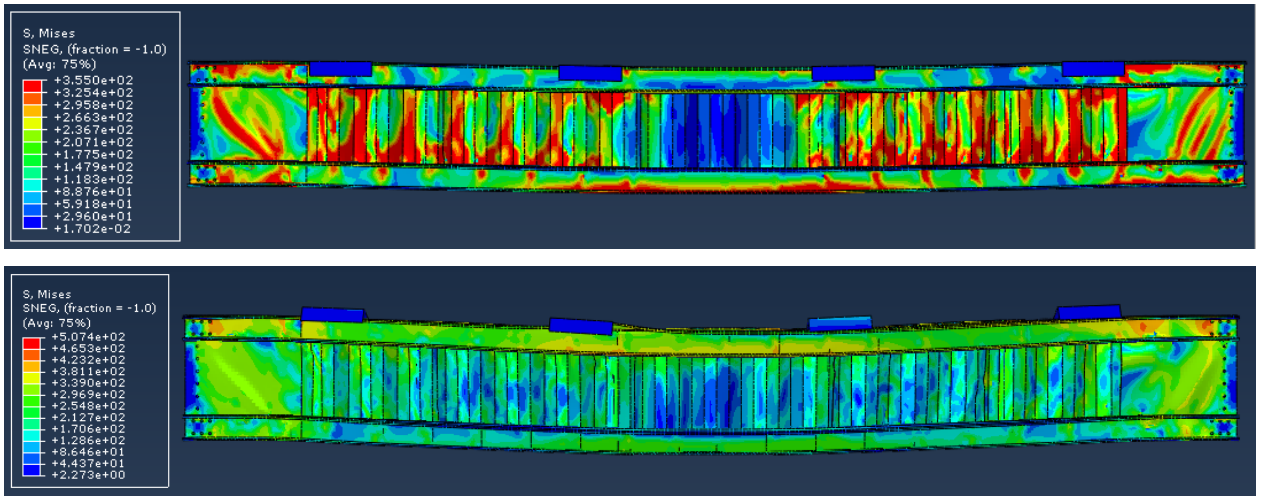

Figure 4.11: Development of the mises stresses on CWB SW-2 beam

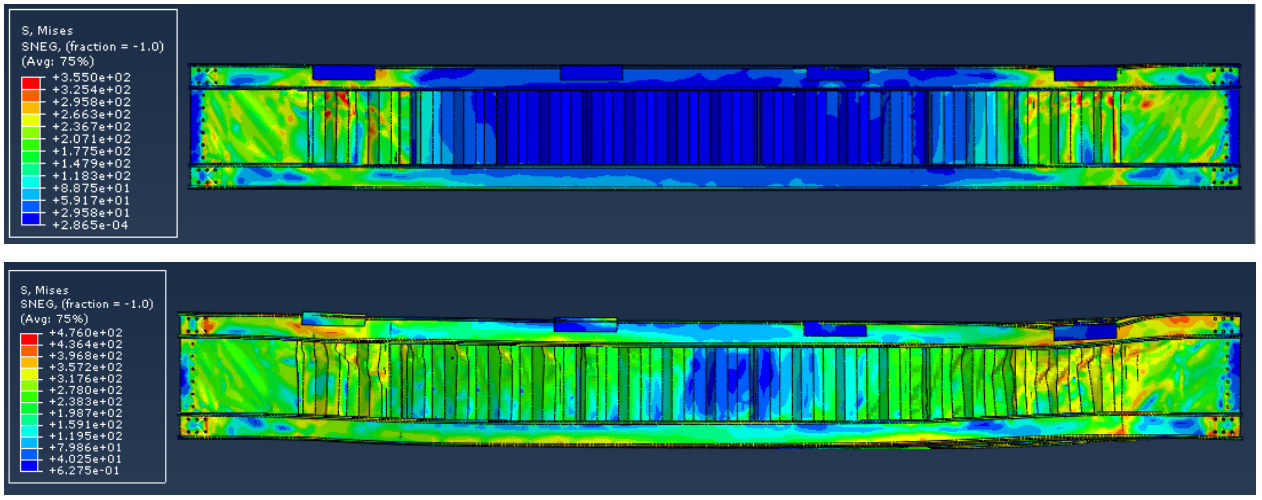

Figure 4.12: Development of the mises stresses on CWB CMT-1 beam

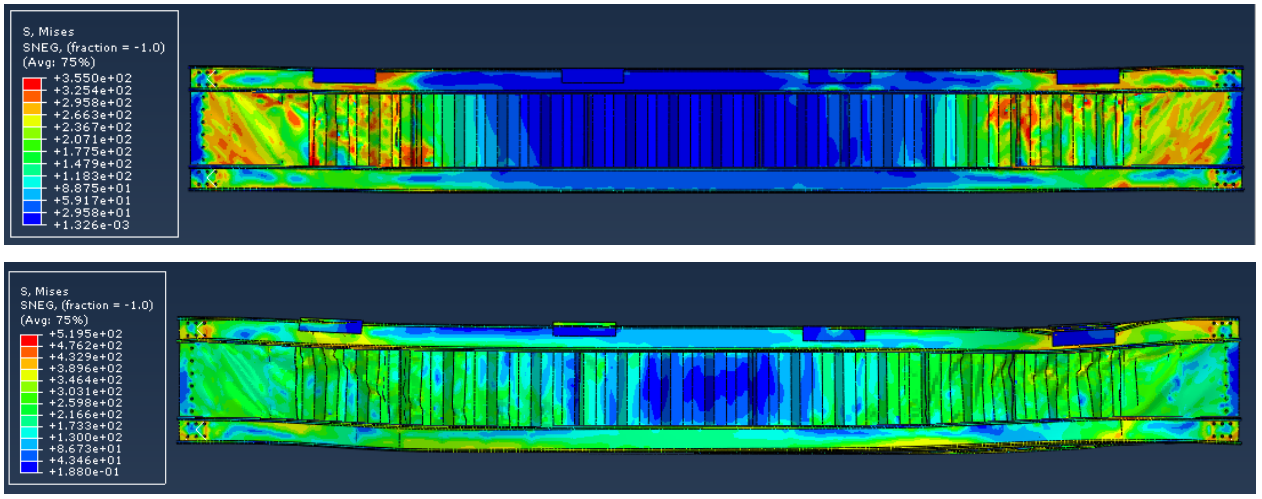

Figure 4.13: Development of the mises stresses on CWB CMT-2 beam

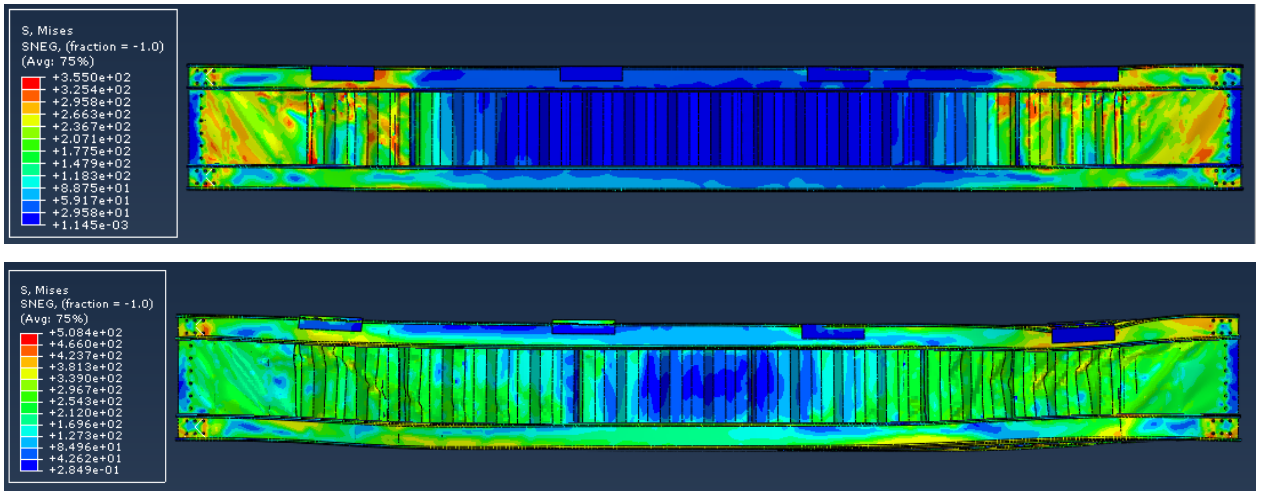

Figure 4.14: Development of the mises stresses on CWB CMT-3 beam

It is predicted from the numerical simulation that the stress developed in the spot-welding beam is higher than the one developed in the CMT-welding beam. It is reasonable because in the case of CMT-welding beam, this type of welding creates a larger contact surface between flanges, shear panels and the corrugation web. Therefore, it helps to prevent the development of the distortion of the beam better than in the case of spot-welding beam. In addition, for the types of beams using the same welding technolody, it can be seen that the stress is greater in the beam with thinner shear panel or thinner outer corrugated sheet of the web.

Figure 4.15: Force-displacement curves of SW beams obtained in ABAQUS/CAE

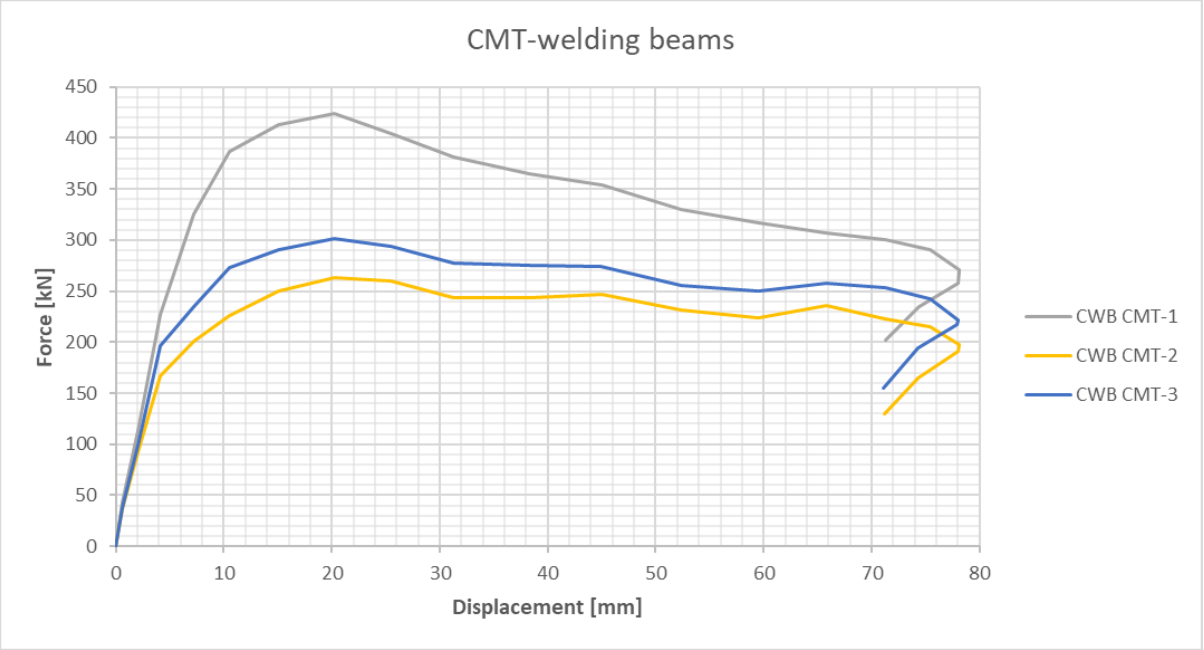

Figure 4.16: Force-displacement curves of CMT beams obtained in ABAQUS/CAE

As a result from numerical simulaton, it can be obviously seen that CMT-welding beams provide higher capacity compared to spot-welding beams. For spot-welding beams, the thickness of shear panels has a small effect on load-bearing capacity of the beam (see Figure 4.15). The thicker shear panel is, the higher load-bearing capacity is. 256.30 kN and 265.71 kN are the values of load-bearing capacities obtained by the beams CWB SW-1 and CWB SW-2 respectively. In the case of CMT-welding beams presented in Figure 4.16, not only the thickness of the shear panels, but also thickness of outer corrugated sheets affect to the final result. The beam CWB CMT-1 with the thickest shear panels of 1.2 mm and the thickest outer corrugated sheets of 1.2 mm witnesses the highest load-bearing capacity at around 424 kN. While the beam CWB CMT-3 with 1.0 mm-thick outer corrugated sheets displays greater load-bearing capacity compared to the beam CWB CMT-2 with 0.8 mm-thick outer corrugated sheets for the same 1.0 mm-thick of the shear panels for both beams. The load-bearing capacities for these beams are nearly 300 kN and 260 kN respectively. The details of five types of beam are provided in Table 3.13.

The Appendix E of the thesis displays the detailed data regarding the force-displacement relationship.

4.2. Parametric study

In order to study about load-bearing capacity of corrugated-web beams due to the effect of the thickness of corrugated webs and the thickness of shear panels. Four additional types of beams,

highlighted in Table 4.7, are taken into account. All parameters including material properties, step type, meshing properties and boundary conditions were kept the same as chapter 4.1 of this thesis.

Table 4.7: Types of beams for parametric study

Name	Welding type	Thickness		
		Outer corrugated sheets	Inner corrugated sheets	Shear panels
CWB SW-0.8	Spot welding	0.8 mm	0.8 mm	0.8 mm
CWB SW-1.2	Spot welding	1.2 mm	1.2 mm	1.2 mm
CWB SW-1	Spot welding	1.2 mm	0.8 mm	1.0 mm
CWB SW-2	Spot welding	1.2 mm	0.8 mm	1.2 mm
CWB CMT-0.8	CMT welding	0.8 mm	0.8 mm	0.8 mm
CWB CMT-1.2	CMT welding	1.2 mm	1.2 mm	1.2 mm
CWB CMT-1	CMT welding	1.2 mm	0.8 mm	1.2 mm
CWB CMT-2	CMT welding	0.8 mm	0.8 mm	1.0 mm
CWB CMT-3	CMT welding	1.0 mm	0.8 mm	1.0 mm

The numerical results of the additional beams are displayed in visualization module as following.

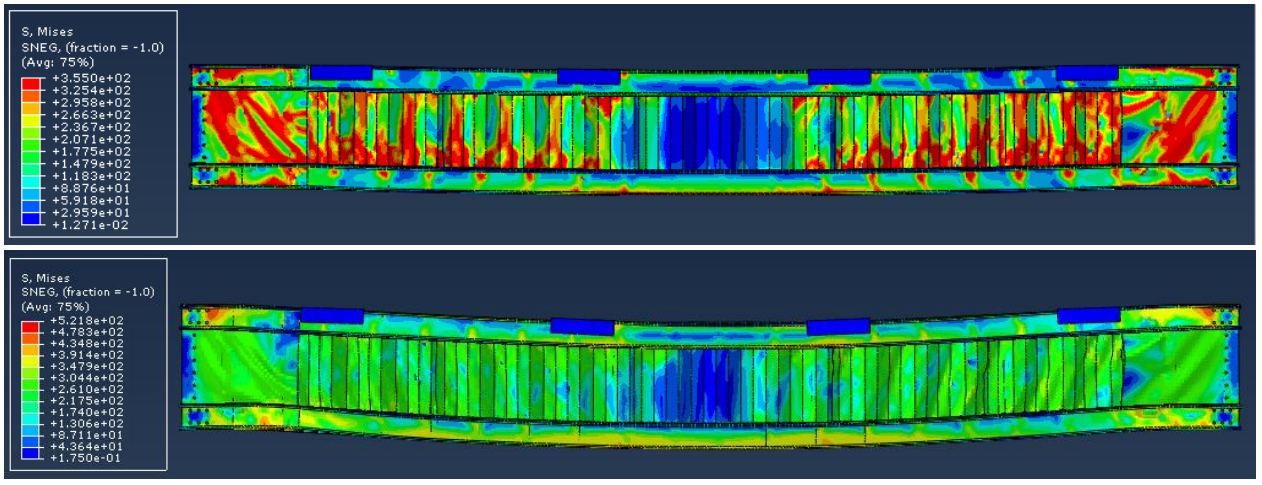

Figure 4.17: Development of the mises stresses on CWB SW-0.8 beam

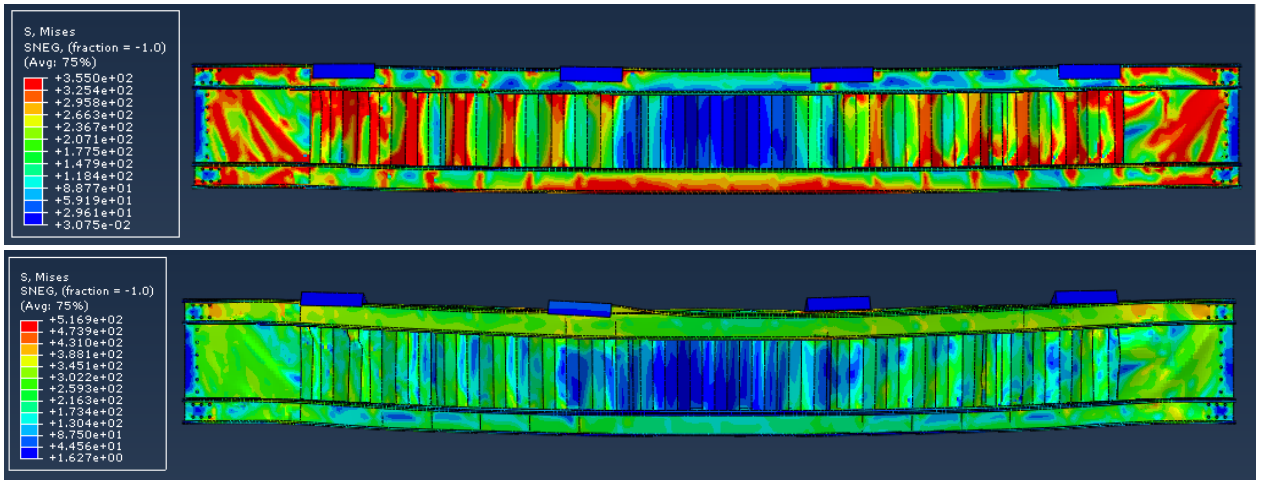

Figure 4.18: Development of the mises stresses on CWB SW-1.2 beam

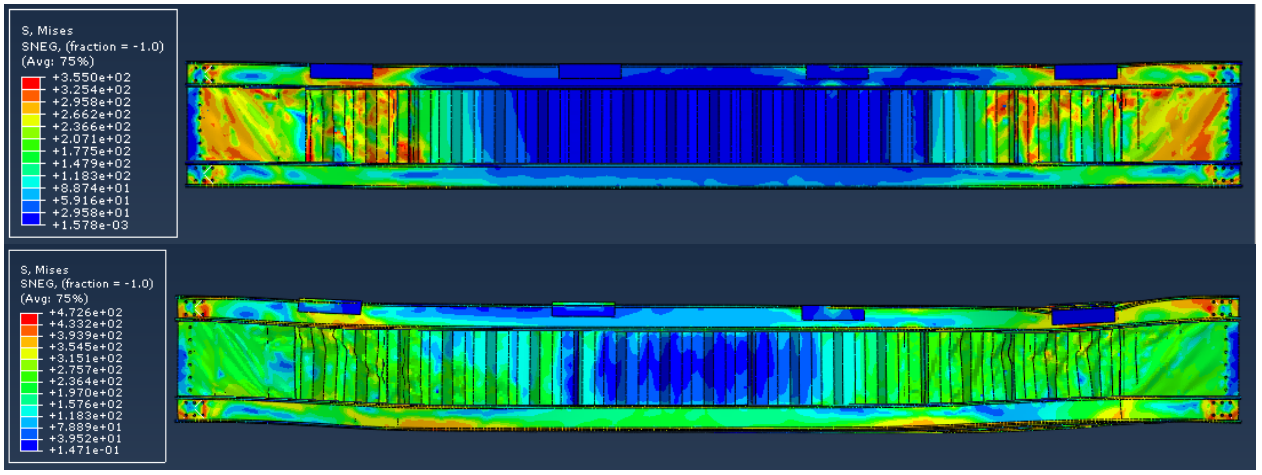

Figure 4.19: Development of the mises stresses on CWB CMT-0.8 beam

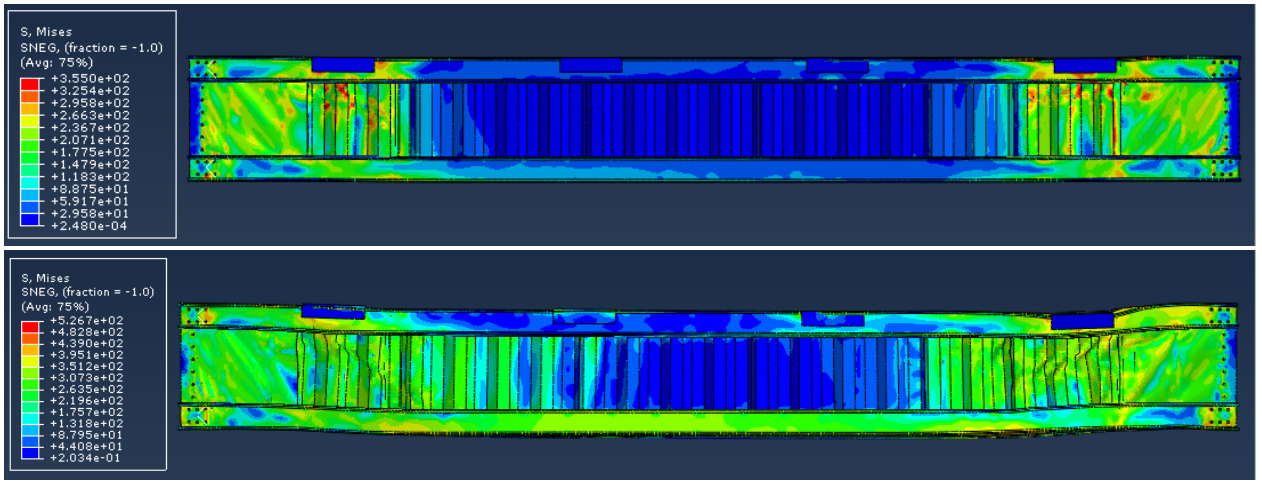

Figure 4.20: Development of the mises stresses on CWB CMT-1.2 beam

The force-displacement curves of all spot-welding beams are shown in Figure 4.21. Once again, it is confirmed that the value of load-bearing capacity of the beam will be increased if the shear panels or corrugated sheets get thicker. In the case of the beams CWB SW-1 and CWB SW-2, in which their corrugated webs are the same, the influence of the thickness of the shear panels on the capacity of the beam is not much.

Figure 4.22 displays the force-displacement relationship for five CMT-welding beams with the difference in the thickness of shear panels and corrugated webs. It can be obviously seen that both shear panels and corrugated webs affect to the load-bearing capacity of the beam. The thicker shear panel or corrugated sheet is, the higher value of the beam capacity. It is observed that there is one noticeable thing in the case of the beams CWB CMT-1 and CWB CMT-1.2. These two beams are modeled to have the same thickness of shear panels and the same thickness of outer corrugated sheets. The only thing different is the thickness of the intermediate corrugated steel sheets for the web that is 0.8 mm and 1.2 mm for CWB CMT-1 and CWB CMT-1.2 respectively. However, the

maximum force recorded from numerical analysis for these two beams are almost the same at nearly 430 kN as shown in Figure 4.22.

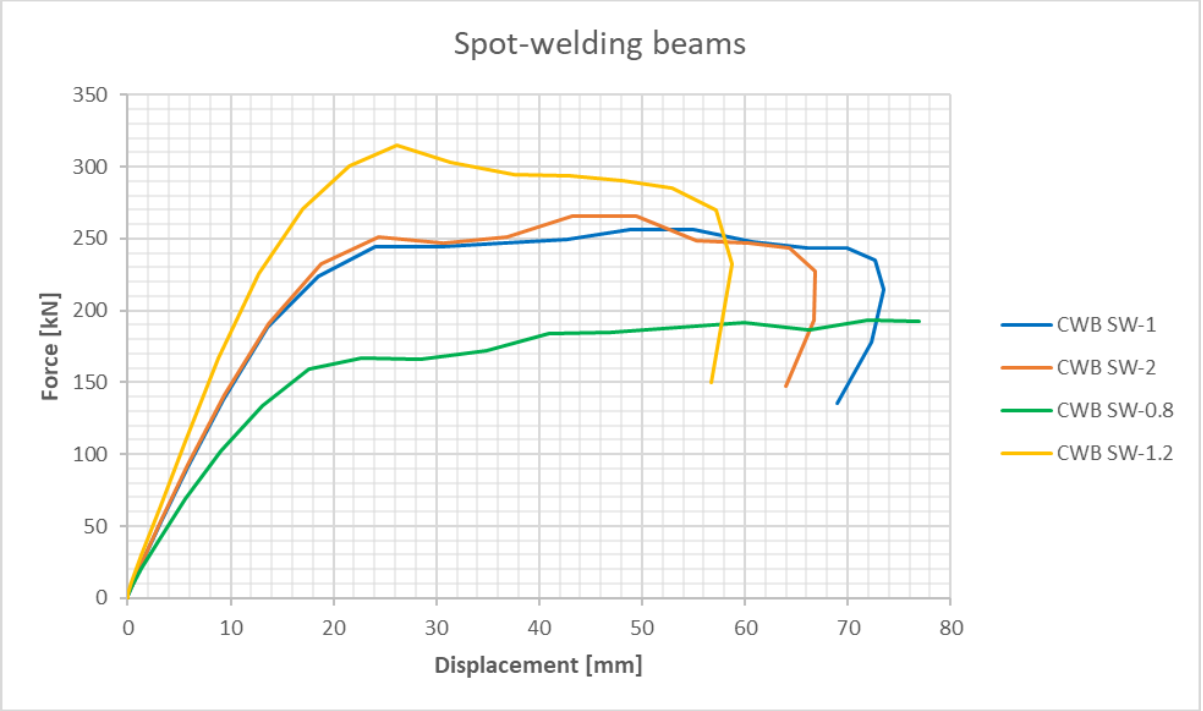

Figure 4.21: Force-displacement curves of SW beams used in parametric study

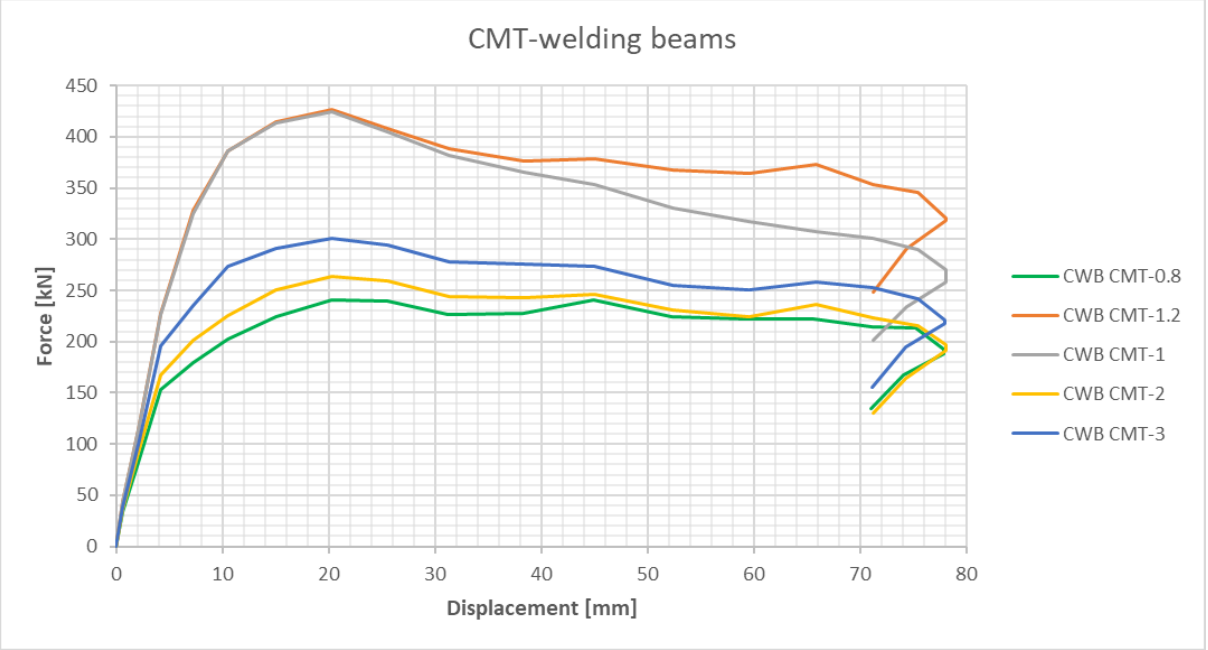

Figure 4.22: Force-displacement curves of CMT beams used in parametric study

The Appendix E of the thesis displays the detailed data regarding the force-displacement relationship of all beams that have been simulated for parametric study.

4.3. Comparison between experimental tests and FEM

- **For CWB SW-1 beam:**

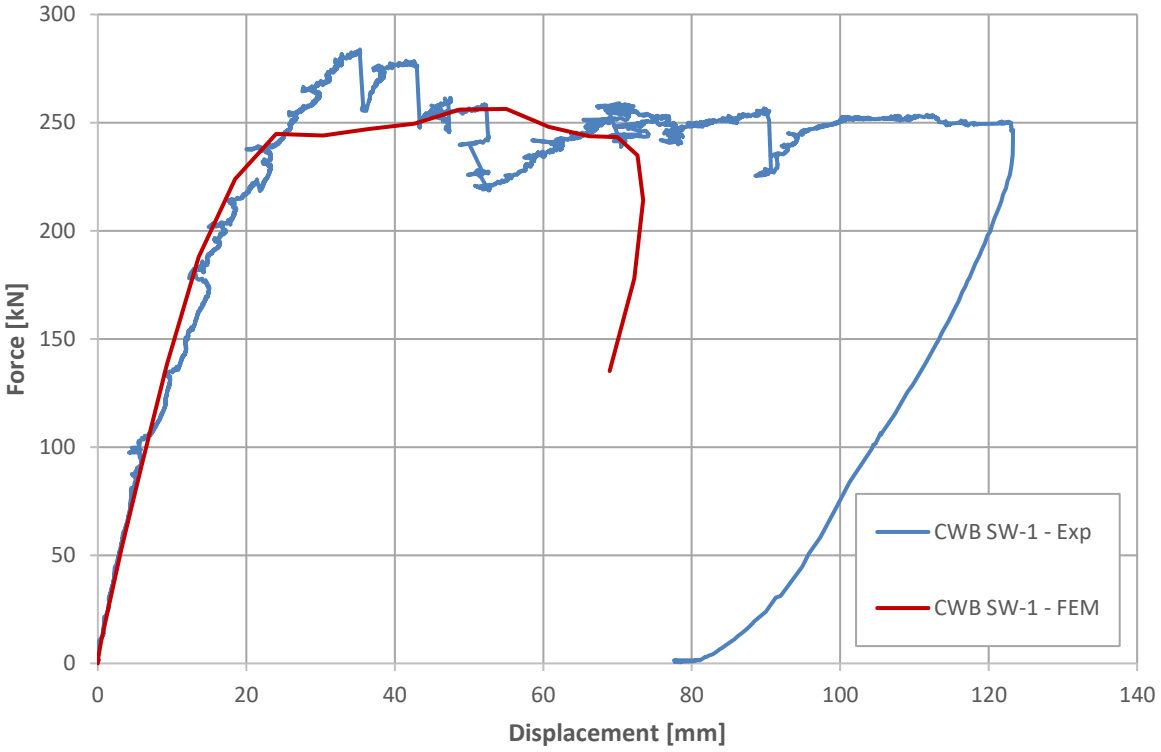

Figure 4.23: FEM/experimental force-displacement curves for CWB SW-1 beam

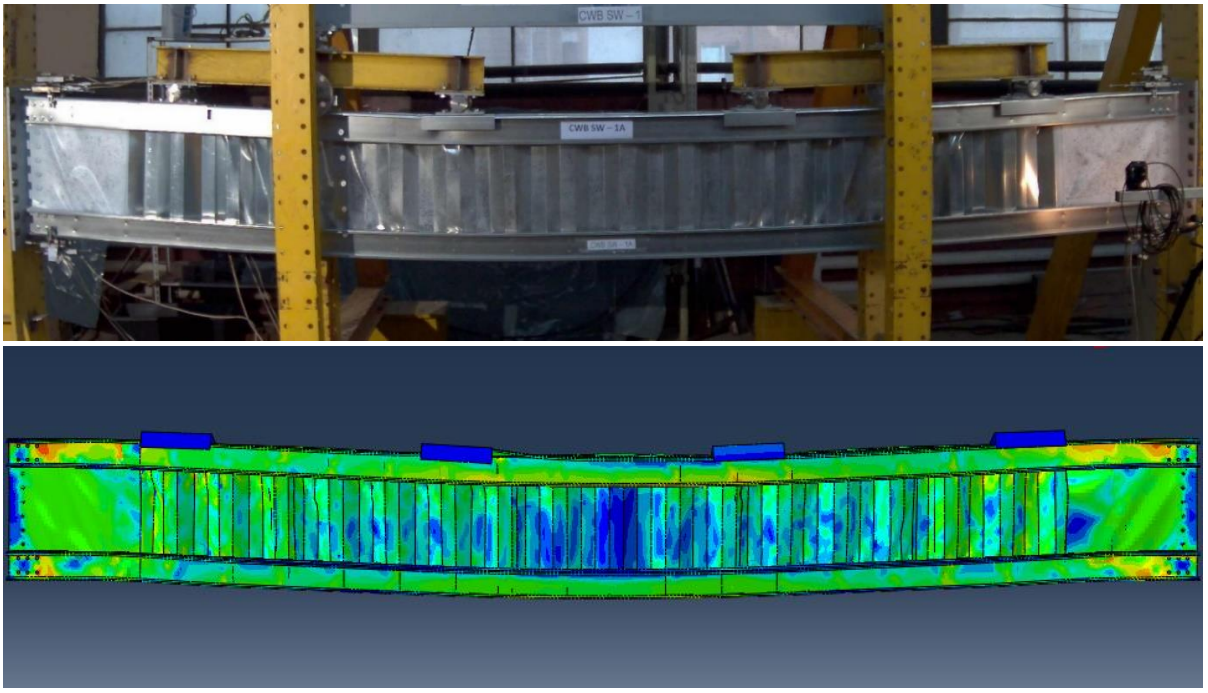

Figure 4.24 - a

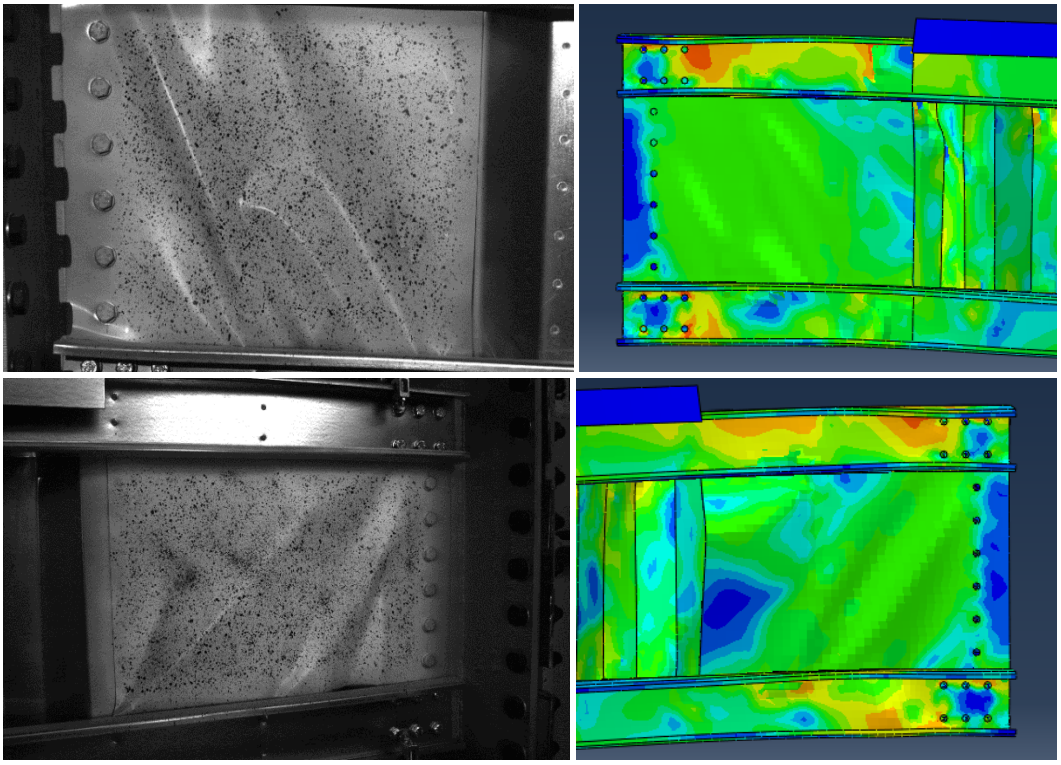

Figure 4.24 - b

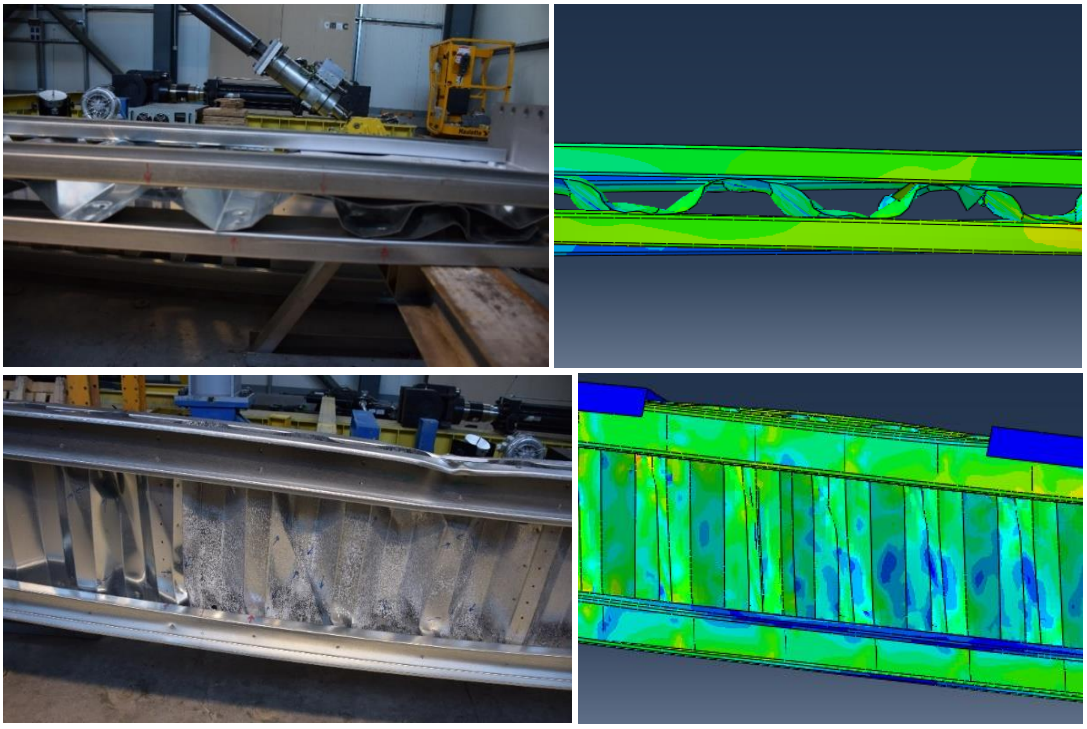

Figure 4.24 - c

Figure 4.24: Failure mode comparison between test and simulation for CWB SW-1 beam a. The entire beam; b. The shear panels; c. The corrugated web

It can be seen from Figure 4.23 that the result of numerical simulation is quite similar to the test result in terms of both initial stiffness and maximum force. When it comes to failure mode, the result from the FE simulation corresponds to the one identified during the test. The comparison of the failure mode is shown in Figure 4.24. The shapes of the buckling of the shear panels and distortion of corrugated web on FE model are almost the same as the ones on the tested specimen. As a results, it is concluded that the response of the FE model has a very good matching with the experimental test in the case of CWB SW-1 beam.

- **For CWB SW-2 beam:**

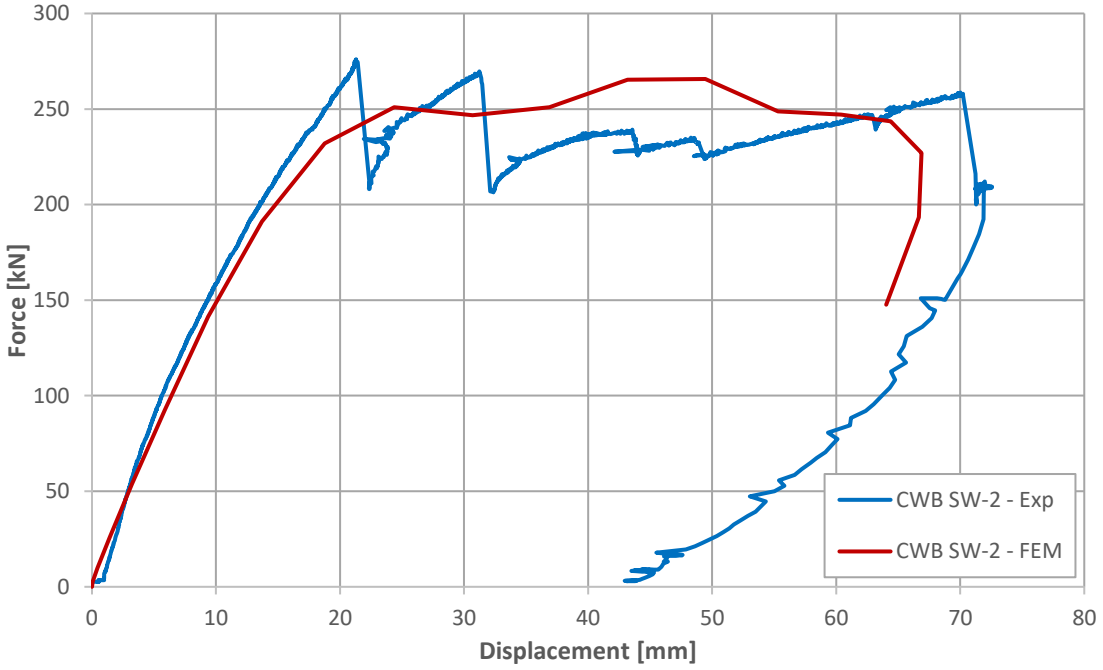

Figure 4.25: FEM/experimental force-displacement curves for CWB SW-2 beam

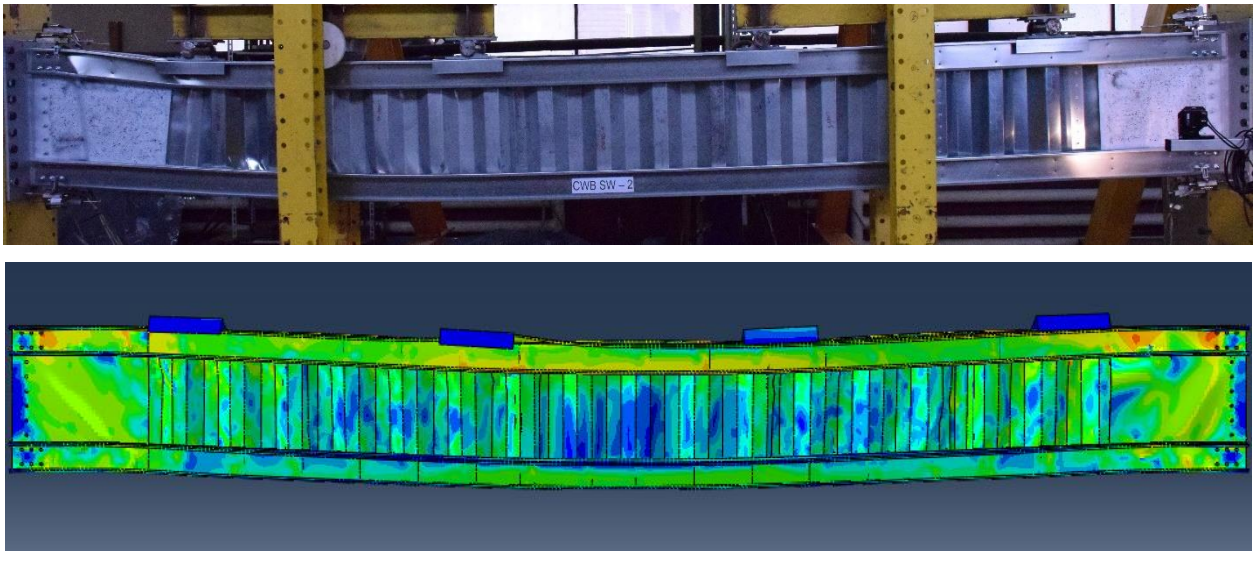

Figure 4.26 - a

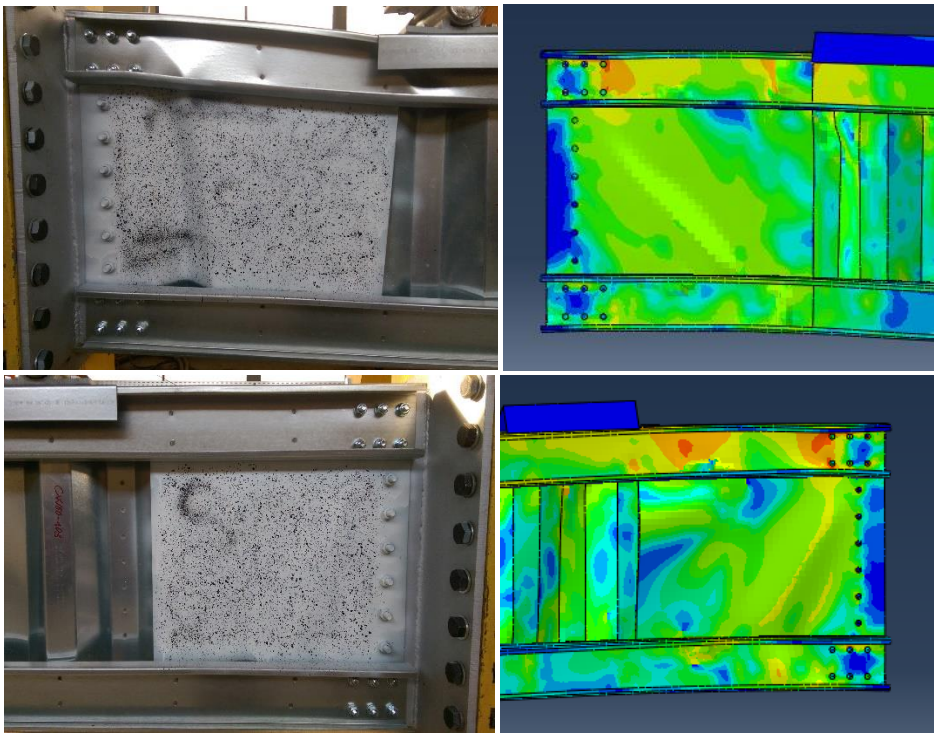

Figure 4.26 - b

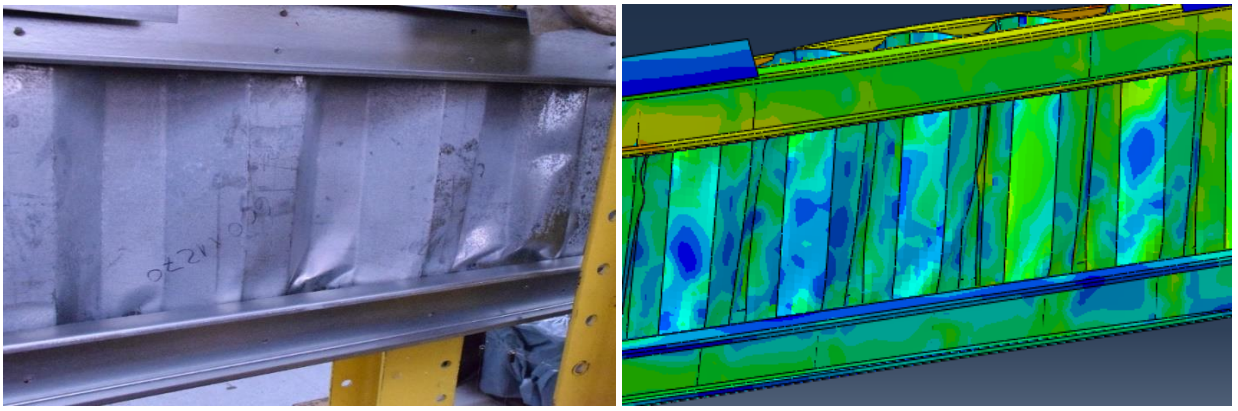

Figure 4.26 - c

Figure 4.26: Failure mode comparison between test and simulation for CWB SW-2 beam a. The entire beam; b. The shear panels; c. The corrugated web

Figure 4.25 shows a very good matching of the force-displacement curves between numerical simulation and the test result in terms of both initial stiffness and maximum force. As for the comparison of the failure mode of the beam components, the result from the FE simulation is quite similar to the one identified during the test which is displayed in Figure 4.26. The distortion of corrugated web and the deformed shape of the beam on FE model are almost the same as the ones on the tested specimen. To conclude, there is a good aggrement between FEM and experiment in the case of CWB SW-2 beam.

- **For CWB CMT-1 beam:**

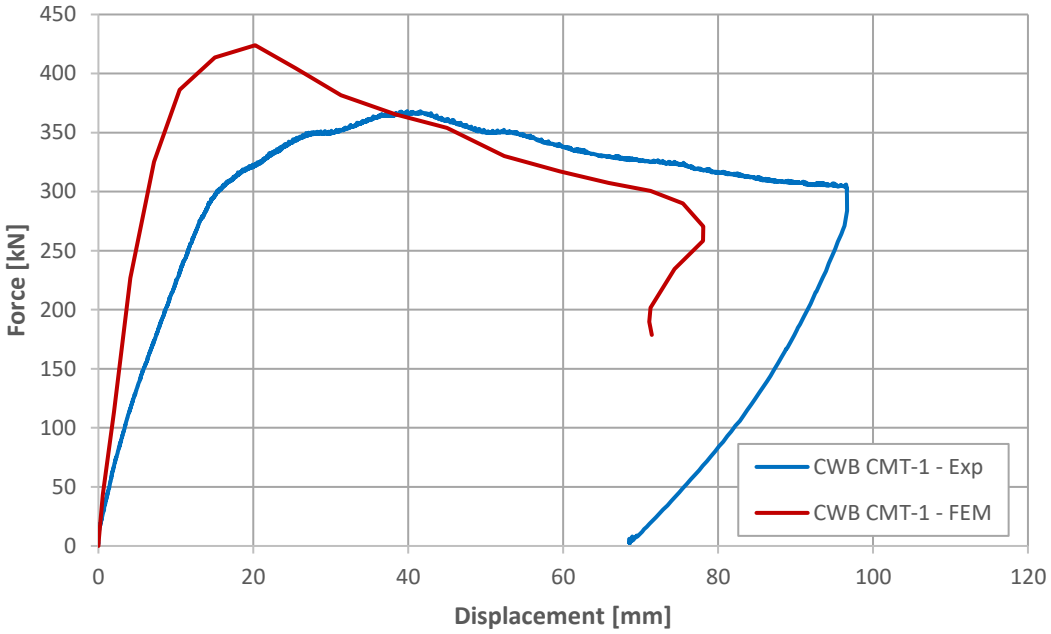

Figure 4.27: FEM/experimental force-displacement curves for CWB CMT-1 beam

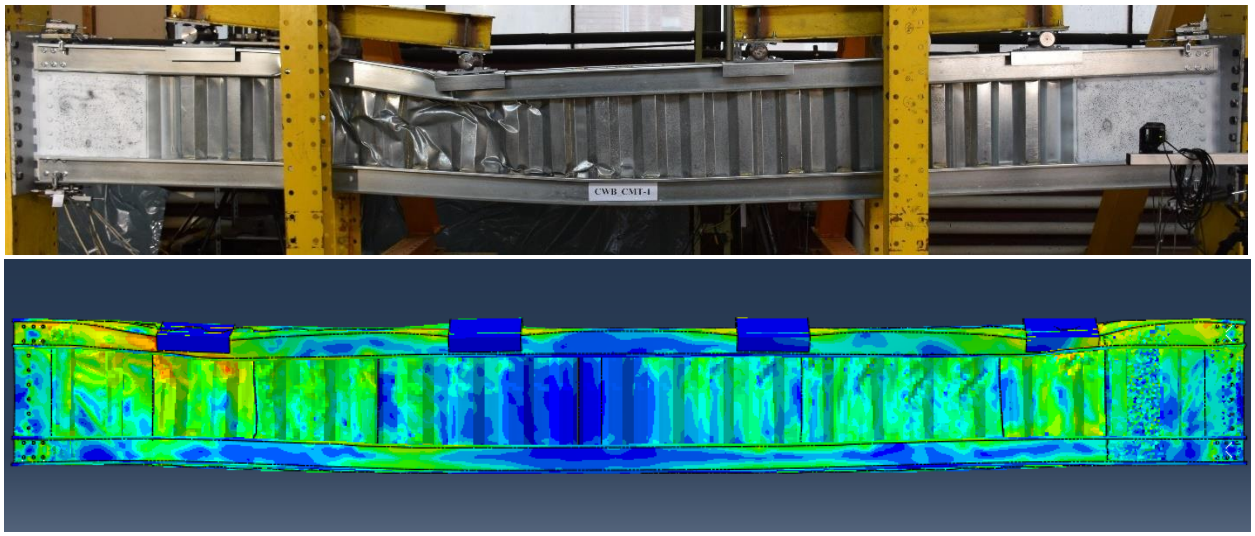

Figure 4.28 - a

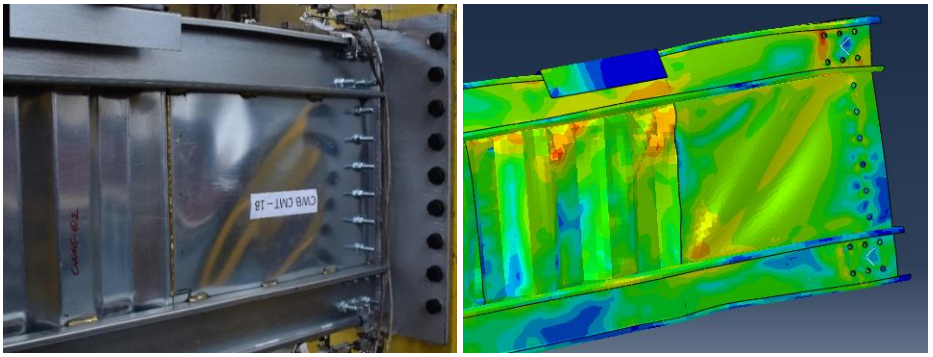

Figure 4.28 - b

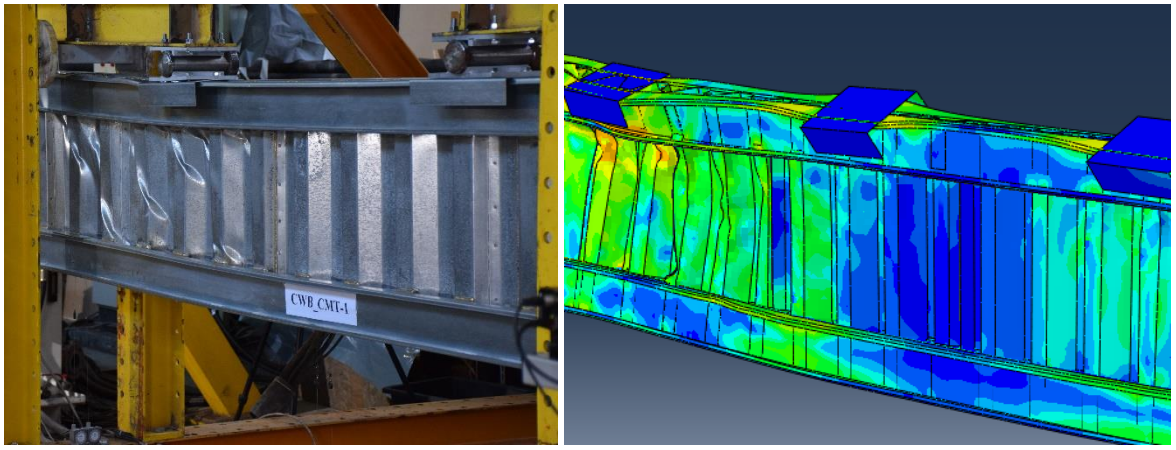

Figure 4.28 - c

Figure 4.28: Failure mode comparison between test and simulation for CWB CMT-1 beam a) The entire beam; b) The shear panels; c) The corrugated web

The comparison of the force-displacement curves of CWB CMT-1 beam between numerical and experimental analyses is shown in Figure 4.27. Regarding the ultimate force, the result obtained from ABAQUS is higher than the one from the experiment, and also the beam in ABAQUS is stronger than the actual beam in term of stiffness. This is due to the fact that the way to assign the constraint condition between the beam components ("Tie" constraint) is not exactly the same as the way how CMT welds really connect the parts of the beam together. However, the FE simulation shows quite similar failure modes compared to the experimental test in the cases of the deformed shape of the beam, the buckling of the shear panel and the distortion of corrugated web (see Figure 4.28). In conclusion, the constraint condition of finite element model is needed to be reconsider in order to make a better matching between FEM and experiment in the case of CWB CMT-1 beam.

In summary, the comparison in terms of initial stiffness and maximum capacity between numerical and experimental analyses of three beams that have been tested in laboratory is displayed in Table 4.8. Good agreements were obtained in the cases of CWB SW-1 and CWB SW-2 beams in terms of both failure modes and force-displacement curves. Further modifications need to be done for the FE model in the case of CWB CMT-1 beam.

Table 4.8: Initial stiffness and ultimate load: FEM vs. experimental results

Beam type	$K_{0\text{-Exp}}$ (N/mm)	$K_{0\text{-FEM}}$ (N/mm)	$F_{max\text{-Exp}}$ (kN)	$F_{max\text{-FEM}}$ (kN)
CWB SW-1	16483.5	15543.5	283.8	256.3
CWB SW-2	15007.3	15099.1	276.0	265.7
CWB CMT-1	20973.4	36895.1	368.2	424.0

CHAPTER 5: CONCLUSIONS AND RECOMMENDATIONS

5.1. Conclusions

Within the WELLFORMED research project, carried out at the CEMSIG Research Center of the Politehnica University of Timisoara, a new experimental program is discussed in this thesis studied on built-up cold-formed steel beams, made of corrugated webs and back-to-back lipped channel profiles for flanges, connected by welding technique namely spot-welding and CMT (Cold metal transfer)-welding.

This thesis firstly presents the experimental results on small specimens subjected to shear, consisting of two layers of steel sheets, connected by spot welding and CMT welding, in order to investigate and characterize the behaviour of these joints. After that, based on the experimental results on small specimens, five full-scale beams have manufactured to be tested in order to evaluate their performance and demonstrate the feasibility of the proposed solution. However, there were three beams in which two beams used spot-welding technique and another one used CMT-welding technique to be tested in the laboratory due to the limitation of time. The process of the experiments can be hightlighted by the following points:

- The material characteristics including basic yield strength and ultimate strength were determined through the tensile test for different combinations of thicknesses. The adjustment of basic yield strength was made according to Chapter A.6.2 and A.6.3 of EN1993-1-3, and the ultimate strength was adjusted by following European Recommendations (ECCS_124, 2008). After that, the result was used to calculate the resistance for spot welds and CMT welds in the following chapters.
- For spot welds, both the capacity and the ductility obtained for the tested specimens are very good. It was observed that there are two types of failure modes for spot-welding specimens namely full button pullout (or nugget pullout) and interfacial fracture. The calculation of the resistance for spot weld loaded in shear was determined using Table 8.5, Chapter 8.4, EN1993-1-3, and it was taken to compare with the result obtained from the experiment.
- For CMT welds, the specimens used this technique witness higher capacity compared to spot-welding specimens with the same steel thicknesses. There are two types of failure modes for this type of specimens, included nearly weld fracture and breaking out of heat affected zone. The design resistance of CMT welded connection was determined in

accordance with formula 8.4c in Chapter 8.5.2, EN1993-1-3. And a good agreement can be seen from the comparison between the theoretical and experimental results for CMT-welding specimens.

- The corrugated-web beams used welding technique bring huge advantage due to provide higher values in terms of both ultimate load and initial stiffness in comparison with the corrugated-web beams used self-drilling screws.

In the second part of the thesis, the experimental research was followed by numerical simulations, and parametric studies were carried out to see the limits of the system. Some conclusions can be drawn as follwing:

- CMT-welding beams provide higher capacity compared to spot-welding beams.
- For simulation of spot-welding beams, the load-bearing capacity of the beam was affected by the shear panels. It is increased with the increase in the thickness of the shear panels.
- For simulation of CMT-welding beams, both the thickness of shear panels and the thickness of outer corrugated sheets have an effect on the capacity of the beam. The thicker outer corrugated sheet or shear panel is, the higher value of load-bearing capacity is.
- Parametric study was implemented by changing some parameters of the beam such as thickness of shear panels and thickness of corrugated web in order to see how the beams behave. A general conclusion can be drawn that the load-bearing capacity of the beams will get higher if the corrugated webs or shear panels get thicker.
- It can also be seen that a very good agreement was obtained between numerical models and experimental ones in the case of the beams CWB SW-1 and CWB SW-2, in terms of both failure modes and load - displacement curves.

5.2. Recommendations

Finally, although the results look promising, significant works still have to be done in order to investigate, validate and optimize such a solution for mass production, i.e.:

- To continue to perform the experimental test for the rest of CMT-welding beams and take comparison with numerical simulations.
- To optimize the arrangement/distribution of welding connections by parametric study.

The results are encouraging and demonstrating the potential of this solution for standardization and industrial manufacturing.

REFERENCES

[1] EN 1993-1-5, Eurocode 3: Design of steel structures - Part 1-5: Plated structural elements, CEN, Brussels, 2006.

[2] EN 1993-1-1, Eurocode 3: Design of steel structures - Part 1-1: General rules and rules for buildings, CEN, Brussels, 2005.

[3] EN 1993-1-3, Eurocode 3: Design of steel structures - Part 1-3: General Rules. Supplementary rules for cold-formed thin gauge members and sheeting, CEN, Brussels, 2006.

[4] Zhao W. Behaviour and design of cold-formed steel hollow flange sections under axial compression. (PhD thesis). Brisbane, Australia: School of Civ. Eng., Queensland Univ.; 2005.

[5] Wanniarachchi S. Flexural behaviour of cold-formed steel beams with rectangular hollow flanges. (PhD thesis). Brisbane, Australia: School of Civ. Eng., Queensland University; 2005.

[6] Landolfo R, Mammana O, Portioli F, Di Lorenzo G, Guerrieri MR. Laser welded built-up cold-formed steel beams: experimental investigations. Thin-Walled Struct 2008;46(7-9):781–91.

[7] Elgaaly M., Dagher H.: Beams and girders with corrugated webs. In: Proceedings of the SSRC annual technical session. St. Louis, MO; 1990.

[8] Smith D. Behavior of corrugated plates subjected to shear. (MSc thesis). Orono, ME: Dept. of Civil Engineering, University of Maine; 1992.

[9] Hamilton R. Behavior of welded girders with corrugated web. (Ph.D. thesis). Orono, ME: Dept. of Civ. Engr., Univ. of Maine; 1993.

[10] Elgaaly M, Hamilton R, Seshadri A. Shear Strength of Beams with Corrugated Webs. J Struct Eng ASCE, 122; 1996.

[11] Luo R, Edlund B. Numerical simulation of shear tests on plate girders with trapezoidally corrugated webs. Sweden: Div. Steel and Timber Structures, Chalmers Univ. of Tech.; 1995.

[12] Elgaaly, M., Seshadri, A., Hamilton, R. W.: Bending strength of steel beams with corrugated webs. Journal of Structural Engineering, ASCE, vol. 123, 1997, No. 6, pp. 772–782.

[13] Chan CL, Khalid YA, Sahari BB, Hamouda AMS. Finite element analysis of corrugated web beams under bending. J Constr Steel Res 2002;58:1391–406.

[14] Johnson R, Cafolla J. Local flange buckling in plate girders with corrugated webs. Proc Inst Civil Eng Struct Build 1997:148–56.

[15] Lindner J. Lateral-torsional buckling of beams with trapezoidally corrugated webs. In: Proc of the fourth international colloquium on stability of steel structures. Budapest, Hungary; 1990.

[16] Jiho M, Jong W, Byung HC, Hak-Eun L. Lateral-torsional buckling of I-girder with corrugated webs under uniform bending. Thin Walled Struct. 2009. p. 21–30.

[17] Moon J, Yi JW, Choi BH, Lee HE. Lateral-torsional buckling of I-girder with corrugated webs under uniform bending. Thin-Walled Struct 2009;47:21–30.

[18] Pasternak H., Robra J., Kubieniec G. New proposals for EN 1993-1-5, Annex D: plate girders with corrugated webs. In: Codes in structural engineering, joint IABSE-fib conference, 2, 1365-1372, Dubrovnik, Croatia; 2010.

[19] Pasternak H., Kubieniec G. Flange buckling of sinusoidal corrugated girders. In: Int. Conf. in thin walled structures - ICTWS2011. Timisoara, Romania; 5-7.09.2011. 625-633; 2011.

[20] Moon J, Lim NH, Lee HE. Moment gradient correction factor and inelastic flexural torsional buckling of I-girder with corrugated steel webs. ThinWalled Struct 2013;62:18–27.

[21] Leiva-Aravena L., Edlund B. Buckling of trapezoidally corrugated webs. In: Proceedings of the ECCS colloquium on stability of plates and shells. Ghent, Belgium; 1987.

[22] Elgaaly M, Seshadri A. Girders with corrugated webs under partial compressive edge loading. J Struct Eng ASCE 1997;123(6):783–91.

[23] Luo R, Edlund B. Ultimate strength of girders with trapezoidally corrugated webs under patch loading. Thin-Walled Struct 2006;24:135–56.

[24] Nguyen ND, Han SR, Kim JH, Kim SN, Kang YJ. Moment modification factors of I-girder with trapezoidal web corrugations under moment gradient. ThinWalled Struct 2012;57:1–12.

[25] Tahir M, Sulaiman A, Anis S. Experimental tests on composite and noncomposite connections using trapezoid web profiled steel sections. Steel Struct 2008;8:43–58.

[26] Kövesdi B, Jáger B, Dunai L. Stress distribution in the flanges of girders with corrugated webs. J Constr Steel Res 2012;79:204–15.

[27] Neagoie B., Ungureanu V., Dubina D. Beams with cold-formed steel sections for flanges and corrugated web. In: Stability and ductility of steel structures recent research. Academic days; 27 May 2005, Timisoara, Romania, 978-973-661-977-9, 57-70 (in Romanian).

[28] Prefabricated steel structures for low-rise buildings in seismic areas (Precasteel), final report. isbn: 978-92-79-29011-4, Research Fund for Coal and Steel, RFSR-CT-2007-00038; 2013.

[29] D. Dubina, V. Ungureanu, L. Gîlia, Experimental investigations of cold-formed steel beams of corrugated web and built-up section for flanges, Thin-Walled Structures 90 (2015) 159-170.

[30] D. Dubina, V. Ungureanu, L. Gîlia, Cold-formed steel beams with corrugated web and discrete web-to-flange fasteners, Steel Construction, 6(2) (2013) 74-81.

[31] P. Briskham, N. Blundell, L. Han, R. Hewitt, K. Young, D. Boomer, Comparison of self-pierce riveting, resistance spot welding and spot friction joining for aluminium automotive sheet, SAE 2006 Congress, Technical paper, 2006-01-0774, 2006.

[32] G. Snow, Strength of arc spot welds made in single and multiple steel sheets, MsC Thesis, Blacksburg, Virginia, USA, 2008.

[33] Milwaukee, Wisconsin, Spot welding techical information, Title-spot welders, inc.

[34] J. Radakovic, M. Tumuluru, Predicting Resistance Spot Weld Failure Modes in Shear Tension Tests of Advanced High-Strength Automotive Steels, Welding Journal, 87 (2008) 96-105.

[35] M. Pouranvari, P. Marashi, M. Goodarzi, A. Abedi, An analytical model predicting failure mode of resistance spot welds, Metal 2008, 13. – 15. 5. 2008, Hradec nad Moravicí.

[36] M. Pouranvari, P. Marashi, M. Goodarzi, A. Abedi, Failure Mode Transition in AISI 304 Resistance Spot Welds, Welding Journal.

[37] Y.J. Chao, Failure mode of spot welds: interfacial versur pullout, Department of Mechanical Engineering University of South Caroline, Columbia, 2003 IoM Communications Ltd.

[38] Y.J. Chao, Ultimate Strength and Failure Mechanism of Resistance Spot Weld Subjected to Tensile, Shear or Combined Tensile/Shear Loads, Journal of Engineering Materials and Technology, 125 (2003) 125-132.

[39] E. Rusinski, A. Kopczynski, J. Czmochowskia, Tests of thin-walled beams joined by spot welding, Journal of Materials Processing Technology, 157–158 (2004) 405–409.

[40] Premium Automotive Research and Development Project (PARDP), Cold Metal Transfer (CMT) Brazing of Galvanised Steel Sheets, PARDP (C. Pickin) / AJT (mshergo1), 14/02/2017.

[41] R. Cao, J. Y. Yu, J. H. Chen, Pei-Chung Wang, Feasibility of Cold-Metal-Transfer Welding Magnesium AZ31 to Galvanized Mild Steel, Welding Journal, September 2013, Vol. 92.

[42] Janusz Rykała, Tomasz Pfeifer, Robotised CMT welding of 6xxx series aluminium alloys, Research by NC, No. 6/2013.

[43] Sriwongras Piyapong, dostal Petr, Effetc of corrosion process on mechanical properties and acoustic emission characteristics of Al/Zinc-coated steel welded by cold metal transfer, Mendel Net 2015.

[44] Lin Jian, Ma Ninshu, Lei Yongping, Murakawa Hidekazu, Investigation of interface layer failure and shear strength of CMT brazed lap joints in dissimiliar materials, Transactions of JWRI, Vol. 40 (2011), No.1.

[45] S. Kodama, Y. Ishida, S. Furusako, M. Saito, Y. Miyazaki, T. Nose, Arc Welding Technology for Automotive Steel Sheets, Nippon Steel Technical Report, No. 103, 2013, pp. 83-90.

[46] International standard ISO 6892-1, Metallic materials - Tensile testing - Part 1: Method of test at room temperature, First edition 2009-08-15.

APPENDIX A: PRE- AND POST- STATUS OF SPECIMENS FOR TENSILE TEST

This section consists of the figures to show the status of all specimens before and after performing the tensile test for six different combination of thickness, including 0.8 mm, 1.0 mm, 1.2 mm, 1.5 m, 2.0 mm and 2.5 mm. Each specimen is denoted in the format as "T - Norminal thickness - Number".

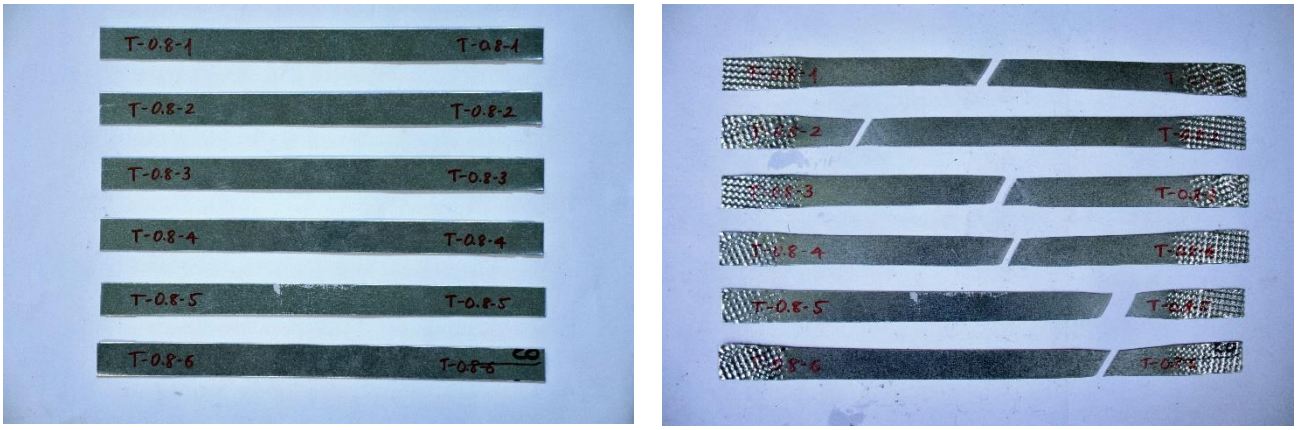

Figure A.1: Status of T-0.8 specimens before and after the tensile test

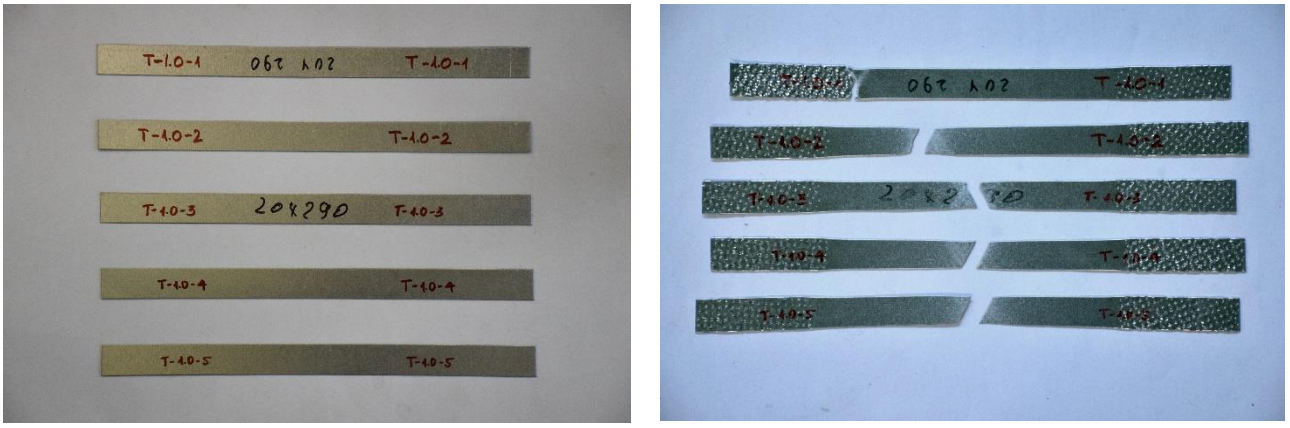

Figure A.2: Status of T-1.0 specimens before and after the tensile test

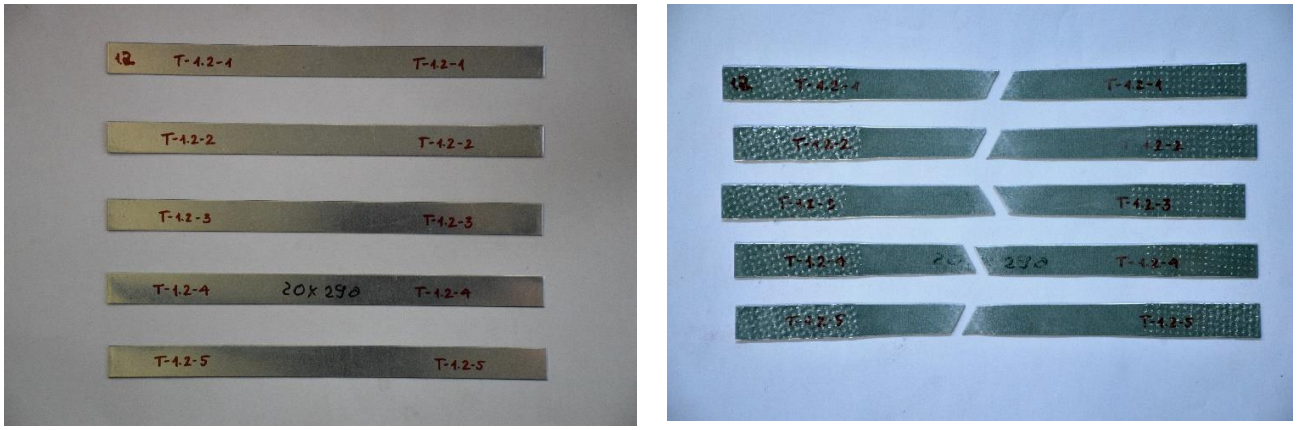

Figure A.3: Status of T-1.2 specimens before and after the tensile test

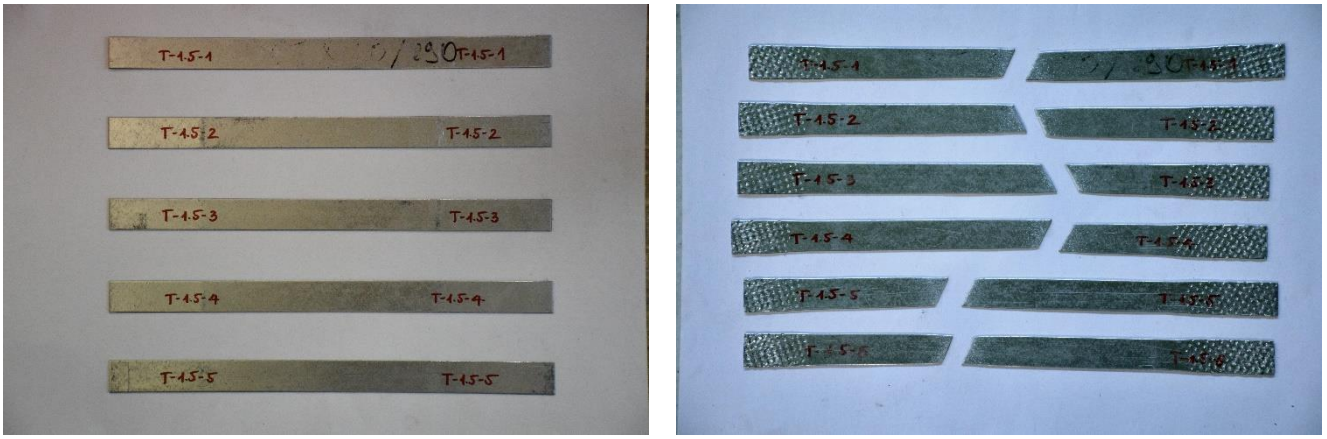

Figure A.4: Status of T-1.5 specimens before and after the tensile test

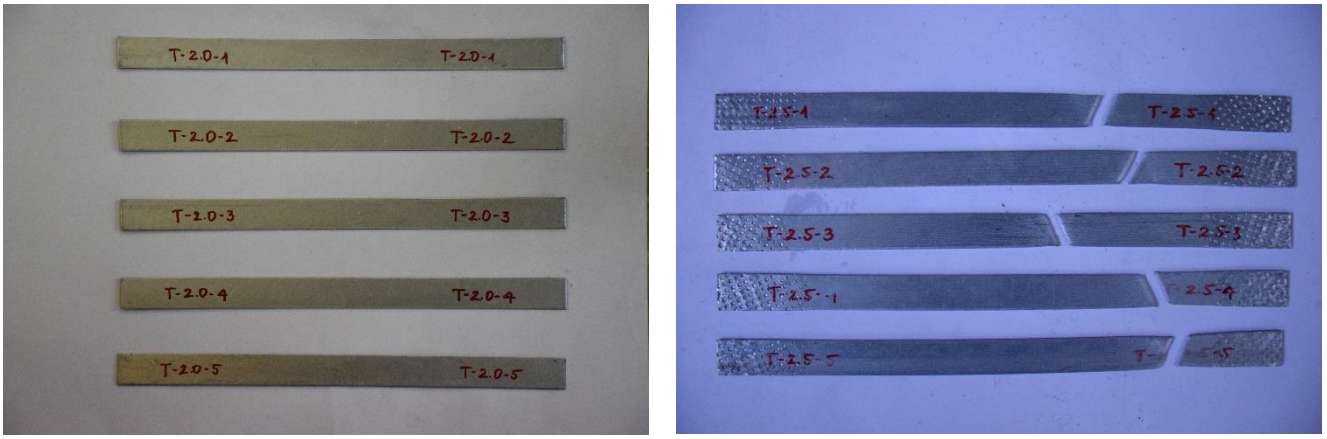

Figure A.5: Status of T-2.0 specimens before and after the tensile test

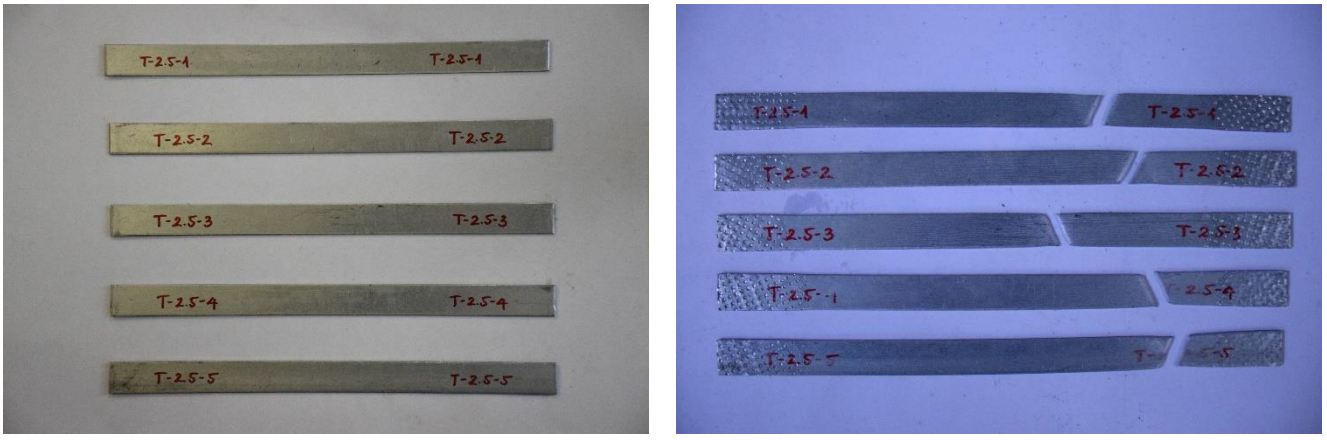

Figure A.6: Status of T-2.5 specimens before and after the tensile test

APPENDIX B: EVALUATION OF TENSILE TEST RESULTS

This section displays the evaluation of test results under static loads according to European Recommendations (ECCS_124, 2008) for the ultimate strength and according to EN1993-1-3 for the basic yield strength. All equations used to calculate are provided in Chapter 3.1.4 of this thesis.

Table B.1: Characteristic value of yield strength for series of 0.8 mm

Specimens	t_1 (mm)		b_1 (mm)		f_{yb} (MPa)						
	$t_{1,obs}$	δ	$b_{1,obs}$	δ	$f_{yb,obs}$	δ	α	β	μ_R	$f_{yb,adj}$	R_k
T - 0.8 - 1	0.82	2.04%	21.45	6.76%	283.57	1.26%	1	2	1.058	268.11	266.65
T - 0.8 - 2	0.80	-0.42%	21.61	7.44%	277.47	-0.91%	0	1	0.996	278.70	
T - 0.8 - 3	0.80	-0.42%	21.56	7.24%	279.87	-0.05%	0	1	0.996	281.11	
T - 0.8 - 4	0.79	-0.84%	21.61	7.45%	282.98	1.05%	1	1	1.002	282.48	
T - 0.8 - 5	0.80	0.00%	20.64	3.09%	277.07	-1.06%	0	1	1.000	277.07	
T - 0.8 - 6	0.80	-0.42%	21.83	8.38%	277.70	-0.83%	0	1	0.996	278.92	
Mean value	0.80		21.45		279.78					277.73	
Nominal value	0.80		20.00		280.00					280.00	
Standard deviation	8.43E-03		0.42		2.88					5.08	
Variance	7.11E-05		0.17		8.32					25.85	

Table B.2: Characteristic value of ultimate strength for series of 0.8 mm

Specimens	t_1 (mm)		b_1 (mm)		f_u(MPa)					
	$t_{1,obs}$	δ	$b_{1,obs}$	δ	$f_{u,obs}$	δ	α	μ_R	$f_{u,adj}$	R_k
T - 0.8 - 1	0.82	2.04%	21.45	6.76%	365.36	1.47%	1	1.037	352.27	350.98
T - 0.8 - 2	0.80	-0.42%	21.61	7.44%	360.08	0.02%	1	0.996	361.59	
T - 0.8 - 3	0.80	-0.42%	21.56	7.24%	362.03	0.56%	1	1.001	361.59	
T - 0.8 - 4	0.79	-0.84%	21.61	7.45%	365.87	1.60%	1	1.007	363.19	
T - 0.8 - 5	0.80	0.00%	20.64	3.09%	358.15	-0.52%	0	1.000	358.15	
T - 0.8 - 6	0.80	-0.42%	21.83	8.38%	359.05	-0.26%	0	0.996	360.63	
Mean value	0.80		21.45		361.76				359.57	
Nominal value	0.80		20.00		360.00				360.00	
Standard deviation	0.01		0.42		3.26				3.94	
Variance	7.11E-05		0.17		10.63				15.52	

Table B.3: Characteristic value of yield strength for series of 1.0 mm

Specimens	t_1 (mm)		b_1 (mm)		f_{yb} (MPa)						
	$t_{1,obs}$	δ	$b_{1,obs}$	δ	$f_{yb,obs}$	δ	α	β	μ_R	$f_{yb,adj}$	R_k
T - 1.0 - 1	1.01	0.99%	20.75	3.61%	278.06	-0.70%	0	2	1.021	272.36	269.18
T - 1.0 - 2	1.01	1.32%	20.59	2.85%	280.26	0.09%	1	2	1.029	272.38	
T - 1.0 - 3	1.00	0.33%	20.54	2.61%	282.79	0.99%	1	2	1.017	278.07	
T - 1.0 - 4	1.01	0.99%	20.83	3.97%	281.04	0.37%	1	2	1.025	274.26	
T - 1.0 - 5	1.00	0.33%	20.72	3.49%	283.04	1.08%	1	2	1.018	278.07	
T - 1.0 - 6	1.01	0.99%	20.91	4.35%	279.80	-0.07%	0	2	1.021	274.06	
T - 1.0 - 7	1.00	0.00%	21.25	5.88%	281.49	0.53%	1	1	1.005	280.00	
Mean value	1.01		20.80		280.93					275.60	
Nominal value	1.00		20.00		280.00					280.00	
Standard deviation	4.88E-03		0.24		1.74					3.07	
Variance	2.38E-05		0.06		3.03					9.43	

Table B.4: Characteristic value of ultimate strength for series of 1.0 mm

Specimens	t_1 (mm)		b_1 (mm)		f_u(MPa)					
	$t_{1,obs}$	δ	$b_{1,obs}$	δ	$f_{u,obs}$	δ	α	μ_R	$f_{u,adj}$	R_k
T - 1.0 - 1	1.01	0.99%	20.75	3.61%	370.65	2.87%	1	1.040	356.29	353.58
T - 1.0 - 2	1.01	1.32%	20.59	2.85%	370.96	2.95%	1	1.045	355.07	
T - 1.0 - 3	1.00	0.33%	20.54	2.61%	376.32	4.34%	1	1.049	358.75	
T - 1.0 - 4	1.01	0.99%	20.83	3.97%	372.57	3.37%	1	1.046	356.29	
T - 1.0 - 5	1.00	0.33%	20.72	3.49%	375.83	4.21%	1	1.048	358.75	
T - 1.0 - 6	1.01	0.99%	20.91	4.35%	371.85	3.19%	1	1.044	356.29	
T - 1.0 - 7	1.00	0.00%	21.25	5.88%	375.63	4.16%	1	1.043	360.00	
Mean value	1.01		20.80		373.40				357.35	
Nominal value	1.00		20.00		360.00				360.00	
Standard deviation	4.88E-03		0.24		2.45				1.81	
Variance	2.38E-05		0.06		6.00				3.26	

Table B.5: Characteristic value of yield strength for series of 1.2 mm

Specimens	t_1 (mm)		b_1 (mm)		f_{yb} (MPa)						
	$t_{1,obs}$	δ	$b_{1,obs}$	δ	$f_{yb,obs}$	δ	α	β	μ_R	$f_{yb,adj}$	R_k
T - 1.2 - 1	1.21	0.55%	20.80	3.85%	364.88	4.08%	1	2	1.055	346.01	342.56
T - 1.2 - 2	1.20	0.28%	20.99	4.72%	368.83	5.11%	1	2	1.060	348.00	
T - 1.2 - 3	1.20	0.28%	21.17	5.54%	367.99	4.89%	1	2	1.057	348.00	
T - 1.2 - 4	1.21	0.83%	20.77	3.71%	364.66	4.02%	1	2	1.060	344.04	
T - 1.2 - 5	1.21	0.55%	21.04	4.94%	365.88	4.34%	1	2	1.057	346.01	
Mean value	1.21		20.95		366.45					346.41	
Nominal value	1.20		20.00		350.00					350.00	
Standard deviation	2.79E-03		0.17		1.87					1.66	
Variance	7.78E-06		0.03		3.50					2.74	

Table B.6: Characteristic value of ultimate strength for series of 1.2 mm

Specimens	t_1 (mm)		b_1 (mm)		f_u(MPa)					
	$t_{1,obs}$	δ	$b_{1,obs}$	δ	$f_{u,obs}$	δ	α	μ_R	$f_{u,adj}$	R_k
T - 1.2 - 1	1.21	0.55%	20.80	3.85%	419.17	-0.20%	0	1.006	416.78	414.03
T - 1.2 - 2	1.20	0.28%	20.99	4.72%	422.14	0.51%	1	1.008	418.80	
T - 1.2 - 3	1.20	0.28%	21.17	5.54%	422.96	0.70%	1	1.010	418.80	
T - 1.2 - 4	1.21	0.83%	20.77	3.71%	418.89	-0.26%	0	1.009	415.31	
T - 1.2 - 5	1.21	0.55%	21.04	4.94%	420.25	0.06%	1	1.006	417.60	
Mean value	1.21		20.95		420.68				417.46	
Nominal value	1.20		20.00		420.00				420.00	
Standard deviation	2.79E-03		0.17		1.80				1.47	
Variance	7.78E-06		0.03		3.24				2.17	

Table B.7: Characteristic value of yield strength for series of 1.5 mm

Specimens	t_1 (mm)		b_1 (mm)		f_{yb} (MPa)						
	$t_{1,obs}$	δ	$b_{1,obs}$	δ	$f_{yb,obs}$	δ	α	β	μ_R	$f_{yb,adj}$	R_k
T - 1.5 - 1	1.51	0.66%	20.70	3.40%	408.86	14.40%	1	2	1.184	345.25	324.45
T - 1.5 - 2	1.52	1.32%	20.55	2.69%	412.18	15.09%	1	2	1.210	340.60	
T - 1.5 - 3	1.51	0.88%	20.75	3.61%	406.66	13.93%	1	2	1.183	343.69	
T - 1.5 - 4	1.54	2.60%	20.71	3.41%	402.97	13.14%	1	2	1.215	331.58	
T - 1.5 - 5	1.54	2.81%	20.77	3.71%	399.37	12.36%	1	2	1.210	330.11	
T - 1.5 - 6	1.51	0.66%	20.72	3.47%	408.43	14.31%	1	2	1.183	345.25	
Mean value	1.52		20.70		406.41					339.42	
Nominal value	1.50		20.00		350.00					350.00	
Standard deviation	0.02		0.08		4.58					6.87	
Variance	2.29E-04		0.01		20.97					47.16	

Table B.8: Characteristic value of ultimate strength for series of 1.5 mm

Specimens	t_1 (mm)		b_1 (mm)		f_u(MPa)					
	$t_{1,obs}$	δ	$b_{1,obs}$	δ	$f_{u,obs}$	δ	α	μ_R	$f_{u,adj}$	R_k
T - 1.5 - 1	1.51	0.66%	20.70	3.40%	509.43	17.56%	1	1.221	417.14	404.44
T - 1.5 - 2	1.52	1.32%	20.55	2.69%	499.43	15.90%	1	1.205	414.32	
T - 1.5 - 3	1.51	0.88%	20.75	3.61%	495.51	15.24%	1	1.191	416.20	
T - 1.5 - 4	1.54	2.60%	20.71	3.41%	484.11	13.24%	1	1.184	408.80	
T - 1.5 - 5	1.54	2.81%	20.77	3.71%	490.76	14.42%	1	1.203	407.89	
T - 1.5 - 6	1.51	0.66%	20.72	3.47%	511.69	17.92%	1	1.227	417.14	
Mean value	1.52		20.70		498.49				413.58	
Nominal value	1.50		20.00		420.00				420.00	
Standard deviation	0.02		0.08		10.68				4.19	
Variance	2.29E-04		0.01		114.00				17.60	

Table B.9: Characteristic value of yield strength for series of 2.0 mm

Specimens	t_1 (mm)		b_1 (mm)		f_{yb} (MPa)						
	$t_{1,obs}$	δ	$b_{1,obs}$	δ	$f_{yb,obs}$	δ	α	β	μ_R	$f_{yb,adj}$	R_k
T - 2.0 - 1	1.97	-1.52%	20.33	1.62%	420.51	16.77%	1	1	1.183	355.44	354.22
T - 2.0 - 2	1.96	-2.21%	20.33	1.61%	431.69	18.92%	1	1	1.206	357.91	
T - 2.0 - 3	1.97	-1.69%	20.34	1.69%	436.84	19.88%	1	1	1.227	356.06	
T - 2.0 - 4	1.96	-1.87%	20.34	1.69%	431.56	18.90%	1	1	1.210	356.67	
T - 2.0 - 5	1.96	-2.21%	20.33	1.62%	438.70	20.22%	1	1	1.226	357.91	
Mean value	1.96		20.33		431.86					356.80	
Nominal value	2.00		20.00		350.00					350.00	
Standard deviation	0.01		0.01		7.08					1.11	
Variance	3.56E-05		6.44E-05		50.16					1.22	

Table B.10: Characteristic value of ultimate strength for series of 2.0 mm

Specimens	t_1 (mm)		b_1 (mm)		f_u(MPa)					
	$t_{1,obs}$	δ	$b_{1,obs}$	δ	$f_{u,obs}$	δ	α	μ_R	$f_{u,adj}$	R_k
T - 2.0 - 1	1.97	-1.52%	20.33	1.62%	461.77	9.05%	1	1.083	426.53	425.06
T - 2.0 - 2	1.96	-2.21%	20.33	1.61%	466.07	9.88%	1	1.085	429.50	
T - 2.0 - 3	1.97	-1.69%	20.34	1.69%	468.48	10.35%	1	1.096	427.27	
T - 2.0 - 4	1.96	-1.87%	20.34	1.69%	460.87	8.87%	1	1.077	428.01	
T - 2.0 - 5	1.96	-2.21%	20.33	1.62%	465.09	9.70%	1	1.083	429.50	
Mean value	1.96		20.33		464.46				428.16	
Nominal value	2.00		20.00		420.00				420.00	
Standard deviation	0.01		0.01		3.13				1.33	
Variance	3.56E-05		6.44E-05		9.82				1.76	

Table B.11: Characteristic value of yield strength for series of 2.5 mm

Specimens	t_1 (mm)		b_1 (mm)		f_{yb} (MPa)						
	$t_{1,obs}$	δ	$b_{1,obs}$	δ	$f_{yb,obs}$	δ	α	β	μ_R	$f_{yb,adj}$	R_k
T - 2.5 - 1	2.50	0.13%	20.37	1.82%	377.57	7.30%	1	2	1.082	349.05	341.57
T - 2.5 - 2	2.50	-0.13%	20.44	2.17%	369.43	5.26%	1	1	1.054	350.47	
T - 2.5 - 3	2.50	-0.13%	20.44	2.17%	374.76	6.61%	1	1	1.069	350.47	
T - 2.5 - 4	2.51	0.27%	20.43	2.09%	378.87	7.62%	1	2	1.088	348.11	
T - 2.5 - 5	2.52	0.92%	20.53	2.60%	395.82	11.58%	1	2	1.152	343.45	
Mean value	2.51		20.44		379.29					348.31	
Nominal value	2.50		20.00		350.00					350.00	
Standard deviation	0.01		0.06		9.93					2.90	
Variance	1.20E-04		3.44E-03		98.52					8.39	

Table B.12: Characteristic value of ultimate strength for series of 2.5 mm

Specimens	t_1 (mm)		b_1 (mm)		f_u(MPa)					
	$t_{1,obs}$	δ	$b_{1,obs}$	δ	$f_{u,obs}$	δ	α	μ_R	$f_{u,adj}$	R_k
T - 2.5 - 1	2.50	0.13%	20.37	1.82%	455.64	7.82%	1	1.086	419.43	414.78
T - 2.5 - 2	2.50	-0.13%	20.44	2.17%	447.87	6.22%	1	1.065	420.57	
T - 2.5 - 3	2.50	-0.13%	20.44	2.17%	452.71	7.23%	1	1.076	420.57	
T - 2.5 - 4	2.51	0.27%	20.43	2.09%	455.71	7.84%	1	1.088	418.86	
T - 2.5 - 5	2.52	0.92%	20.53	2.60%	453.28	7.34%	1	1.089	416.05	
Mean value	2.51		20.44		453.04				419.10	
Nominal value	2.50		20.00		420.00				420.00	
Standard deviation	0.01		0.06		3.19				1.86	
Variance	1.20E-04		3.44E-03		10.20				3.44	

APPENDIX C: SPOT WELDING SPECIMENS

This section displays all detailed information regarding the measured dimensions, the load-displacement relationships, the pictures that shows status of specimens before and after the experimental test and the types of failure modes for some combinations of specimens connected by single spot welds.

Table B.13: Dimensions and failure modes of spot-welding specimens

Specimen	t_1	t_2	b_1	b_2	e_{11}	e_{12}	e_{21}	e_{22}	Failure mode
	mm	mm	mm	mm	mm	mm	mm	mm	
SW - 0.8 - 0.8 - 1S	0.81	0.80	27.40	27.36	17.46	22.84	12.98	13.97	Nugget pullout
SW - 0.8 - 0.8 - 2S	0.81	0.80	28.20	27.53	17.62	22.06	12.71	15.00	Nugget pullout
SW - 0.8 - 0.8 - 3S	0.80	0.80	28.06	27.12	19.59	20.32	12.47	14.94	Nugget pullout
SW - 0.8 - 0.8 - 4S	0.81	0.80	27.53	27.02	19.92	19.93	12.78	14.35	Nugget pullout
SW - 0.8 - 0.8 - 5S	0.80	0.80	27.54	27.33	20.75	18.85	12.81	14.36	Nugget pullout
SW - 0.8 - 0.8 - 6S	0.80	0.79	27.56	27.44	20.28	19.45	13.04	14.19	Nugget pullout
SW - 0.8 - 0.8 - 7S	0.81	0.81	27.58	27.08	19.96	19.46	12.30	14.54	Nugget pullout
SW - 0.8 - 1.0 - 1S	0.80	1.02	27.76	30.35	21.05	19.32	11.56	15.67	Nugget pullout
SW - 0.8 - 1.0 - 2S	0.81	1.01	27.40	30.20	20.82	18.91	13.30	13.65	Nugget pullout
SW - 0.8 - 1.0 - 3S	0.79	1.00	27.31	30.35	20.79	19.03	13.19	13.69	Nugget pullout
SW - 0.8 - 1.0 - 4S	0.79	0.99	27.40	30.44	21.42	18.65	13.15	13.94	Nugget pullout
SW - 0.8 - 1.0 - 5S	0.81	1.00	27.46	30.69	21.20	18.83	13.27	13.52	Nugget pullout
SW - 0.8 - 1.0 - 6S	0.81	1.01	27.30	30.70	20.60	19.13	13.38	13.40	Nugget pullout
SW - 0.8 - 1.0 - 7S	0.81	1.01	27.27	30.41	15.43	24.54	13.83	13.19	Nugget pullout
SW - 0.8 - 1.2 - 1S	0.80	1.21	27.78	33.32	21.67	18.02	13.56	13.75	Nugget pullout
SW - 0.8 - 1.2 - 2S	0.80	1.21	27.76	33.41	20.64	19.24	13.18	14.08	Nugget pullout
SW - 0.8 - 1.2 - 3S	0.79	1.22	27.29	33.24	20.97	18.69	12.74	13.96	Nugget pullout
SW - 0.8 - 1.2 - 4S	0.81	1.22	27.27	33.26	20.21	19.72	13.04	13.77	Nugget pullout
SW - 0.8 - 1.2 - 5S	0.80	1.21	27.13	33.26	19.46	20.12	13.29	13.58	Nugget pullout
SW - 0.8 - 1.2 - 6S	0.81	1.20	27.27	33.32	18.41	21.09	12.90	13.65	Nugget pullout
SW - 0.8 - 1.2 - 7S	0.79	1.20	27.68	33.33	19.48	20.13	13.61	13.71	Nugget pullout
SW - 0.8 - 1.5 - 1S	0.80	1.54	27.40	37.32	22.48	17.48	11.01	15.54	Nugget pullout
SW - 0.8 - 1.5 - 2S	0.81	1.54	27.64	37.32	21.87	17.78	12.51	14.53	Nugget pullout
SW - 0.8 - 1.5 - 3S	0.81	1.55	27.49	37.19	20.91	19.21	13.50	13.51	Nugget pullout
SW - 0.8 - 1.5 - 4S	0.80	1.54	27.47	37.15	20.45	19.56	13.10	13.83	Nugget pullout
SW - 0.8 - 1.5 - 5S	0.79	1.54	27.45	37.22	21.30	18.17	12.85	14.38	Nugget pullout
SW - 0.8 - 1.5 - 6S	0.80	1.54	27.77	37.24	20.65	19.22	12.98	14.14	Nugget pullout
SW - 0.8 - 1.5 - 7S	0.81	1.53	27.49	37.23	20.53	19.15	13.14	13.97	Nugget pullout
SW - 0.8 - 2.0 - 1S	0.80	1.97	27.74	42.31	21.41	18.31	14.46	12.68	Nugget pullout
SW - 0.8 - 2.0 - 2S	0.84	2.00	27.10	42.25	19.45	20.75	13.82	12.82	Nugget pullout
SW - 0.8 - 2.0 - 3S	0.80	2.00	27.33	42.11	19.32	20.73	13.77	12.89	Nugget pullout

SW - 0.8 - 2.0 - 4S	0.79	1.94	27.13	42.08	19.97	19.95	14.29	12.34	Nugget pullout
SW - 0.8 - 2.0 - 5S	0.80	1.94	27.20	42.00	20.02	19.53	13.94	12.72	Nugget pullout
SW - 0.8 - 2.0 - 6S	0.80	1.96	27.58	42.45	19.51	20.06	14.38	12.92	Nugget pullout
SW - 0.8 - 2.0 - 7S	0.81	1.96	27.55	42.09	19.38	20.85	14.07	12.96	Nugget pullout
SW - 0.8 - 2.5 - 1S	0.80	2.51	27.39	42.51	22.39	17.39	13.68	13.53	Nugget pullout
SW - 0.8 - 2.5 - 2S	0.79	2.49	27.57	42.49	21.38	18.38	13.61	13.51	Nugget pullout
SW - 0.8 - 2.5 - 3S	0.79	2.48	27.23	42.43	21.16	18.62	21.12	18.71	Nugget pullout
SW - 0.8 - 2.5 - 4S	0.80	2.50	27.23	42.38	22.49	17.48	13.84	12.84	Nugget pullout
SW - 0.8 - 2.5 -5S	0.80	2.49	27.30	42.45	21.71	18.04	13.97	12.80	Nugget pullout
SW - 0.8 - 2.5 - 6S	0.80	2.50	27.38	42.51	21.72	18.12	13.58	13.40	Nugget pullout
SW - 0.8 - 2.5 - 7S	0.80	2.50	27.29	42.48	22.61	17.27	13.32	13.33	Nugget pullout
SW - 1.0 - 1.0 - 1S	1.01	1.01	30.66	30.38	24.29	25.83	15.03	15.49	Nugget pullout
SW - 1.0 - 1.0 - 2S	1.01	1.01	31.14	30.63	24.48	25.29	14.72	15.71	Nugget pullout
SW - 1.0 - 1.0 - 3S	1.01	1.01	30.41	30.46	25.15	25.20	14.92	15.27	Nugget pullout
SW - 1.0 - 1.0 - 4S	1.00	1.00	30.22	30.92	23.00	27.37	14.25	15.27	Nugget pullout
SW - 1.0 - 1.0 - 5S	1.01	1.00	30.27	30.64	24.30	25.60	14.85	14.92	Nugget pullout
SW - 1.0 - 1.0 - 6S	1.00	1.00	30.77	30.39	24.23	25.56	14.73	15.26	Nugget pullout
SW - 1.0 - 1.0 - 7S	1.00	0.99	30.97	30.48	25.15	25.08	14.49	15.67	Nugget pullout
SW - 1.0 - 1.2 - 1S	1.00	1.20	30.73	33.20	23.66	25.65	13.55	16.35	Nugget pullout
SW - 1.0 - 1.2 - 2S	1.01	1.20	30.60	33.23	30.70	19.14	13.51	16.27	Nugget pullout
SW - 1.0 - 1.2 - 3S	1.00	1.20	30.96	33.05	25.42	24.24	13.94	16.42	Nugget pullout
SW - 1.0 - 1.2 - 4S	1.00	1.21	30.48	33.21	27.54	22.13	13.58	16.57	Nugget pullout
SW - 1.0 - 1.2 - 5S	1.01	1.20	30.60	33.48	26.04	23.74	13.56	16.54	Nugget pullout
SW - 1.0 - 1.2 - 6S	1.00	1.21	31.03	33.22	25.45	23.89	13.80	16.76	Nugget pullout
SW - 1.0 - 1.2 - 7S	1.02	1.22	30.44	33.21	25.27	24.23	13.79	16.21	Nugget pullout
SW - 1.0 - 1.5 - 1S	1.01	1.54	30.49	37.26	25.48	23.61	15.59	14.51	Nugget pullout
SW - 1.0 - 1.5 - 2S	1.00	1.53	30.34	37.32	25.45	23.85	15.77	14.28	Nugget pullout
SW - 1.0 - 1.5 - 3S	1.01	1.54	30.34	37.33	25.19	24.72	15.88	13.84	Nugget pullout
SW - 1.0 - 1.5 - 4S	1.01	1.53	30.69	37.34	25.42	23.89	16.27	13.91	Nugget pullout
SW - 1.0 - 1.5 - 5S	1.01	1.53	30.48	37.18	25.11	25.19	15.91	14.18	Nugget pullout
SW - 1.0 - 1.5 - 6S	1.00	1.52	30.49	37.41	25.08	25.05	16.20	14.10	Nugget pullout
SW - 1.0 - 1.5 - 7S	1.01	1.53	30.33	37.35	24.78	24.85	16.40	13.53	Nugget pullout
SW - 1.0 - 2.0 - 1S	1.00	1.98	30.45	42.04	25.97	24.19	15.26	15.08	Nugget pullout
SW - 1.0 - 2.0 - 2S	1.00	1.99	30.38	42.42	26.44	22.82	15.81	14.37	Nugget pullout
SW - 1.0 - 2.0 - 3S	1.00	2.02	31.12	42.29	25.46	24.13	15.74	15.16	Nugget pullout
SW - 1.0 - 2.0 - 4S	1.01	1.98	30.85	42.04	26.31	23.50	15.72	14.76	Nugget pullout
SW - 1.0 - 2.0 - 5S	1.00	1.99	30.41	42.48	24.94	23.95	14.88	15.20	Nugget pullout
SW - 1.0 - 2.0 - 6S	1.03	2.00	30.29	42.20	26.43	23.41	15.22	14.86	Nugget pullout
SW - 1.0 - 2.0 - 7S	1.01	1.99	31.02	41.92	26.32	23.30	15.60	14.97	Nugget pullout
SW - 1.0 - 2.5 - 1S	1.01	2.50	30.69	42.53	26.85	22.46	15.43	14.74	Nugget pullout
SW - 1.0 - 2.5 - 2S	1.01	2.50	30.48	42.20	27.46	21.95	15.23	14.87	Nugget pullout

SW - 1.0 - 2.5 - 3S	1.00	2.49	30.66	41.52	26.49	22.83	15.47	14.69	Nugget pullout
SW - 1.0 - 2.5 - 4S	1.01	2.50	30.60	42.26	27.73	22.07	15.24	14.88	Nugget pullout
SW - 1.0 - 2.5 - 5S	1.01	2.53	30.26	42.28	26.24	23.23	15.65	14.41	Nugget pullout
SW - 1.0 - 2.5 - 6S	1.01	2.49	30.81	42.38	25.52	23.58	15.57	15.31	Nugget pullout
SW - 1.0 - 2.5 - 7S	1.00	2.49	30.40	42.26	26.76	23.36	15.65	14.43	Nugget pullout
SW - 1.2 - 1.2 - 1S	1.19	1.20	33.56	33.13	24.70	24.71	14.48	18.11	Nugget pullout
SW - 1.2 - 1.2 - 2S	1.20	1.20	33.27	33.10	23.60	25.67	14.65	18.09	Nugget pullout
SW - 1.2 - 1.2 - 3S	1.20	1.20	32.99	33.29	25.31	24.33	14.41	17.99	Nugget pullout
SW - 1.2 - 1.2 - 4S	1.20	1.20	33.25	33.23	25.62	24.04	14.94	17.55	Nugget pullout
SW - 1.2 - 1.2 - 5S	1.20	1.20	33.29	33.23	24.76	24.54	14.22	18.34	Nugget pullout
SW - 1.2 - 1.2 - 6S	1.20	1.21	33.26	33.01	25.21	23.81	14.76	17.71	Nugget pullout
SW - 1.2 - 1.2 - 7S	1.20	1.20	33.23	33.06	24.91	24.96	15.02	18.17	Nugget pullout
SW - 1.2 - 1.5 - 1S	1.21	1.54	32.85	37.18	25.50	23.64	17.02	15.56	Nugget pullout
SW - 1.2 - 1.5 - 2S	1.21	1.54	33.30	37.19	26.21	23.38	17.13	15.71	Nugget pullout
SW - 1.2 - 1.5 - 3S	1.21	1.55	33.07	37.12	26.00	24.05	17.09	15.46	Nugget pullout
SW - 1.2 - 1.5 - 4S	1.19	1.55	33.23	37.20	26.51	23.27	17.36	15.42	Nugget pullout
SW - 1.2 - 1.5 - 5S	1.20	1.53	33.44	37.30	26.58	22.95	17.12	15.83	Nugget pullout
SW - 1.2 - 1.5 - 6S	1.20	1.53	33.33	37.34	26.03	23.64	17.31	15.51	Nugget pullout
SW - 1.2 - 1.5 - 7S	1.20	1.53	33.24	37.21	26.38	23.19	17.17	15.44	Nugget pullout
SW - 1.2 - 2.0 - 1S	1.21	1.97	33.28	42.38	25.23	24.15	16.07	16.58	Nugget pullout
SW - 1.2 - 2.0 - 2S	1.21	1.97	33.46	42.31	27.55	22.86	16.29	16.73	Nugget pullout
SW - 1.2 - 2.0 - 3S	1.21	1.99	33.23	42.46	25.64	24.62	16.16	16.61	Nugget pullout
SW - 1.2 - 2.0 - 4S	1.20	1.97	33.27	42.44	26.33	22.98	16.51	16.35	Nugget pullout
SW - 1.2 - 2.0 - 5S	1.21	2.00	33.36	42.06	26.01	24.07	16.57	16.20	Nugget pullout
SW - 1.2 - 2.0 - 6S	1.20	1.98	33.23	42.28	25.43	23.59	16.40	16.37	Nugget pullout
SW - 1.2 - 2.0 - 7S	1.21	2.01	33.12	42.08	26.53	23.38	16.19	16.44	Nugget pullout
SW - 1.2 - 2.5 - 1S	1.20	2.51	33.36	42.31	25.98	23.17	16.64	16.29	Nugget pullout
SW - 1.2 - 2.5 - 2S	1.21	2.49	33.29	40.96	26.50	23.20	17.09	15.63	Nugget pullout
SW - 1.2 - 2.5 - 3S	1.21	2.50	33.24	42.45	27.01	22.33	16.09	16.61	Nugget pullout
SW - 1.2 - 2.5 - 4S	1.20	2.49	33.33	42.41	27.23	21.93	16.31	16.47	Nugget pullout
SW - 1.2 - 2.5 - 5S	1.20	2.52	33.37	42.47	26.53	23.22	16.56	16.28	Nugget pullout
SW - 1.2 - 2.5 - 6S	1.23	2.51	33.16	42.28	27.18	22.50	16.13	16.45	Nugget pullout
SW - 1.2 - 2.5 - 7S	1.21	2.50	33.31	42.29	26.36	23.01	16.19	16.59	Nugget pullout
SW - 1.5 - 1.5 - 1S	1.54	1.54	37.30	37.29	31.61	27.76	20.61	16.21	Interfacial fracture
SW - 1.5 - 1.5 - 2S	1.52	1.51	37.18	37.23	30.04	29.79	17.55	18.94	Interfacial fracture
SW - 1.5 - 1.5 - 3S	1.53	1.53	37.32	37.24	30.08	30.24	17.64	18.98	Interfacial fracture
SW - 1.5 - 1.5 - 4S	1.53	1.53	37.25	37.24	29.75	30.01	17.75	18.81	Interfacial fracture
SW - 1.5 - 1.5 - 5S	1.53	1.53	37.28	37.29	28.94	30.47	17.78	18.83	Interfacial fracture
SW - 1.5 - 1.5 - 6S	1.54	1.53	37.36	37.28	29.65	30.47	17.97	18.74	Interfacial fracture
SW - 1.5 - 1.5 - 7S	1.54	1.55	37.42	37.28	28.73	30.51	17.73	18.96	Interfacial fracture
SW - 1.5 - 1.5 - S1	1.54		37.42						Interfacial fracture

SW - 1.5 - 1.5 - S2	1.54		37.42						Interfacial fracture
SW - 1.5 - 1.5 - S3	1.54		37.42						Interfacial fracture
SW - 1.5 - 1.5 - S4	1.54		37.42						Interfacial fracture
SW - 1.5 - 1.5 - S5	1.54		37.26						Interfacial fracture
SW - 1.5 - 1.5 - S6	1.54		37.61						Interfacial fracture
SW - 1.5 - 1.5 - S7	1.54		37.34						Interfacial fracture
SW - 1.5 - 2.0 - 1S	1.55	2.01	37.29	42.61	31.40	28.35	18.46	18.48	Nugget pullout
SW - 1.5 - 2.0 - 2S	1.54	2.01	37.25	42.12	30.74	29.40	18.22	18.24	Interfacial fracture
SW - 1.5 - 2.0 - 3S	1.54	1.98	37.19	41.90	31.59	28.58	18.24	18.39	Nugget pullout
SW - 1.5 - 2.0 - 4S	1.54	2.00	37.17	42.33	31.72	27.23	18.56	18.36	Nugget pullout
SW - 1.5 - 2.0 - 5S	1.54	2.02	37.14	42.38	31.71	28.00	18.27	18.29	Nugget pullout
SW - 1.5 - 2.0 - 6S	1.55	1.98	37.24	42.08	30.88	28.60	18.31	18.33	Nugget pullout
SW - 1.5 - 2.0 - 7S	1.54	1.99	37.32	42.26	31.00	20.64	18.29	18.20	Nugget pullout
SW - 1.5 - 2.5 - 1S	1.52	2.52	37.48	42.39	31.57	27.57	18.82	18.22	Nugget pullout
SW - 1.5 - 2.5 - 2S	1.55	2.52	37.13	42.25	31.75	27.62	18.07	18.34	Nugget pullout
SW - 1.5 - 2.5 - 3S	1.54	2.51	37.28	42.57	31.59	27.84	18.42	18.43	Nugget pullout
SW - 1.5 - 2.5 - 4S	1.54	2.48	37.37	42.21	31.06	28.56	18.36	18.41	Nugget pullout
SW - 1.5 - 2.5 - 5S	1.54	2.50	37.24	42.42	31.06	28.42	18.26	18.25	Nugget pullout
SW - 1.5 - 2.5 - 6S	1.51	2.48	37.40	42.65	30.65	29.34	18.41	18.42	Nugget pullout
SW - 1.5 - 2.5 - 7S	1.54	2.51	37.31	42.33	32.31	27.51	18.15	18.32	Nugget pullout
SW - 2.0 - 2.0 - 1S	1.99	1.99	41.95	41.77	36.52	32.89	20.77	20.41	Interfacial fracture
SW - 2.0 - 2.0 - 2S	2.01	1.99	42.35	41.99	36.39	33.35	21.13	20.14	Interfacial fracture
SW - 2.0 - 2.0 - 3S	2.00	1.99	42.66	42.15	36.28	33.24	20.73	20.81	Interfacial fracture
SW - 2.0 - 2.0 - 4S	1.98	1.97	41.94	41.96	35.89	34.07	21.29	20.54	Interfacial fracture
SW - 2.0 - 2.0 - 5S	2.00	1.97	42.25	41.98	37.61	32.32	20.49	20.70	Interfacial fracture
SW - 2.0 - 2.0 - 6S	1.98	1.99	42.44	42.09	36.06	23.75	20.55	20.76	Interfacial fracture
SW - 2.0 - 2.0 - 7S	2.00	1.99	42.09	42.31	35.51	24.95	20.67	21.21	Interfacial fracture
SW - 2.0 - 2.0 - S1	2.00		42.09						Interfacial fracture
SW - 2.0 - 2.0 - S2	2.00		42.09						Interfacial fracture
SW - 2.0 - 2.0 - S3	2.00		42.09						Interfacial fracture
SW - 2.0 - 2.0 - S4	2.00		42.09						Interfacial fracture
SW - 2.0 - 2.0 - S5	2.00		41.66						Interfacial fracture
SW - 2.0 - 2.0 - S6	2.00		42.22						Interfacial fracture
SW - 2.0 - 2.0 - S7	2.00		41.95						Interfacial fracture
SW - 2.0 - 2.5 - 1S	1.97	2.49	42.61	42.77	35.99	33.18	20.34	21.24	Interfacial fracture
SW - 2.0 - 2.5 - 2S	1.99	2.51	42.28	42.77	36.25	32.49	20.48	20.89	Interfacial fracture
SW - 2.0 - 2.5 - 3S	2.00	2.52	42.37	42.07	36.63	32.91	21.27	21.08	Interfacial fracture
SW - 2.0 - 2.5 - 4S	1.99	2.51	42.22	42.84	36.01	33.64	20.49	21.04	Interfacial fracture
SW - 2.0 - 2.5 - 5S	1.99	2.50	42.36	42.55	36.31	34.20	20.75	20.76	Interfacial fracture
SW - 2.0 - 2.5 - 6S	1.99	2.49	42.35	42.07	36.26	33.62	21.14	20.20	Interfacial fracture
SW - 2.0 - 2.5 - 7S	2.01	2.49	42.20	42.04	36.22	33.99	21.39	20.50	Interfacial fracture

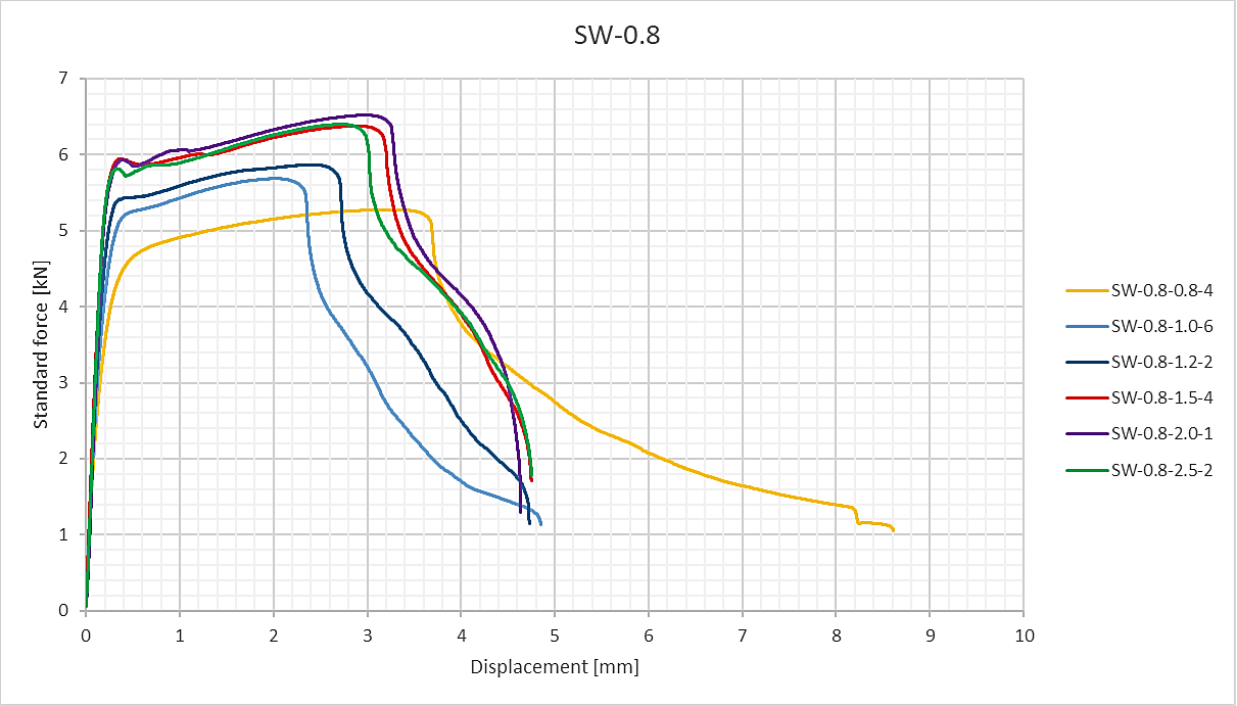

Figure B.1: Load-displacement curves of series SW-0.8

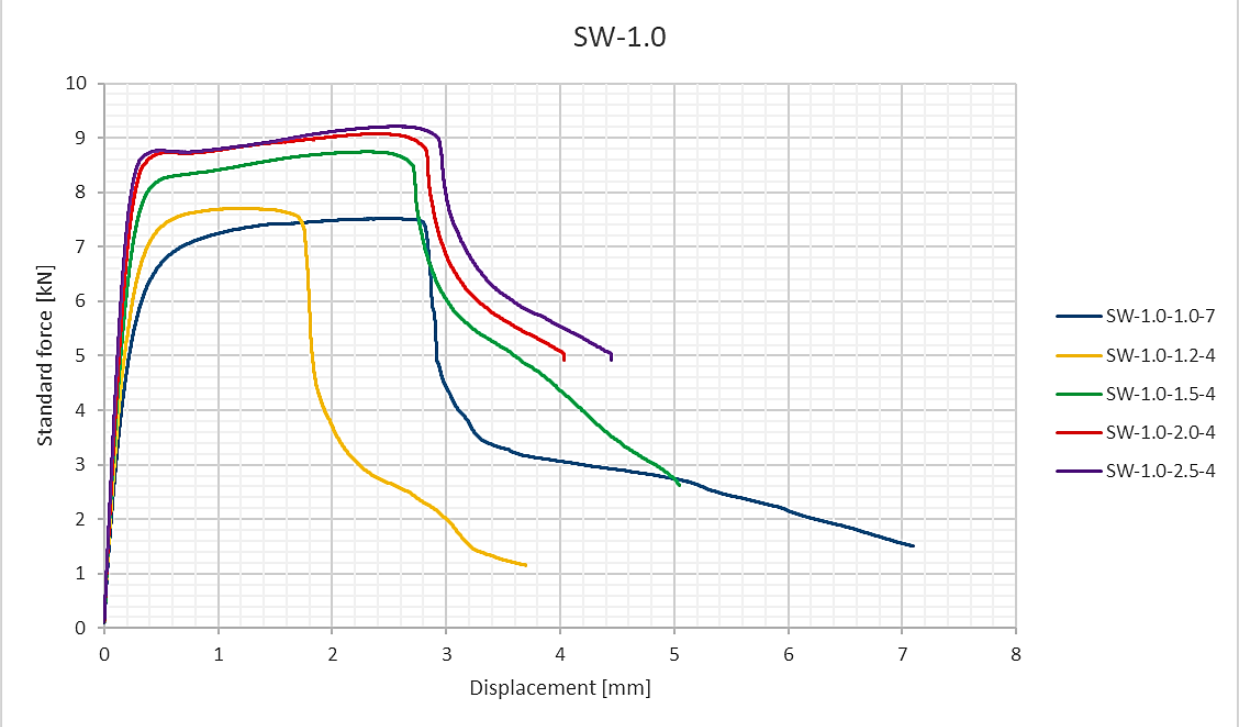

Figure B.2: Load-displacement curves of series SW-1.0

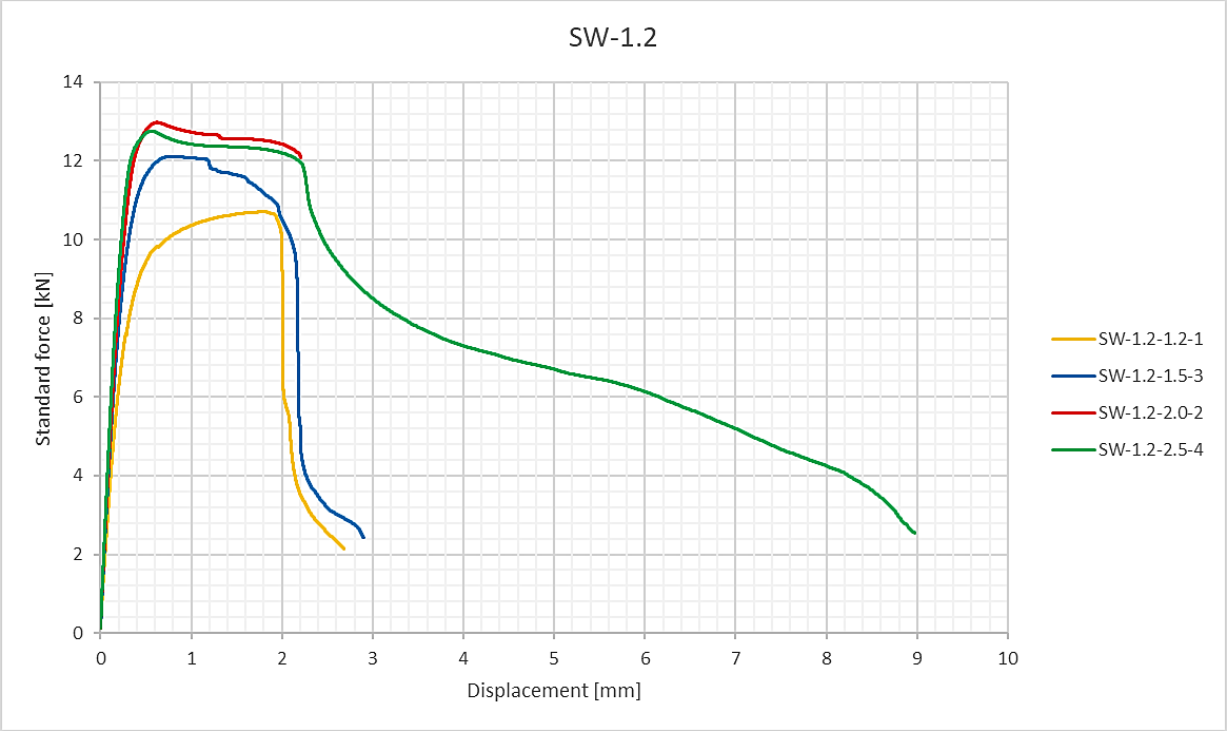

Figure B.3: Load-displacement curves of series SW-1.2

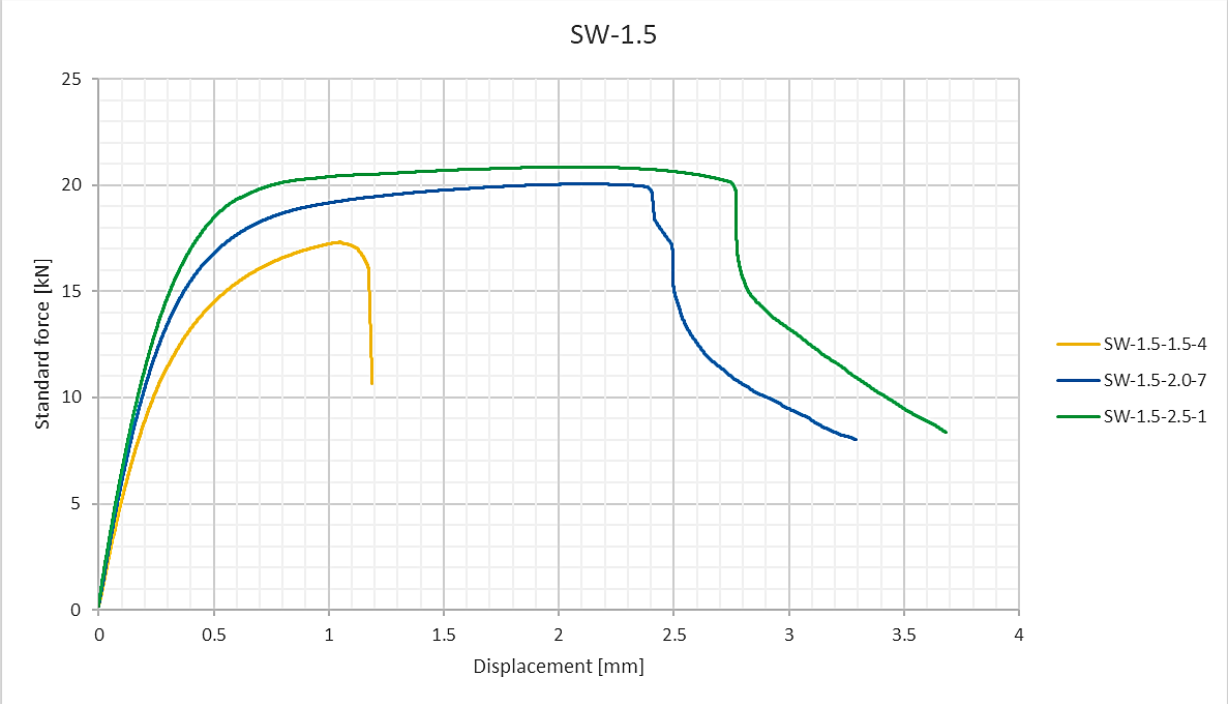

Figure B.4: Load-displacement curves of series SW-1.5

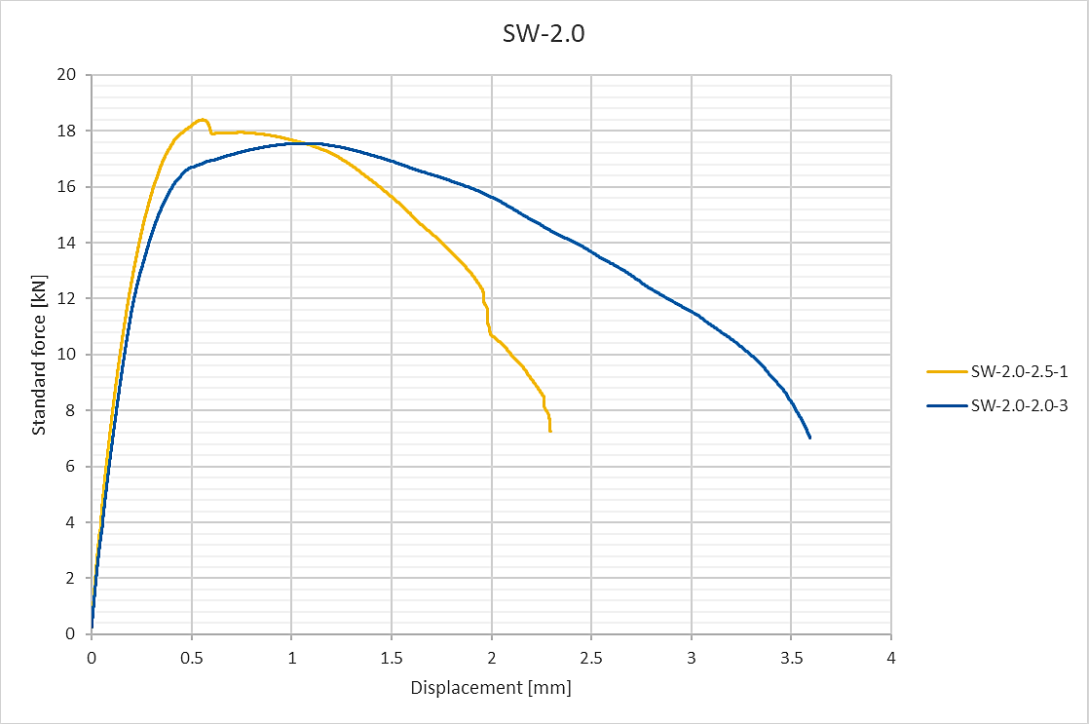

Figure B.5: Load-displacement curves of series SW-2.0

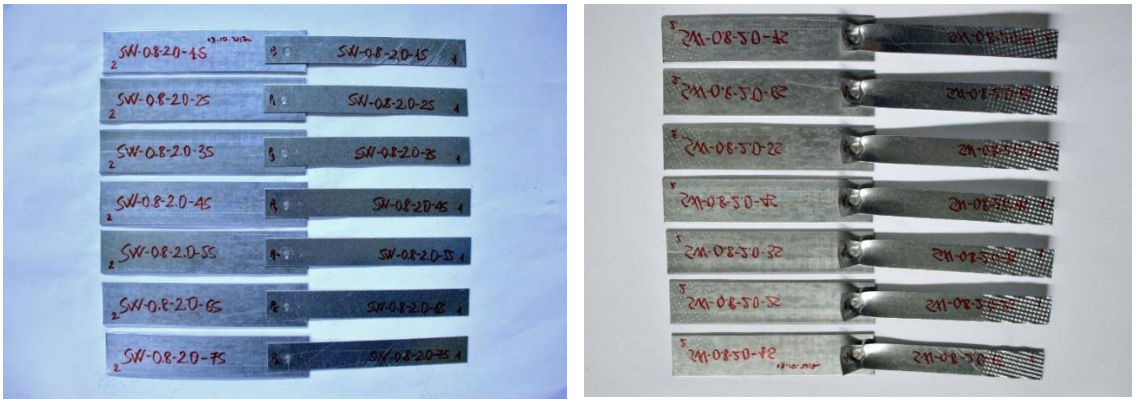

Figure B.6: SW-0.8-2.0 specimens before and after testing

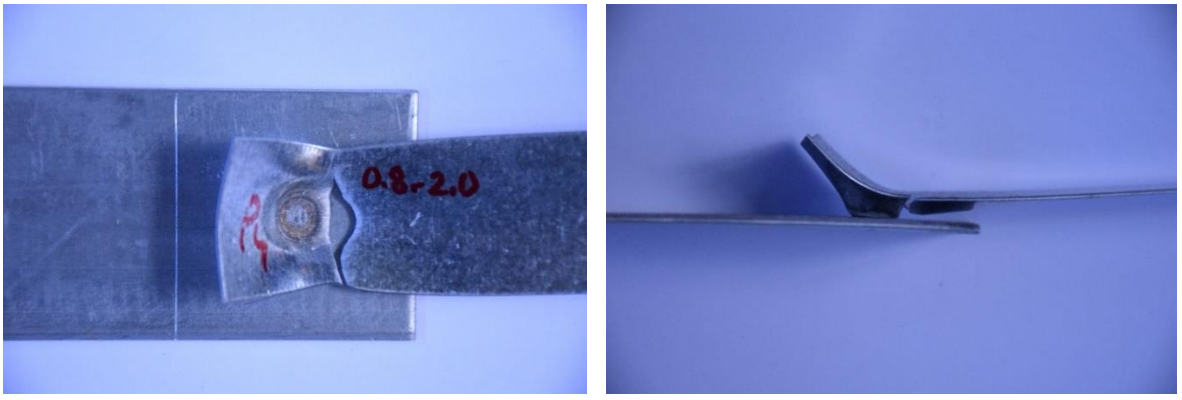

Figure B.7: Failure mode of SW-0.8-2.0 specimens

Figure B.8: SW-1.0-2.5 specimens before and after testing

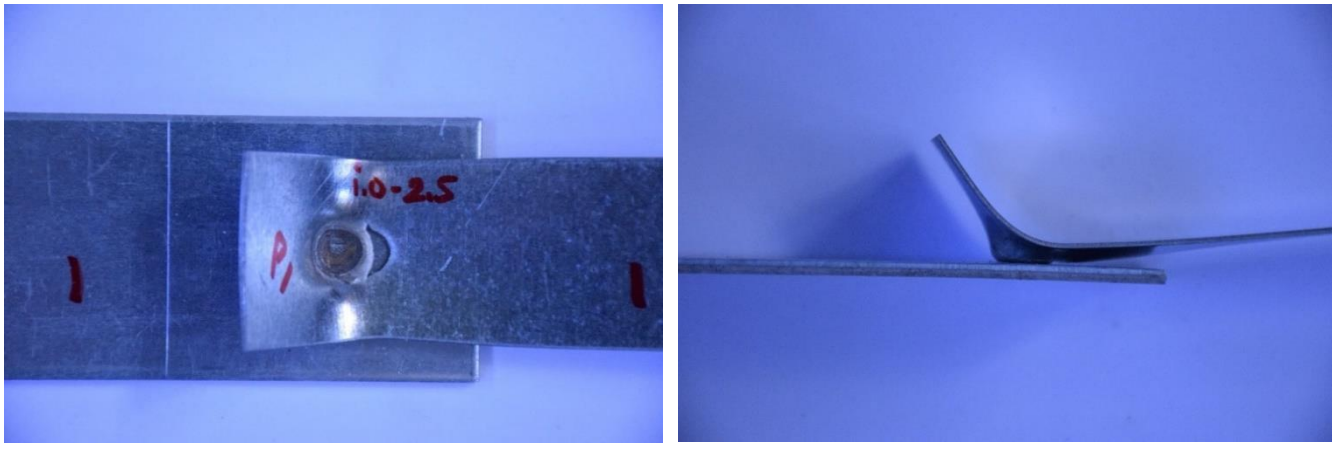

Figure B.9: Failure mode of SW-1.0-2.5 specimens

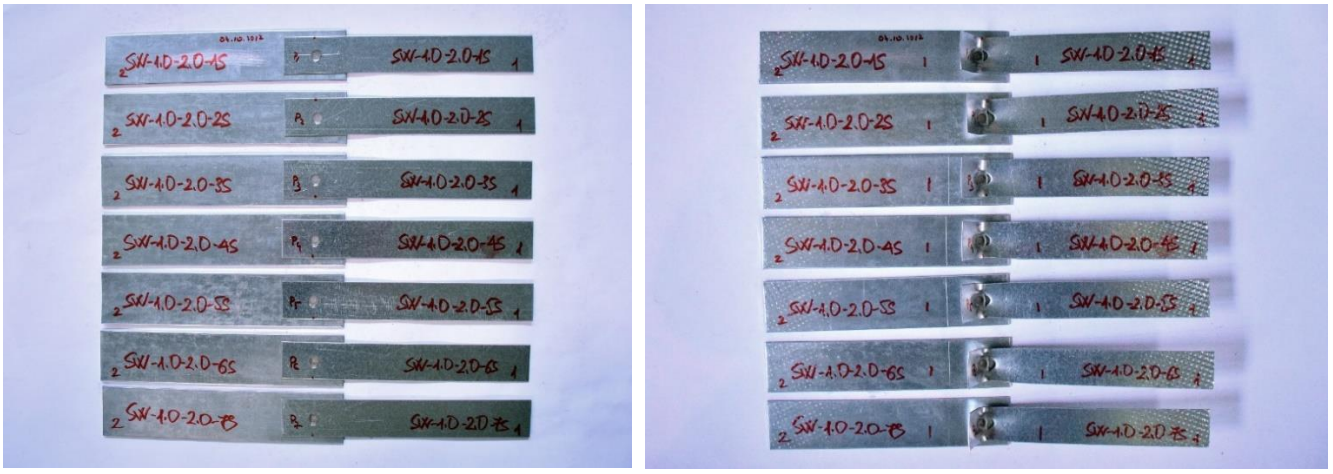

Figure B.10: SW-1.2-2.0 specimens before and after testing

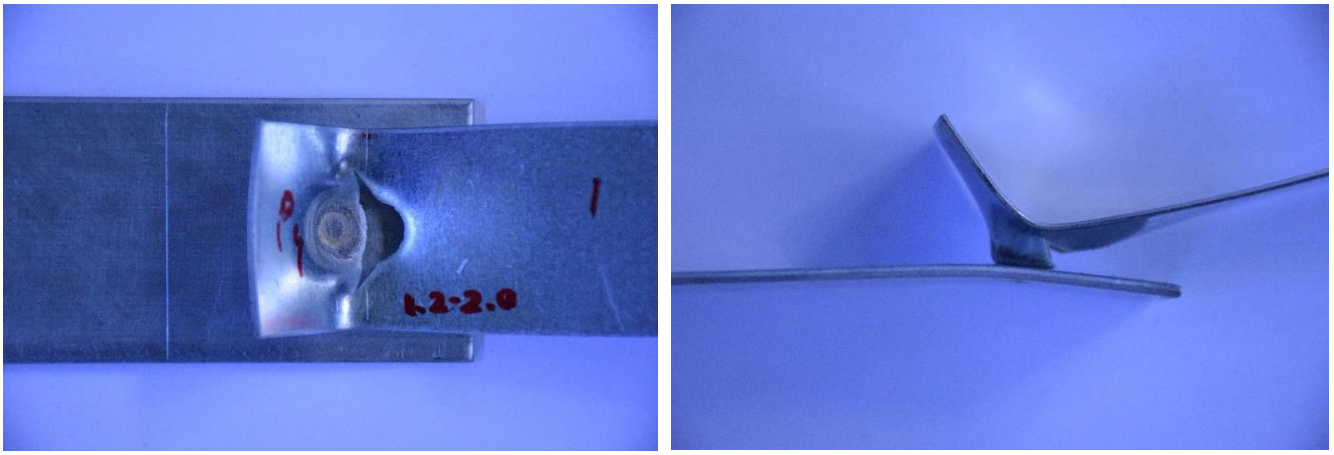

Figure B.11: Failure mode of SW-1.2-2.0 specimens

Figure B.12: SW-1.5-1.5 specimens before and after testing and failure mode

Figure B.13: SW-2.0-2.5 specimens before and after testing and failure mode

APPENDIX D: CMT WELDING SPECIMENS

This section displays all detailed information regarding the measured dimensions, the load-displacement relationships, the pictures that shows status of specimens before and after the experimental test and the types of failure modes for some combinations of specimens connected by CMT welds.

Table B.14: Dimensions and failure modes of CMT-welding specimens

Specimen	t_1	t_2	b_1	b_2	Failure mode
	mm	mm	mm	mm	
CMT-0.8-0.8-1	0.80	0.83	49.07	49.25	Near weld fracture
CMT-0.8-0.8-2	0.82	0.80	49.34	49.09	Near weld fracture
CMT-0.8-0.8-3	0.80	0.82	48.94	49.52	Near weld fracture
CMT-0.8-0.8-4	0.79	0.79	49.77	49.76	Near weld fracture
CMT-0.8-0.8-5	0.80	0.80	49.80	49.75	Near weld fracture
CMT-0.8-0.8-6	0.80	0.81	49.73	49.71	Near weld fracture
CMT-0.8-0.8-7	0.80	0.80	49.81	49.79	Near weld fracture
CMT-0.8-1.0-1	0.80	0.99	49.08	49.17	Near weld fracture
CMT-0.8-1.0-2	0.80	1.01	49.10	49.09	Near weld fracture
CMT-0.8-1.0-3	0.80	0.99	49.10	49.27	Near weld fracture
CMT-0.8-1.0-4	0.79	1.00	49.76	49.76	Near weld fracture
CMT-0.8-1.0-5	0.80	1.00	49.66	49.76	Breaking out of heat affected zone
CMT-0.8-1.0-6	0.80	0.99	49.69	49.72	Near weld fracture
CMT-0.8-1.0-7	0.81	1.00	49.62	49.72	Near weld fracture
CMT-0.8-1.2-1	0.77	1.20	49.47	49.18	Near weld breaking
CMT-0.8-1.2-2	0.80	1.20	49.12	49.14	Near weld breaking
CMT-0.8-1.2-3	0.80	1.21	49.20	49.19	Near weld breaking
CMT-0.8-1.2-4	0.79	1.20	49.73	49.90	Breaking out of heat affected zone
CMT-0.8-1.2-5	0.79	1.21	49.73	49.87	Near weld fracture
CMT-0.8-1.2-6	0.80	1.21	49.78	49.87	Near weld breaking
CMT-0.8-1.2-7	0.80	1.22	49.72	49.81	Near weld breaking
CMT-0.8-1.5-1	0.79	1.51	48.93	49.19	Near weld fracture
CMT-0.8-1.5-2	0.81	1.51	49.01	49.14	Breaking out of heat affected zone
CMT-0.8-1.5-3	0.79	1.49	49.07	49.04	Near weld fracture
CMT-0.8-1.5-4	0.80	1.50	49.85	49.73	Near weld breaking
CMT-0.8-1.5-5	0.80	1.49	49.81	49.71	Near weld fracture
CMT-0.8-1.5-6	0.81	1.51	49.77	49.71	Near weld fracture
CMT-0.8-1.5-7	0.80	1.49	49.77	49.73	Near weld breaking
CMT-0.8-2.0-1	0.81	2.03	49.07	49.00	Near weld fracture
CMT-0.8-2.0-2	0.81	2.03	49.00	49.08	Near weld fracture

CMT-0.8-2.0-3	0.81	2.02	49.01	48.98	Near weld fracture
CMT-0.8-2.0-4	0.80	2.01	49.83	50.06	Near weld fracture
CMT-0.8-2.0-5	0.81	2.00	49.67	49.90	Near weld breaking
CMT-0.8-2.0-6	0.81	2.00	49.67	49.93	Near weld breaking
CMT-0.8-2.0-7	0.80	2.01	49.74	50.01	Breaking out of heat affected zone
CMT-0.8-2.5-1	0.81	2.47	49.09	49.09	Near weld breaking
CMT-0.8-2.5-2	0.80	2.50	49.09	49.13	Near weld breaking
CMT-0.8-2.5-3	0.81	2.49	48.72	49.20	Breaking out of heat affected zone
CMT-0.8-2.5-4	0.81	2.49	49.69	49.69	Near weld fracture
CMT-0.8-2.5-5	0.82	2.50	49.82	49.74	Near weld fracture
CMT-0.8-2.5-6	0.80	2.50	49.69	49.66	Near weld fracture
CMT-0.8-2.5-7	0.81	2.49	49.72	49.62	Near weld fracture
CMT-1.0-1.0-1	1.03	1.03	49.20	49.35	Near weld fracture
CMT-1.0-1.0-2	1.02	1.01	49.22	49.35	Near weld fracture
CMT-1.0-1.0-3	1.02	1.05	49.16	49.31	Near weld fracture
CMT-1.0-1.0-4	1.00	1.01	49.85	49.76	Near weld fracture
CMT-1.0-1.0-5	1.01	1.01	49.82	49.69	Near weld fracture
CMT-1.0-1.0-6	1.01	1.01	49.78	49.76	Near weld fracture
CMT-1.0-1.0-7	1.00	1.00	49.84	49.87	Near weld fracture
CMT-1.0-1.2-1	1.02	1.19	49.87	49.58	Near weld fracture
CMT-1.0-1.2-2	1.01	1.20	49.77	49.78	Near weld fracture
CMT-1.0-1.2-3	1.00	1.21	49.88	49.67	Near weld fracture
CMT-1.0-1.2-4	1.01	1.20	49.88	49.77	Near weld fracture
CMT-1.0-1.2-5	1.01	1.21	49.82	49.75	Near weld fracture
CMT-1.0-1.2-6	1.00	1.21	49.75	49.65	Near weld fracture
CMT-1.0-1.2-7	1.00	1.21	49.84	49.78	Near weld fracture
CMT-1.0-1.5-1	0.98	1.46	49.23	49.18	Near weld fracture
CMT-1.0-1.5-2	1.00	1.45	49.50	49.45	Breaking out of heat affected zone
CMT-1.0-1.5-3	0.99	1.47	49.42	49.34	Near weld fracture
CMT-1.0-1.5-4	1.01	1.49	50.06	49.97	Near weld fracture
CMT-1.0-1.5-5	1.00	1.50	49.38	49.97	Near weld fracture
CMT-1.0-1.5-6	1.00	1.49	50.01	49.89	Near weld fracture
CMT-1.0-1.5-7	0.99	1.51	49.94	49.77	Near weld fracture
CMT-1.0-2.0-1	1.00	1.98	50.33	50.36	Near weld fracture
CMT-1.0-2.0-2	1.01	2.00	50.33	49.98	Near weld fracture
CMT-1.0-2.0-3	1.01	2.00	50.20	50.21	Near weld fracture
CMT-1.0-2.0-4	1.01	2.01	49.87	50.25	Near weld fracture
CMT-1.0-2.0-5	1.01	2.00	49.66	49.87	Breaking out of heat affected zone
CMT-1.0-2.0-6	1.00	2.00	49.64	49.80	Near weld fracture
CMT-1.0-2.0-7	1.00	2.00	49.69	49.90	Near weld fracture
CMT-1.0-2.5-1	1.03	2.48	50.08	49.94	Near weld fracture

CMT-1.0-2.5-2	1.01	2.49	50.12	50.20	Near weld fracture
CMT-1.0-2.5-3	1.05	2.52	50.01	50.07	Near weld fracture
CMT-1.0-2.5-4	1.00	2.45	50.03	50.06	Near weld fracture
CMT-1.0-2.5-5	0.99	2.47	50.02	50.03	Near weld fracture
CMT-1.0-2.5-6	1.00	2.48	50.06	50.09	Near weld fracture
CMT-1.0-2.5-7	1.01	2.45	50.07	50.01	Near weld fracture
CMT-1.2-1.2-1	1.22	1.25	49.38	49.50	Near weld fracture
CMT-1.2-1.2-2	1.21	1.22	49.31	49.26	Near weld fracture
CMT-1.2-1.2-3	1.22	1.24	49.37	49.46	Near weld fracture
CMT-1.2-1.2-4	1.20	1.19	49.56	49.72	Near weld fracture
CMT-1.2-1.2-5	1.19	1.19	49.78	49.63	Near weld fracture
CMT-1.2-1.2-6	1.20	1.18	49.54	49.68	Near weld fracture
CMT-1.2-1.2-7	1.21	1.20	49.68	49.64	Near weld fracture
CMT-1.2-1.5-1	1.21	1.52	49.24	49.39	Near weld fracture
CMT-1.2-1.5-2	1.22	1.53	49.31	49.39	Near weld fracture
CMT-1.2-1.5-3	1.23	1.52	49.47	49.52	Near weld fracture
CMT-1.2-1.5-4	1.20	1.49	49.43	49.77	Near weld fracture
CMT-1.2-1.5-5	1.21	1.49	49.60	49.77	Near weld fracture
CMT-1.2-1.5-6	1.20	1.50	49.59	49.74	Near weld fracture
CMT-1.2-1.5-7	1.20	1.48	49.55	49.76	Near weld fracture
CMT-1.2-2.0-1	1.20	1.96	49.34	49.30	Near weld fracture
CMT-1.2-2.0-2	1.20	2.01	49.43	49.31	Breaking out of heat affected zone
CMT-1.2-2.0-3	1.21	2.00	49.35	49.55	Near weld fracture
CMT-1.2-2.0-4	1.21	1.97	49.74	49.64	Near weld fracture
CMT-1.2-2.0-5	1.20	1.97	49.73	49.73	Near weld fracture
CMT-1.2-2.0-6	1.20	2.00	49.57	49.55	Near weld fracture
CMT-1.2-2.0-7	1.20	1.98	49.84	49.90	Near weld fracture
CMT-1.2-2.5-1	1.21	2.49	49.38	49.43	Near weld fracture
CMT-1.2-2.5-2	1.21	2.50	49.39	49.44	Near weld fracture
CMT-1.2-2.5-3	1.20	2.50	49.33	49.33	Near weld fracture
CMT-1.2-2.5-4	1.21	2.49	49.66	49.65	Near weld fracture
CMT-1.2-2.5-5	1.21	2.51	49.73	49.56	Near weld fracture
CMT-1.2-2.5-6	1.21	2.48	49.82	49.72	Near weld fracture
CMT-1.2-2.5-7	1.20	2.49	49.82	49.65	Near weld fracture
CMT-1.5-1.5-1	1.50	1.50	49.41	49.37	Near weld fracture
CMT-1.5-1.5-2	1.50	1.50	49.23	49.43	Breaking out of heat affected zone
CMT-1.5-1.5-3	1.50	1.49	49.16	49.33	Near weld breaking
CMT-1.5-1.5-4	1.51	1.51	49.69	49.78	Near weld fracture
CMT-1.5-1.5-5	1.51	1.49	49.91	49.71	Near weld fracture
CMT-1.5-1.5-6	1.50	1.52	49.74	49.82	Near weld fracture
CMT-1.5-1.5-7	1.50	1.51	49.77	49.82	Near weld fracture

CMT-1.5-2.0-1	1.47	1.95	49.87	49.90	Near weld fracture
CMT-1.5-2.0-2	1.47	1.99	50.01	50.12	Near weld fracture
CMT-1.5-2.0-3	1.50	2.03	49.86	49.86	Near weld fracture
CMT-1.5-2.0-4	1.49	2.00	49.76	49.83	Near weld fracture
CMT-1.5-2.0-5	1.50	2.00	49.59	49.75	Breaking out of heat affected zone
CMT-1.5-2.0-6	1.49	2.00	49.65	49.80	Near weld fracture
CMT-1.5-2.0-7	1.51	2.01	49.75	49.81	Near weld fracture
CMT-1.5-2.5-1	1.27	2.55	49.91	50.04	Near weld fracture
CMT-1.5-2.5-2	1.51	2.52	50.02	50.08	Near weld fracture
CMT-1.5-2.5-3	1.55	2.50	49.98	49.99	Near weld fracture
CMT-1.5-2.5-4	1.50	2.49	49.81	49.66	Breaking out of heat affected zone
CMT-1.5-2.5-5	1.50	2.49	49.65	49.64	Near weld fracture
CMT-1.5-2.5-6	1.50	2.48	49.72	49.66	Near weld fracture
CMT-1.5-2.5-7	1.51	2.50	49.72	49.78	Near weld fracture
CMT-2.0-2.0-1	1.96	1.96	49.95	49.76	Near weld fracture
CMT-2.0-2.0-2	2.00	1.99	50.16	49.55	Near weld fracture
CMT-2.0-2.0-3	1.99	1.97	50.00	49.61	Near weld fracture
CMT-2.0-2.0-4	2.00	1.99	49.89	49.93	Near weld fracture
CMT-2.0-2.0-5	2.00	2.00	50.07	50.09	Near weld fracture
CMT-2.0-2.0-6	2.00	2.00	49.99	50.04	Near weld fracture
CMT-2.0-2.0-7	2.00	1.99	49.93	50.03	Near weld fracture
CMT-2.0-2.5-1	2.01	2.54	49.96	49.38	Near weld fracture
CMT-2.0-2.5-2	2.02	2.50	49.83	49.88	Near weld fracture
CMT-2.0-2.5-3	2.00	2.48	49.81	49.11	Near weld fracture
CMT-2.0-2.5-4	1.93	2.49	50.02	49.74	Near weld fracture
CMT-2.0-2.5-5	1.94	2.49	49.95	49.93	Near weld fracture
CMT-2.0-2.5-6	1.93	2.51	49.98	49.73	Near weld fracture
CMT-2.0-2.5-7	1.93	2.50	49.63	49.88	Near weld fracture

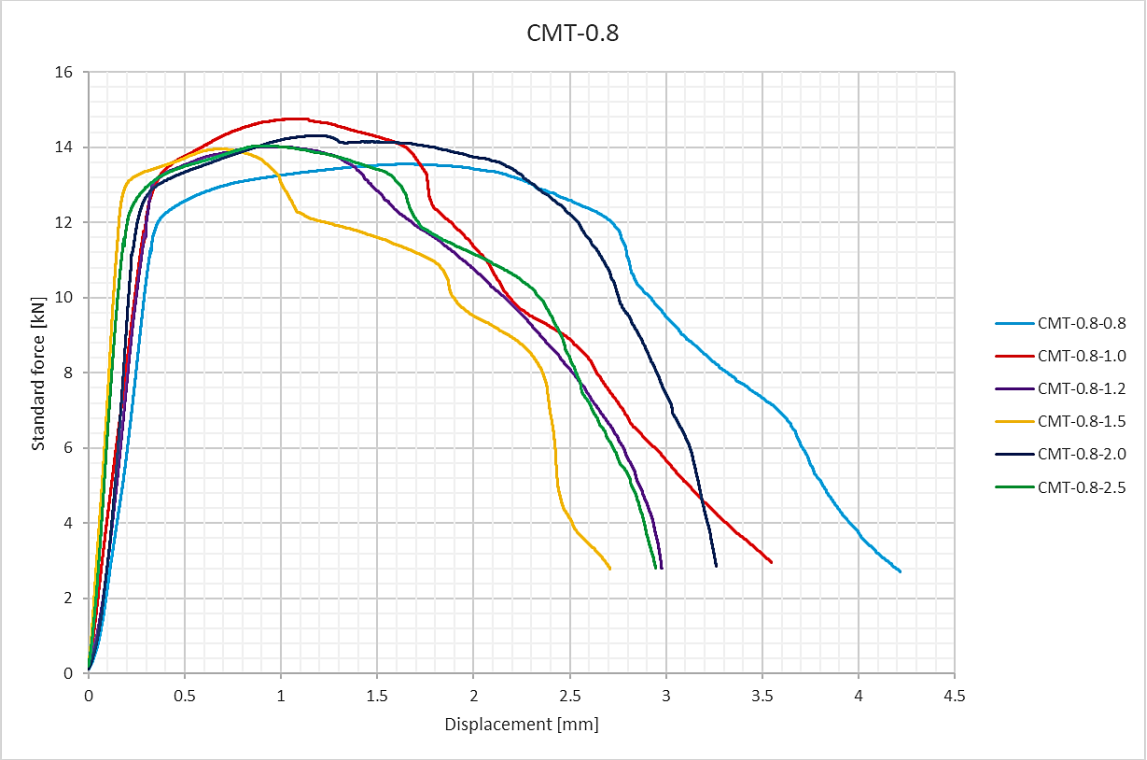

Figure B.14: Load-displacement curves of series CMT-0.8

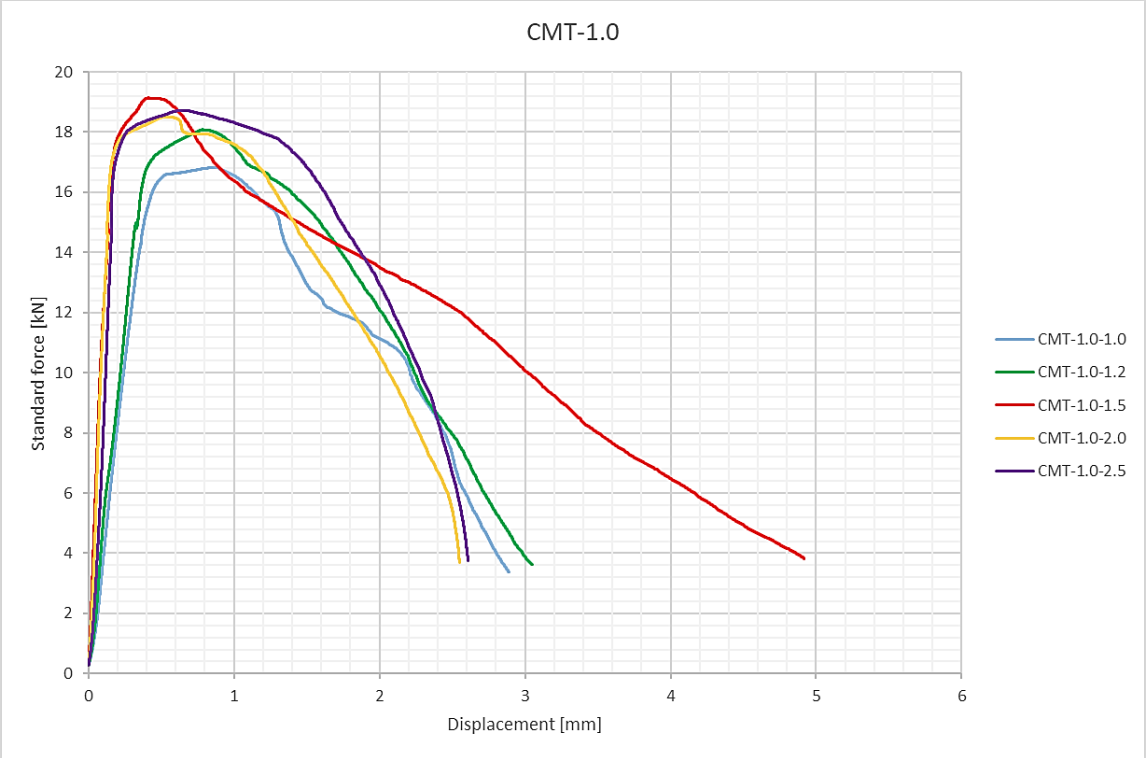

Figure B.15: Load-displacement curves of series CMT-1.0

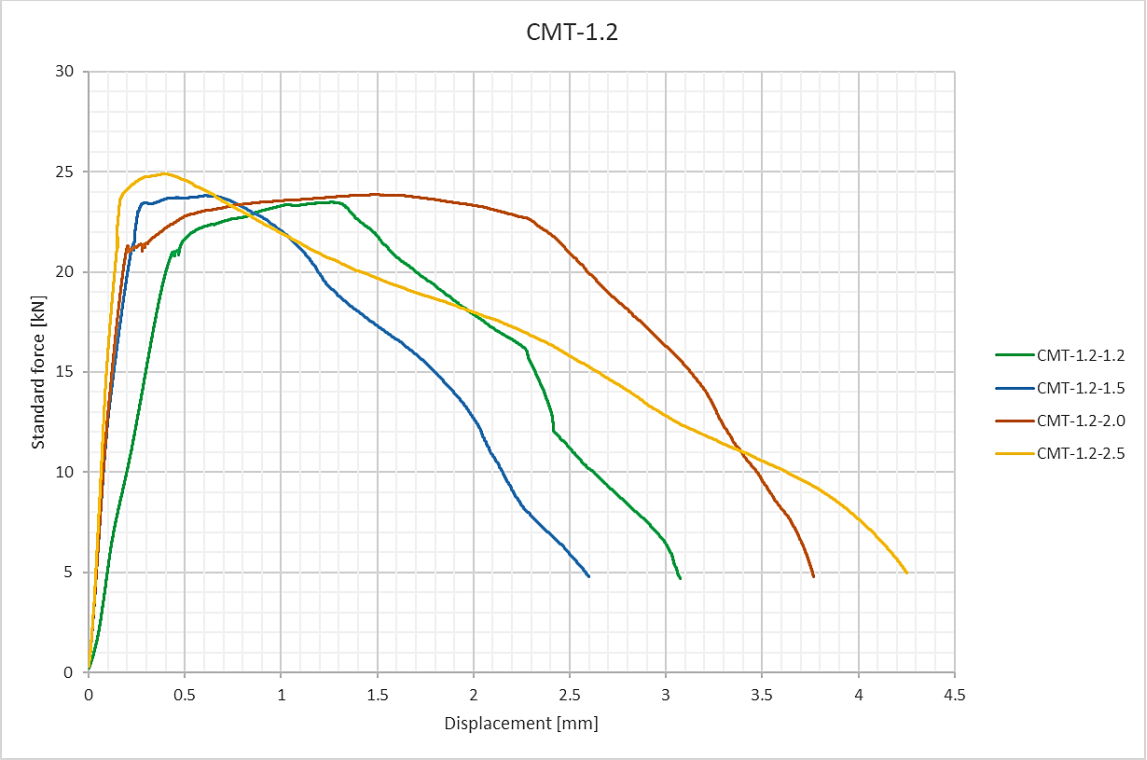

Figure B.16: Load-displacement curves of series CMT-1.2

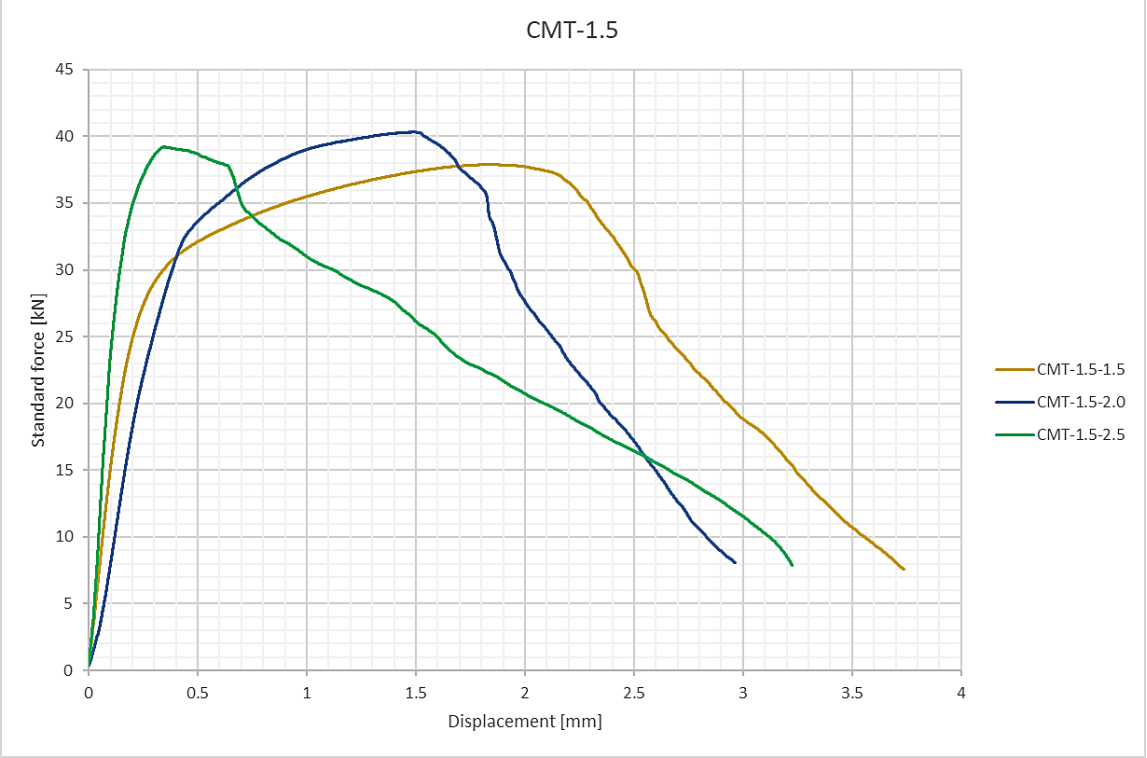

Figure B.17: Load-displacement curves of series CMT-1.5

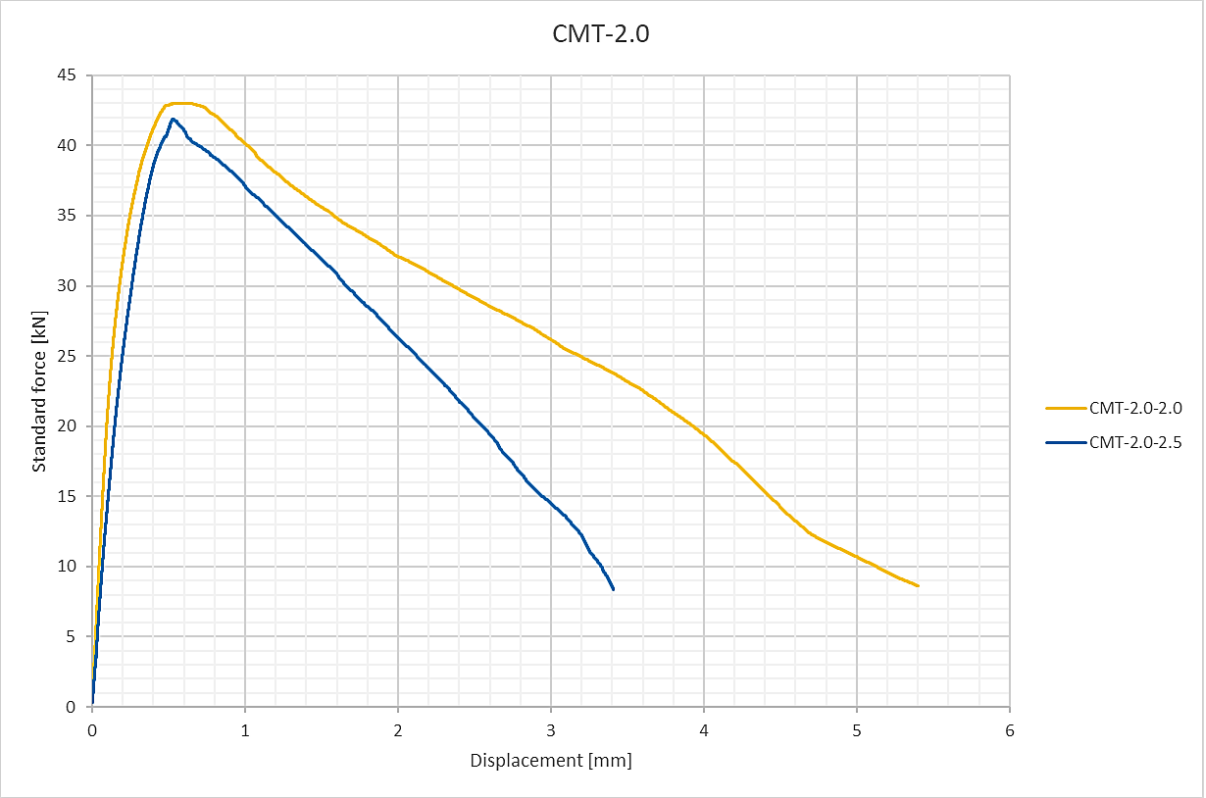

Figure B.18: Load-displacement curves of series CMT-2.0

Figure B.19: CMT-0.8-1.0 specimens before and after testing

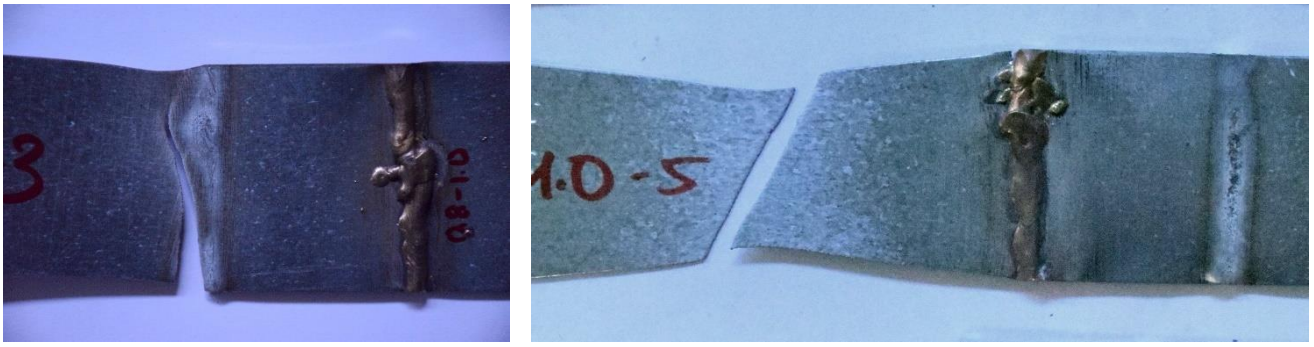

Figure B.20: Failure modes of CMT-0.8-1.0 specimens

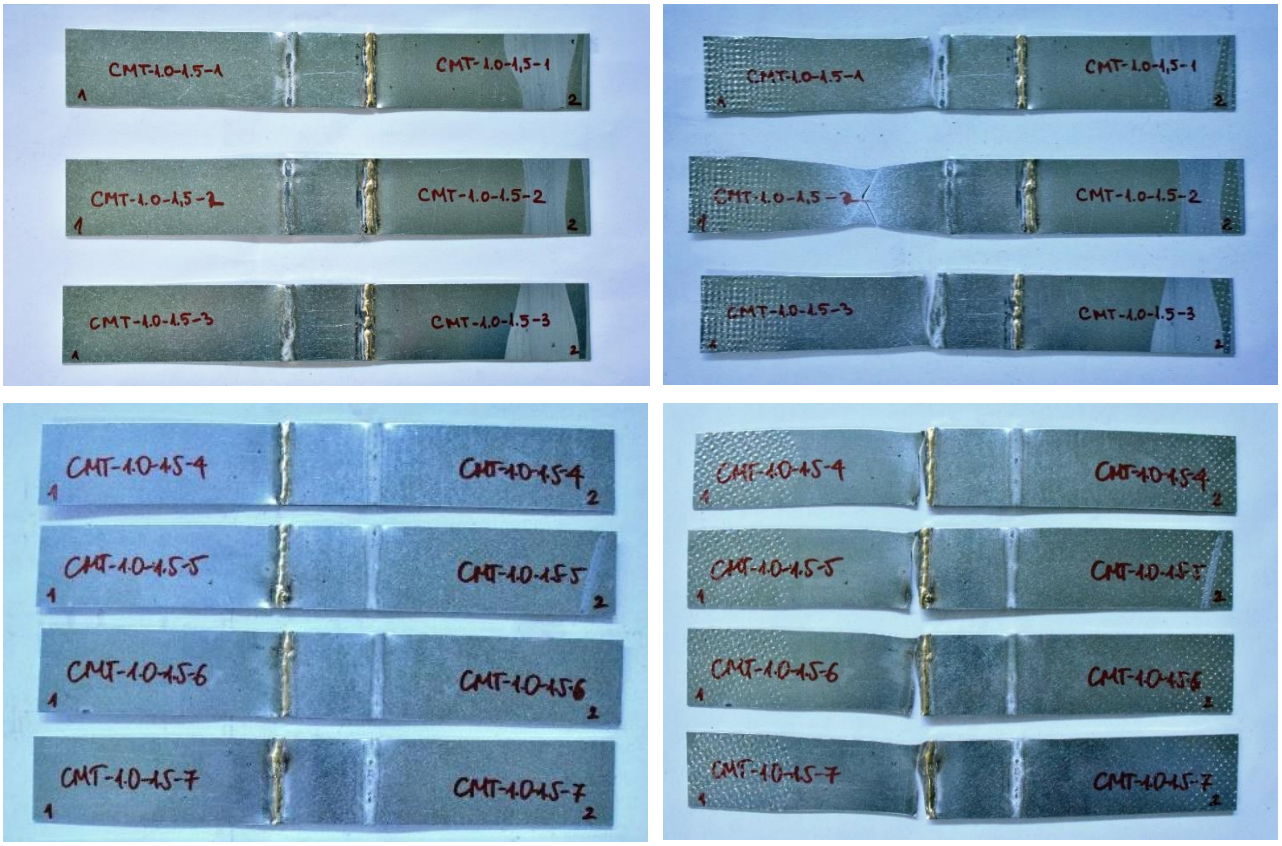

Figure B.21: CMT-1.0-1.5 specimens before and after testing

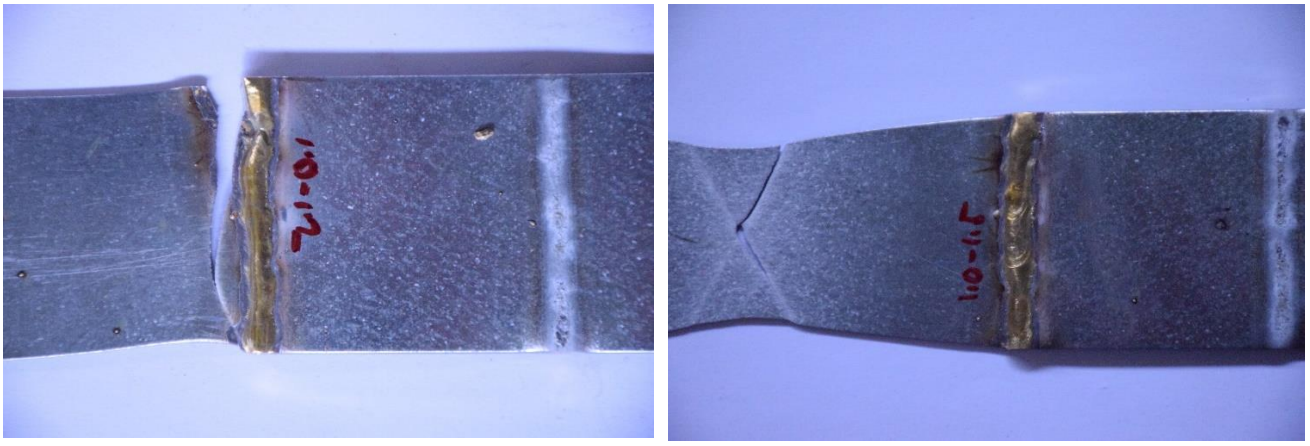

Figure B.22: Failure modes of CMT-1.0-1.5 specimens

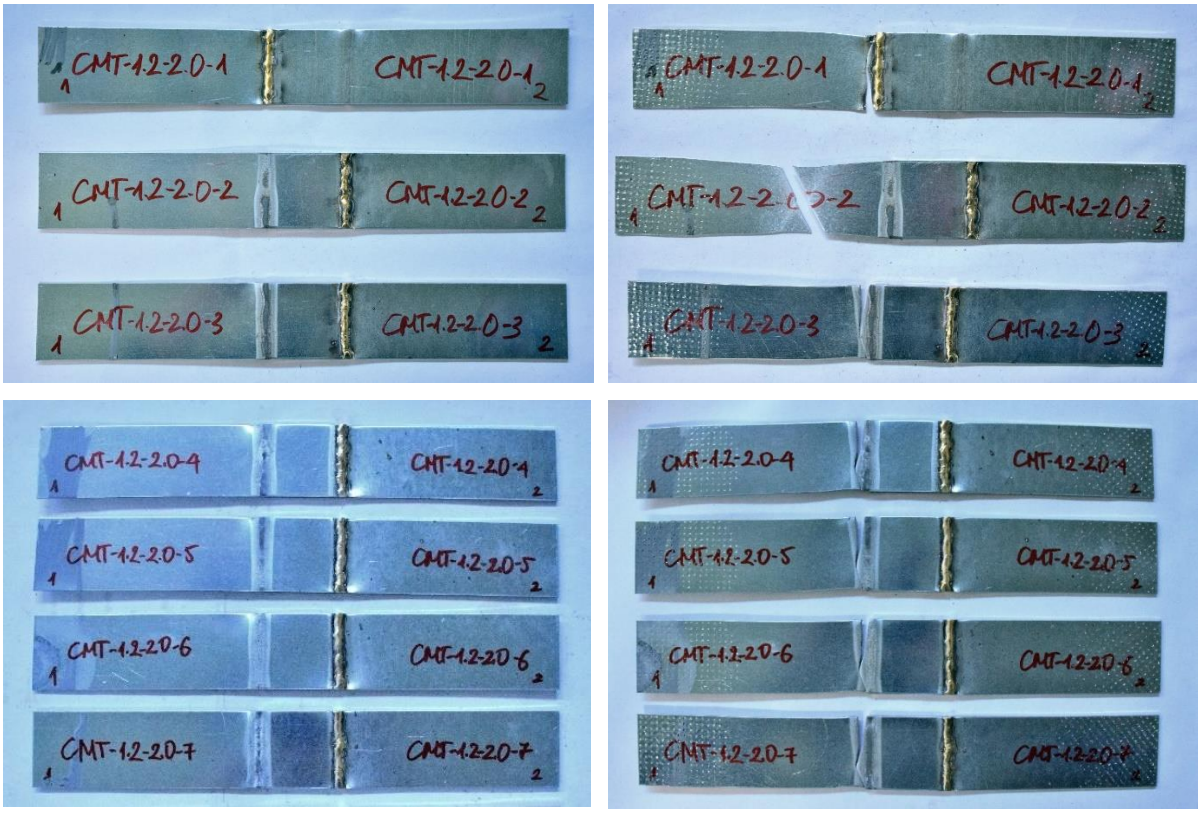

Figure B.23: CMT-1.2-2.0 specimens before and after testing

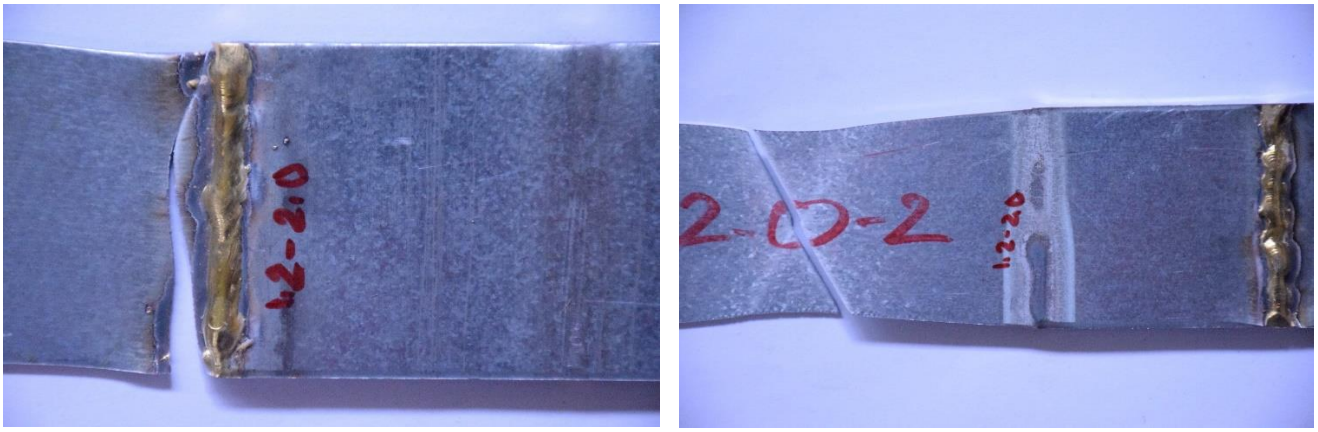

Figure B.24: Failure modes of CMT-1.0-2.0 specimens

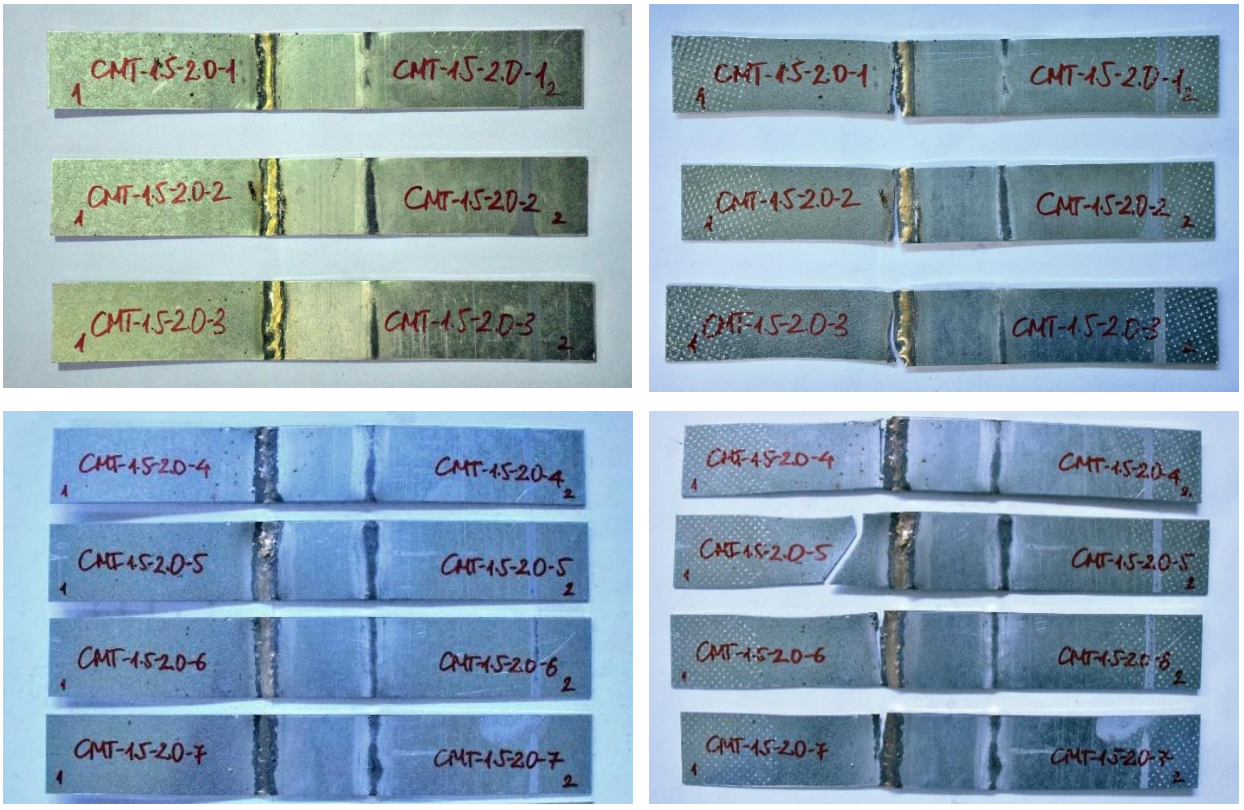

Figure B.25: CMT-1.5-2.0 specimens before and after testing

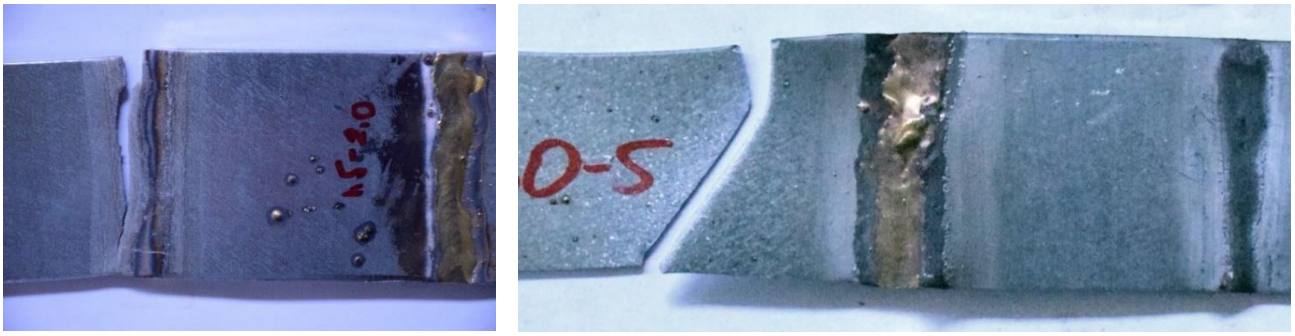

Figure B.26: Failure modes of CMT-1.5-2.0 specimens

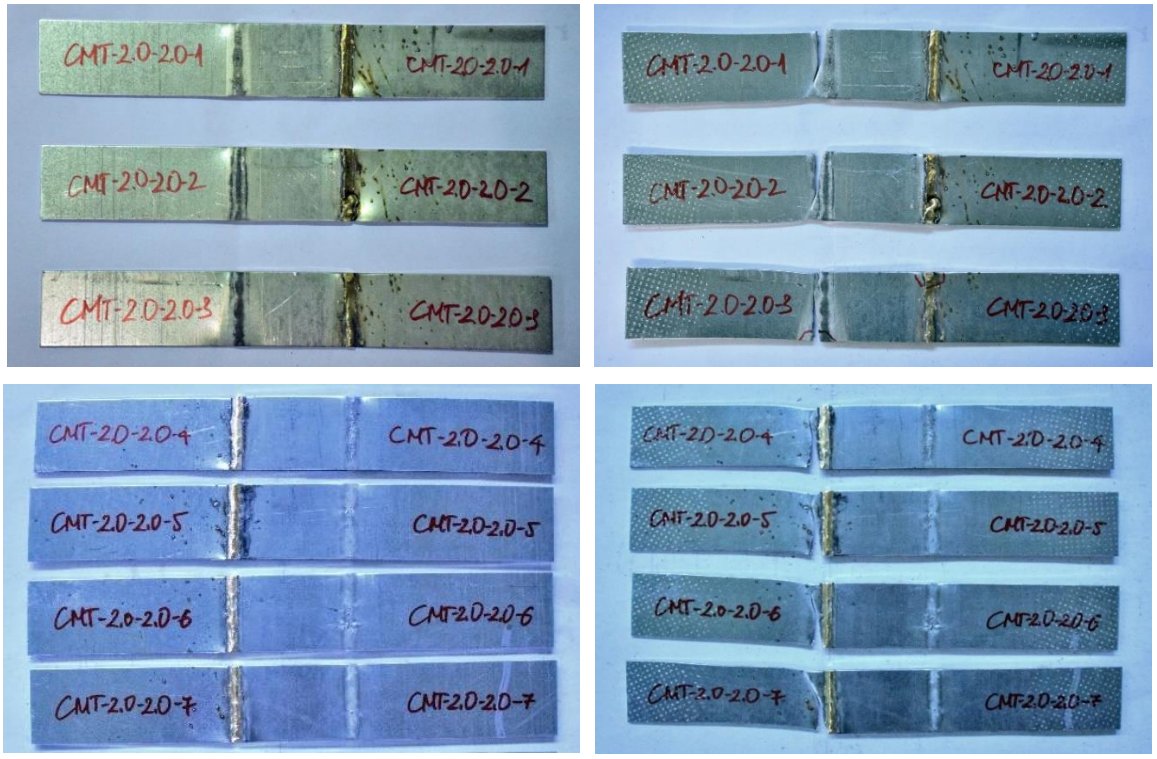

Figure B.27: CMT-2.0-2.0 specimens before and after testing

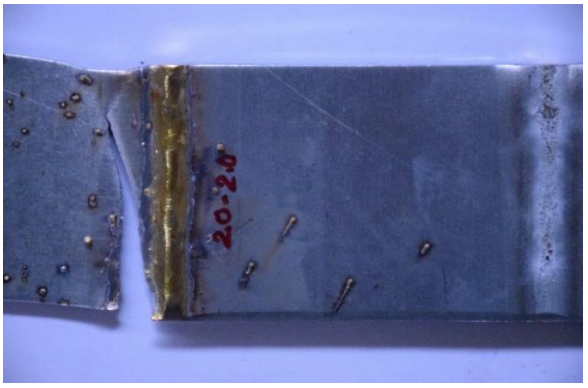

Figure B.28: Failure mode of CMT-2.0-2.0 specimens

APPENDIX E: DATA FOR LOAD-DISPLACEMENT CURVES OBTAINED BY ABAQUS/CAE v.6.14

Table E.1: Data for spot-welding beams obtained from ABAQUS

CWB SW-1		CWB SW-2		CWB SW-0.8		CWB SW-1.2	
Displacement (mm)	Force (kN)	Displacement (mm)	Force (kN)	Displacement (mm)	Force (kN)	Displacement (mm)	Force (kN)
0	0	0	0	0	0	0	0
4.33E-02	2.30	4.36E-02	2.58	4.12E-02	2.25	4.26E-02	2.80
4.29E-01	9.92	4.31E-01	9.89	4.13E-01	8.10	4.09E-01	11.37
1.42	25.59	1.43	25.80	1.37	20.23	1.35	30.15
3.20	52.99	3.22	53.85	3.10	41.04	3.05	62.66
5.85	90.87	5.88	92.77	5.63	68.78	5.55	108.88
9.30	138.19	9.37	141.43	9.00	102.07	8.78	166.78
13.58	187.79	13.69	191.15	13.10	133.48	12.69	225.40
18.51	223.92	18.76	232.07	17.65	159.28	17.02	270.97
24.03	244.75	24.36	250.93	22.71	166.89	21.58	300.16
30.33	244.00	30.68	246.71	28.44	165.69	26.15	314.70
36.39	246.99	36.87	251.01	34.79	171.73	31.41	302.99
42.64	249.53	43.17	265.40	40.90	183.64	37.54	294.37
48.71	256.01	49.46	265.71	47.00	184.61	43.11	293.61
55.01	256.30	55.30	248.80	53.37	188.40	48.22	290.35
60.74	248.05	60.40	247.12	59.96	191.85	52.94	285.45
66.13	243.77	64.40	243.49	66.19	186.78	57.16	269.64
69.96	243.29	66.88	226.94	71.96	193.72	58.73	232.08
72.71	234.79	66.67	193.40	76.93	192.85	56.70	149.73
73.46	214.21	64.02	147.63				
72.28	177.96						
68.96	135.16						

Table E.2: Data for CMT-welding beams obtained from ABAQUS

CWB CMT-1		CWB CMT-2		CWB CMT-3		CWB CMT-0.8		CWB CMT-1.2	
Displacement (mm)	Force (kN)	Displacement (mm)	Force (kN)	Displacement (mm)	Force (kN)	Displacement (mm)	Force (kN)	Displacement (mm)	Force (kN)
0	0	0	0	0	0	0	0	0	0
6.20E-02	6.98	6.20E-02	5.92	6.20E-02	6.35	6.20E-02	5.39	6.20E-02	7.12
5.63E-01	43.41	5.63E-01	36.34	5.63E-01	38.32	5.63E-01	33.49	5.63E-01	43.64
2.02	113.58	2.02	92.34	2.02	99.66	2.02	81.68	2.02	114.04
4.14	227.00	4.14	167.15	4.14	195.99	4.14	152.79	4.14	227.22
7.19	325.38	7.20	201.13	7.19	235.11	7.20	179.50	7.19	328.19
10.47	386.34	10.48	225.96	10.47	273.18	10.47	202.25	10.47	386.59
15.04	413.55	15.05	250.29	15.04	290.87	15.04	224.36	15.04	414.30
20.22	423.97	20.24	263.15	20.23	301.42	20.23	241.03	20.22	426.65
25.51	404.41	25.51	259.49	25.50	293.95	25.48	239.14	25.50	408.15
31.31	381.72	31.31	243.54	31.30	277.52	31.26	226.07	31.30	387.99
38.37	365.39	38.36	243.15	38.35	275.44	38.30	227.83	38.36	376.82
45.01	353.89	44.99	246.67	44.98	273.91	44.91	240.35	44.99	378.55
52.40	330.25	52.38	231.20	52.37	255.22	52.28	224.42	52.38	368.05
59.58	317.28	59.56	223.97	59.55	250.08	59.44	221.82	59.57	364.21
65.85	307.45	65.84	236.23	65.84	258.15	65.70	222.40	65.85	372.75
71.26	300.56	71.27	222.89	71.25	253.23	71.10	214.88	71.26	353.04
75.47	290.10	75.46	215.52	75.43	242.23	75.28	213.59	75.47	346.22
78.09	270.60	78.07	197.41	78.02	221.28	77.87	192.60	78.08	320.61
78.05	258.26	78.03	190.99	77.96	217.50	77.81	187.96	78.05	318.22
74.36	234.53	74.33	164.58	74.25	194.59	74.11	167.74	74.35	291.45
71.26	201.67	71.22	130.20	71.13	154.90	70.99	134.93	71.25	248.33